MASTER THESIS TECHNICAL MEDICINE

MEDICAL IMAGING AND INTERVENTION

Dosimetric consequences of prostate motion with and without endorectal balloon during extremely hypofractionated proton therapy

Lisanne G.M. Zwart

05-07-2019

MASTER THESIS TECHNICAL MEDICINE – MEDICAL IMAGING AND INTERVENTION

Dosimetric consequences of prostate motion with and without endorectal balloon during extremely hypofractionated proton therapy

Lisanne G.M. Zwart

Defense: July 5th 2019, 10:00 AM at the University of Twente, Enschede

Location: Department of Radiation Oncology, University Medical Center Groningen, Groningen

Graduation committee

Chairman	Prof. dr. ir. C.H. Slump *University of Twente, Enschede*
Medical supervisor	Dr. S. Aluwini *University Medical Center Groningen, Groningen*
Technical supervisor	Prof. dr. ir. C.H. Slump *University of Twente, Enschede*
Process supervisor	Drs. A.G. Lovink *University of Twente, Enschede*
Extra member	Dr. ir. C.L. Brouwer *University Medical Center Groningen, Groningen*
Extern member	M.E. Kamphuis, MSc *University of Twente, Enschede*

UNIVERSITY OF TWENTE.

umcg

Preface

In this Master thesis, I proudly present to you the final result of my graduation internship for the Medical Imaging and Intervention track of the master Technical Medicine of the University of Twente in Enschede. From September 2018 to June 2019, I have been working at the Department of Radiation Oncology of the University Medical Center Groningen. This resulted in my thesis entitled "Dosimetric consequences of prostate motion with and without endorectal balloon during extremely hypofractionated proton therapy".

First, I would like to thank my supervisors of the University Medical Center Groningen, Shafak Aluwini and Charlotte Brouwer, and my supervisors of the University of Twente, Kees Slump and Annelies Lovink, for their substantive and personal guidance. A special thank you is addressed to Petra Klinker, who helped me create the proton treatment plans. Moreover, I would like to thank all other colleagues in the department of radiation oncology for their assistance in either my project or during clinical activities. Furthermore, I want to thank the students of the Triade building for their support and the pleasant time. In the end, I would like to thank Marije Kamphuis as extern member of my graduation committee.

Lisanne Zwart
Groningen, 25 June 2019

Summary

Introduction: Conventionally fractionated photon therapy is a potentially curative treatment option for prostate cancer. Challenges are the depth-dose characteristics of photons and the low α/β ratio of prostate cancer. Therefore, extremely hypofractionated proton therapy may be more effective, However, challenges are the increased sensitivity to inter- and intrafraction prostate motion in extreme hypofractionation and the interplay effect in pencil beam scanning (PBS) proton therapy. An endorectal balloon (ERB) reduces intrafraction prostate motion, but its use is also associated with disadvantages. This thesis aimed to evaluate the dosimetric consequences of worst-case inter- and intrafraction prostate motion with and without ERB and the interplay effect during extremely hypofractionated proton therapy.

Materials and methods: Robustly optimized PBS proton treatment plans were created for five conventionally treated Groningen prostate cancer patients, using 5 fractions of 7.5Gy(RBE). For interfraction motion evaluation, PBS proton plans were recalculated on seven weekly repeated CTs (rCTs) and doses of the first five rCTs were deformed and summed to the planning CT (pCT) using deformable image registration (DIR) (accumulated deformed dose).

For combined worst-case prostate motion evaluation (inter- and intrafraction evaluation including the interplay effect), the first five rCTs of two representative patients were selected. Real-time intrafraction prostate motion measurements (three degrees of freedom) were available from 54 Pennsylvanian patients (52% with ERB, 48% without ERB). Worst-case intrafraction motion was selected and applied to the rCTs to create virtual CTs (vCTs) using DIR. To simulate the interplay effect, subplans of one second were created and calculated on the vCTs. Doses were deformed and summed from the vCTs to the rCTs and pCTs using DIR (4D accumulated dose). Target coverage of the prostate and proximal part of the seminal vesicles and bladder and rectum constraints were evaluated for both accumulated deformed and 4D accumulated doses.

Results: For interfraction prostate motion and combined worst-case prostate motion with ERB, D95 of the prostate and seminal vesicles was above the aim for 100% of patients. Bladder and rectum doses were within protocol limits. For combined worst-case prostate motion without ERB, target coverage of the prostate and seminal vesicles was on average 8.3±0.1 and 7.0±8.4Gy below the protocol limits, respectively. Rectum doses were within protocol limits for 3/8 constraints.

Conclusion: Extremely hypofractionated proton plans were robust to interfraction prostate motion and combined worst-case prostate motion with ERB, without violating rectum and bladder dose constraints. For combined worst-case prostate motion without ERB, large concessions had to be made for target coverage and rectal doses. In future research, a more probabilistic description of intrafraction prostate motion is necessary to estimate the actually given dose for the combined prostate motion with and without ERB more realistically.

Abbreviations

3D	Three-dimensional
4D	Four-dimensional
AP	Anterior-posterior
AUC	Area under the curve
CBCT	Cone beam computed tomography
CT	Computed tomography
CTCAE	Common terminology criteria for adverse effects
CTV	Clinical target volume
DIR	Deformable image registration
DRE	Digital rectal examination
DVF	Deformation vector field
EBRT	External beam radiotherapy
EPID	Electronic portal imaging device
ERB	Endorectal balloon
GSS	Gleason sum score
KIM	Kilovoltage intrafraction monitoring
kV	Kilovoltage
IGRT	Image-guided radiotherapy
IMPT	Intensity-modulated proton therapy
IMRT	Intensity-modulated radiation therapy
iPSA	Initial prostate-specific antigen
linac	Linear accelerator
LR	Left-right
MRI	Magnetic resonance imaging
MV	Megavoltage
nERB	Without endorectal balloon
OAR	Organ at risk
PBS	Pencil beam scanning
pCT	Planning computed tomography
PSA	Prostate-specific antigen
RBE	Relative biological effectiveness
rCT	Repeated computed tomography
ROI	Region of interest
RTT	Radiation therapist
SBRT	Stereotactic body radiation therapy
SFUD	Single-field uniform dose
SI	Superior-inferior
TNM	Tumour-node-metastases
UMCG	University medical center Groningen
US	Ultrasound
vCT	Virtual computed tomography
VMAT	Volumetric modulated arc therapy
wERB	With endorectal balloon

Table of contents

Chapter 1

General introduction

1.1 Introduction

In the Netherlands, prostate cancer is the most common cancer among males aged 45 years or older [1]. On 1 January 2018, the estimated ten-year prevalence was 9.8 per 1000 men, which means that 83,800 living Dutch men were diagnosed with prostate cancer in the previous ten years [1]. Approximately 12,600 new cases of prostate cancer were diagnosed in 2018 [1,2]. Because of the aging population, it is expected that the absolute incidence will substantially increase in the coming years [3].

External Beam Radiotherapy (EBRT) is a potentially curative treatment option for localized prostate cancer [4,5]. At the moment, photons are used for EBRT in the University Medical Center Groningen (UMCG), using a conventional fractionation scheme of 35 fractions of 2.2 Gy. However, conventionally fractionated photon therapy is associated with some challenges. First, because of the physical characteristics of photons, a low to moderate dose is spread over the surrounding healthy tissues, which eventually may result in side effects such as rectal bleeding [6,7]. Second, the use of a conventionally fractionated scheme with daily treatments over roughly seven weeks is associated with several limitations, including patient inconvenience, high costs and resource utilization [8]. Moreover, from a radiobiological point of view, prostate cancer cells are more sensitive to a few high-dose fractions rather than low-dose long treatment courses [8–10].

Given these limitations for the conventionally fractionated photon therapy, the use of protons in a hypofractionated scheme may be more effective. First, because protons may reduce the dose-volume related side effects because of their beneficial dose distribution properties and potential of sparing healthy tissues [6,11–13]. And second, because a hypofractionated scheme is expected to be more effective and offers the potential to increase patient convenience and decrease healthcare expenditures. In the last years, several phase I and II extreme hypofractionation trials have been conducted and have shown that the biochemical control and toxicity rates seem acceptable. However, the follow-up has been relatively short and trials were conducted with small sample sizes, so extreme hypofractionation is not implemented in clinical practice yet [8,10,14].

One of the major challenges of extreme hypofractionation is the increased sensitivity to geometrical uncertainties, including inter- and intrafraction prostate motion. Because of the high fractional dose and a small amount of fractions, a positional error in even a single fraction may result in a large alteration of the delivered dose on a particular location. Moreover, an additional challenge in pencil beam scanning (PBS) proton therapy is the interplay effect. Intrafraction prostate motion causes ''interplay'' between the timeline of the proton beam delivery and the timeline of the intrafraction prostate motion, leading to misplacement of spots and a subsequent heterogeneous coverage inside the prostate [15–17]. To limit underdosage of the target and overdosage of the organs at risk (OARs), which may result in more side effects, it is important to limit the geometrical uncertainties [18]. From several studies, it followed that an endorectal balloon (ERB) significantly reduced intrafraction prostate motion [19–23]. However, the necessity of an ERB needs further investigation, because of opposing conclusions from studies about the dosimetric impact of an ERB, the possible deformation of the prostate when an ERB is positioned wrongly and the decrease of patient comfort when an ERB is inserted before every treatment delivery [24–26].

The aim of this thesis is to evaluate the dosimetric consequences of prostate motion with and without ERB during extremely hypofractionated PBS proton therapy.

1.2 Clinical Background

1.2.1 Functional anatomy of the prostate

The prostate is an accessory gland that is part of the male reproductive system. It is located in the lower pelvis, anterior to the rectum, inferior to the urinary bladder and it surrounds the proximal urethra. Posteriorly, the prostate is attached to the seminal vesicles. [27,28] The upper and lower narrowed parts of the prostate are called base and apex, respectively. The prostate is divided into a left and right lobe, which both consists of many branching ducts, surrounded by stroma. [28] Its primary function is to secrete a fluid that aids in nourishment and motility of the sperm [29]. Prostate-specific antigen (PSA) is an enzyme that is part of the secreted fluid. The prostate can be functionally divided into different zones, including the fibromuscular, transition, central and peripheral zone. The fibromuscular zone is located anteriorly, the transition zone is located around the prostatic urethra and the central zone surrounds the ejaculatory ducts and extends toward the seminal vesicles. In addition, the peripheral zone envelops the other zones and comprises about three-quarters of the prostate. [29,30] Figure 1 visualizes the anatomy of the prostate and its surrounding organs.

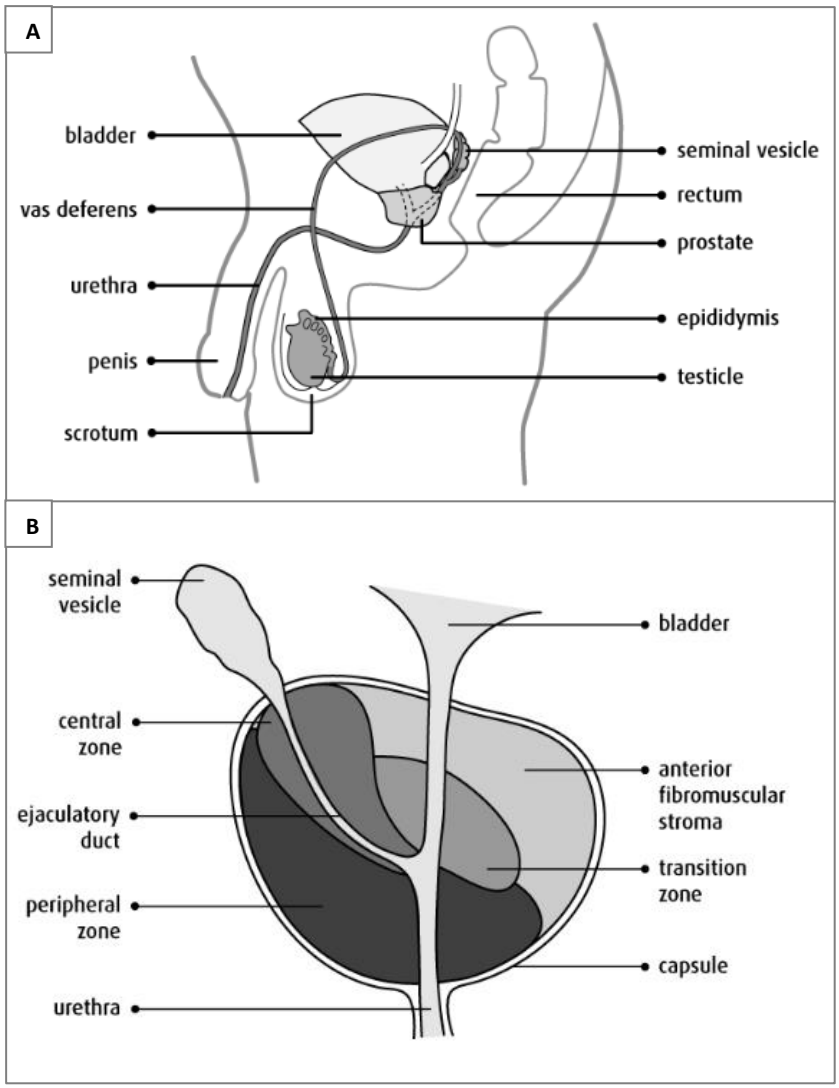

Figure 1: Sagittal aspect of the male pelvic viscera (A) and sagittal dissection of the prostate visualizing the different zones (B) [86].

1.2.2 Pathophysiology of prostate cancer

95% of prostate cancers are adenocarcinomas, which arise from the glandular cells of the prostate [5,29]. They are located in the peripheral zone in 74% of cases [31]. The leading risk factor for developing prostate cancer is advanced age. Prostate cancer is rarely diagnosed in men younger than 40 years, whereas 75% of prostate cancers are diagnosed in men older than 65 years [29]. Another common risk factor is a family history of prostate cancer [5,29]. Men who have a first degree relative with prostate cancer, have a two-fold increased risk of developing prostate cancer themselves [29]. Most adenocarcinomas are of acinar origin and feature glands that lack organization and infiltrate the stroma. Well-differentiated adenocarcinomas show glands with a single layer of neoplastic epithelial cells. On the other hand, progressive loss of differentiation is characterized by rudimentary or no gland formation, increasing variability of gland size and configuration and cribriform or papillary patterns. [30] Prostate cancer aggressiveness is most commonly classified according to the Gleason grading system. The grades are assigned to the two most abundant areas and range from 1 (best-differentiated and least aggressive) to 5 (very poorly differentiated and most aggressive). The total Gleason sum score (GSS) is obtained by adding the primary and secondary grades. For example, a GSS of 4+3=7 means that Gleason pattern 4 was assigned to the most abundant area and Gleason pattern 3 was assigned to the second most abundant area [29,30]. Gleason patterns 1 and 2 are rare, whereas Gleason pattern 3 is the most common. Lower scores are correlated with better prognoses, so the Gleason grading system has prognostic value [30].

1.2.3 Diagnostics

Since most prostate cancers are located in the peripheral zone, most patients with prostate cancer are asymptomatic, especially in the early stages of the disease [5,29]. In most patients, prostate cancer is suspected because of an elevated serum PSA level and/or an abnormal finding on digital rectal examination (DRE). Uncommonly, prostate cancer patients present with lower urinary tract symptoms or symptoms referable to metastases [5,30]. When prostate cancer is suspected, a prostate needle biopsy is indicated. The most widely used method for obtaining prostatic tissue is transrectal ultrasound-guided needle biopsy. The definitive diagnosis of prostate cancer is accomplished by histologic evaluation of the obtained prostatic tissue. [5,29] The necessity of further imaging for prostate cancer staging is based on PSA value, DRE findings and prostate biopsy results, such as GSS, tumour length in the biopsies, vaso-invasive growth and the presence of cribriform growth [5,29]. Prostate cancer staging relies on the Tumour-Node-Metastases (TNM) system. The system describes the extent of the primary tumour (T), the involvement of regional lymph nodes (N) and the presence of distant metastases (M). The extent of the primary tumour is divided into T1-T4. Higher T values are indicative of more involvement of the prostate and the invasion of surrounding structures (see Table 1 and Figure 2). The involvement of regional lymph nodes is either no lymph node involvement (N0) or the presence of positive regional lymph nodes (N1). M0 indicates no distant metastases, whereas M1 indicates the presence of distant metastases. M1 can be subdivided into M1a (non-regional lymph node involvement), M1b (bone metastases) and M1c (other distant metastases, with or without bone metastases). [5,32] The localized prostate carcinoma can be classified in three different risk groups, depending on the T stage, GSS and PSA level. The low-risk patient group consists of patients with T1c-T2a prostate cancer, GSS <7 and PSA <10 ng/ml. The intermediate-risk patient group consists of patients with T2b prostate cancer and/or GSS 7 and/or PSA 10-20 ng/ml. The high-risk patient group consists of patients with T2c-4 prostate cancer, or GSS >7, or PSA >20 ng/ml. [33]

Table 1: T staging of the primary tumour, based on the 8th edition of the cancer staging manual of the American Joint Committee on Cancer [32].

T1	No clinically detectable tumour: not palpable or visible when using imaging techniques.
- T1a	Histological finding of tumour in ≤5% of examined sampled prostatic tissue.
- T1b	Histological finding of tumour in >5% of examined sampled prostatic tissue.
- T1c	Histological finding of tumour in acquired prostatic tissue using needle biopsy.
T2	Tumour is palpable and confined to the prostate.
- T2a	Tumour in ≤50% of one lobe.
- T2b	Tumour in >50% of one lobe.
- T2c	Tumour in both lobes.
T3	Tumour extends through the capsule.
- T3a	Uni- or bilateral extracapsular extension or microscopic bladder neck involvement.
- T3b	Tumour extends into the seminal vesicles.
T4	Tumour invades adjacent structures other than seminal vesicles, for example the external urethral sphincter, bladder, rectum, levator muscles and/or the pelvic wall.

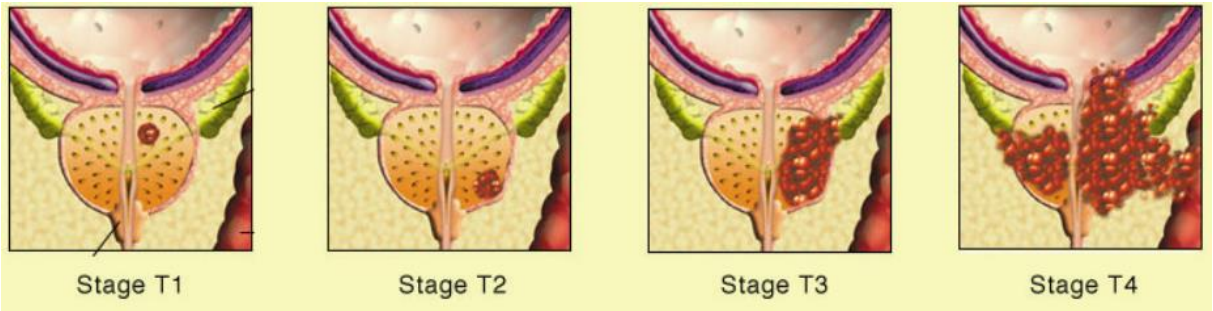

Figure 2: T staging of the primary tumour [87].

1.2.4 Treatment options

When localized prostate cancer is diagnosed, different treatment options are available. Watchful waiting may be an option for patients with a ≤10-year life expectancy because of age or comorbidities [5]. Treatment without curative intention will be offered to these patients when symptomatic progression occurs. Active surveillance may be an appropriate alternative for curative therapy for men with early stage disease [5]. Curative treatment should be offered to patients with more progressive or aggressive prostate cancer [29]. Curative treatment options for localized prostate cancer include radical prostatectomy, EBRT or brachytherapy [5]. Since the mean survival rate is almost equal for the different treatment options, decisions regarding the most appropriate treatment option are dependent on patient and tumour characteristics, personal preferences and resource availability [4,5].

1.3 Technical Background

1.3.1 External beam radiotherapy

In EBRT, a dose of ionizing radiation is delivered externally and eventually causes the accumulation of DNA damage, resulting in apoptosis, mitotic catastrophe or senescence [34]. The most common type of radiation used for EBRT is photons [6]. Photons have no mass or charge and are generated by the collision of accelerated electrons with a metal target. When the generated photons are released by the linear accelerator (linac), there is an initial build-up of energy, followed by a peak-dose only a few centimeters from the entrance surface, after which the dose slowly attenuates (see Figure 3). To deliver the maximal dose to the target, multiple beams are used that converge at the target. [6] Photons can be delivered by different techniques [34]. In three-dimensional (3D) conformal radiotherapy, beams are shaped around the tumour contours using multi-leaf collimators [4,34]. Mostly, four opposed fields are used to create a high-dose overlap zone at the target [4]. The technique developed and intensity-modulated radiotherapy (IMRT) was introduced in the early 2000s [35]. IMRT uses mobile computer-controlled collimators to shape the high-dose region around the target [4]. Volumetric modulated arc therapy (VMAT) was introduced in 2007 [36]. It is an advanced form of IMRT and uses a beam rotating 360 degrees around the patient to achieve a 3D-dose distribution [4,34].

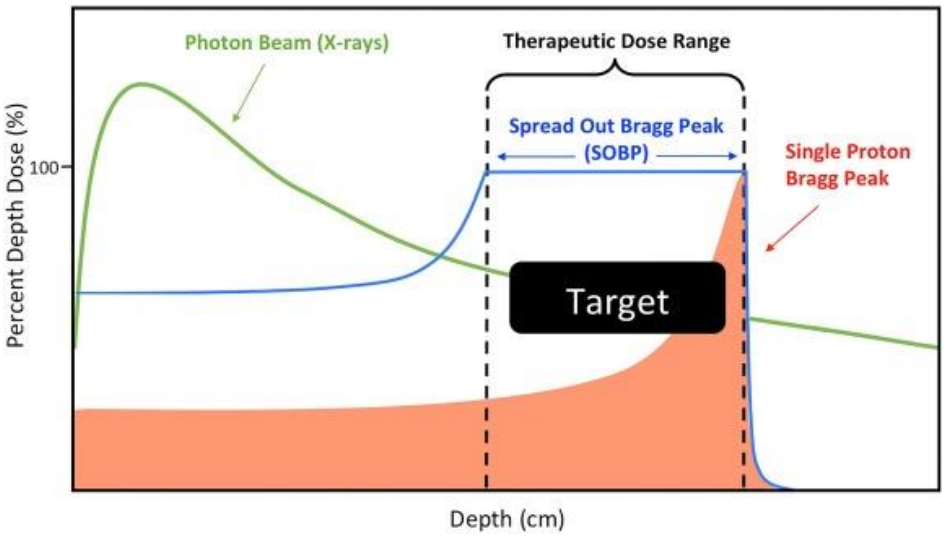

Figure 3: Relative depth-dose distribution for a photon beam (green line) and a proton beam (blue line) [88].

1.3.2 Current workflow for photon therapy in the UMCG

At the moment, photons for EBRT are delivered using VMAT and a conventionally fractionated scheme of 35 fractions of 2.2 Gy. In preparation before the actual irradiation, gold fiducials are placed in the prostate and a planning computed tomography (pCT) scan and magnetic resonance imaging (MRI) scan are acquired. The clinical target volumes (CTVs) and OARs are delineated on the pCT scan, using the MRI scan as a resource. These delineated structures are used to calculate the dose during VMAT treatment planning. Before each treatment fraction on the conventional linac, the patient is positioned based on the alignment of the small tattoo points on the skin and the isocenter of the linac, shown by fixes laser lines. Besides, orthogonal kilovoltage (kV) images or cone beam CT (CBCT) are used to match the position of the gold fiducials with the pCT. One fraction is delivered each working day.

1.3.3 Clinical challenges of the current workflow

The use of a conventionally fractionated scheme, with daily treatments over roughly seven weeks, is associated with several limitations. First, the long treatment duration is inconvenient for patients and increases costs and resource utilization [8]. Second, from a radiobiological point of view, prostate cancer cells are more sensitive to a few high-dose fractions rather than low-dose long treatment courses [8–10]. Given these limitations for the conventionally fractionated scheme, a hypofractionated scheme is expected to be more effective and offers the potential to increase patient convenience and decrease healthcare expenditures.

Another clinical challenge includes the depth-dose characteristics of photons. Because of the physical characteristics of photons, the photon beam always consists of both entrance and exit doses. Therefore, a low to moderate dose is spread over the surrounding healthy tissues, which may eventually result in side effects such as rectal bleeding [6,7]. The severity of side effects e.g. rectal bleeding can be graded according to the Common Terminology Criteria for Adverse Effects (CTCAE) scoring system [37]. Approximately 10% of patients develops ≥grade 2 CTCAE rectal bleeding, which is indicative of medical intervention, within two years after photon radiotherapy [7]. Several studies showed that there is a relationship between the irradiated volume of rectum or rectal wall on the one hand and the severity and frequency of late toxicities on the other hand. For example, Skwarchuk et al. (2000) showed that late rectal bleeding is correlated with higher rectal maximal dose and the exposure of a larger volume of the rectal wall to high dose [38]. Vargas et al. (2005) showed that a strong predictor for chronic rectal toxicity was the volume of rectal wall or rectum radiated to ≥50 Gy [39]. In addition, from Van der Laan et al. (2008) followed that the parameter that was most predictive for Grade 2 or worse late rectal toxicity was the volume of the rectum that receives ≥70 Gy (V70) [40]. At last, from Kim et al. (2014) followed that the absolute volume of the rectum receiving high dose is associated with late toxicity [41]. Given the beneficial dose distribution properties of protons, EBRT using protons may reduce these dose-volume related side effects because they have the potential of sparing healthy tissues [6,11–13].

1.3.4 Proton therapy

Whereas the biological effect of photons and protons is almost the same, protons have beneficial dose distribution properties [11,12]. As opposed to photons, protons are heavy particles, that will stop abruptly in a target after traveling an intended distance [6]. This results in a peak of energy delivery commonly referred to as the Bragg peak. Beyond the Bragg peak, the radiation dose falls off rapidly with essentially no exit dose [11]. To encompass the entire target, multiple proton beams with different energies are used, resulting in a spread out Bragg peak [6]. Figure 3 visualizes the unique relative depth-dose distribution of protons. Protons can be delivered by using two methods. The older method uses large beams of passively scattered protons that are shaped using high-density blocks or apertures [6]. The newer method is called PBS proton therapy and allows for the delivery of single-field uniform dose (SFUD) or intensity-modulated proton beam therapy (IMPT) [6,11].

1.3.5 Extreme hypofractionation

Hypofractionated radiotherapy is the delivery of a larger dose per fraction, in few fractions and with a lower total dose [4]. Prostate cancer has a unique radiobiology since the radiation response of prostate cancer differs compared to the radiation response of other cancer types. To predict the fractionation response, the linear quadratic model of cell killing was established [42]:

$$S = \exp(-\alpha D - \beta D^2) \quad (1)$$

In this equation, S describes the dose survival relationship between the mean number of surviving cells after a radiation dose D and the initial number of cells. The cell-specific coefficients α and β describe the unrepairable lesions and combination of repairable sublethal lesions. So the α/β ratio describes the sensitivity of tumour cells to fractionation and is a measure of the fractionation response. [42]

Most tumours are fast-growing and most sensitive to standard fractionation given in small fractions over a relatively long time period. Therefore the α/β ratio is typically high for most tumours (>10 Gy) [10]. Conversely, prostate cancer cells proliferate slowly and have a high reparation ability of radiation damage over time. Several studies indicated that the α/β ratio of prostate cancer is approximately 1.5 Gy [43–45]. This is even lower than the corresponding α/β ratio of approximately 3 Gy of late responding surrounding OARs such as the bladder and the rectum [10,46,47]. Consequently, the use of a hypofractionated scheme might increase the therapeutic ratio while minimizing late toxicity to surrounding OARs, in a shorter overall treatment time [8–10].

One of the major challenges of extreme hypofractionation is the increased sensitivity to geometrical uncertainties. Because of the high fractional dose and a small amount of fractions, a positional error in even a single fraction may result in a large alteration of the delivered dose on a particular location. To limit underdosage of the target and overdosage of the OARs that may result in more side effects, it is essential to limit the geometrical uncertainty, such as the target motion as much as possible [18].

1.3.6 Prostate motion

Prostate motion may be distinguished into two categories, including inter- and intrafraction prostate motion. Interfraction prostate motion is the day-to-day anatomical variation that can be described as the discrepancy between patient anatomy at the pCT and the beginning of treatment. Intrafraction prostate motion is the motion that occurs during the actual radiation delivery. Several factors can contribute to prostate motion, for example patient movement, femoral head rotation, rectal peristalsis and bladder and rectal filling. Because of the geometrical uncertainties, a treatment margin is added around the CTV to create the planning target volume to ensure adequate target dose coverage. [18]

Interfraction prostate motion

To account for the daily anatomical variation, image guided radiotherapy (IGRT) is increasingly used in the clinic. In current clinical practice, gold fiducials are placed in the prostate. In addition, kV or megavoltage (MV) CBCT images are used to position the patient accurately before starting radiation delivery. Table 2 summarizes the recorded interfraction prostate motion relative to bony anatomy or initial skin tattoo positioning of several studies. In these studies, Van Herk's formalism was used to determine the mean, systematic and random error in the left-right (LR), superior-inferior (SI) and anterior-posterior (AP) direction [48,49].

Table 2: Interfraction prostate motion relative to bony anatomy or initial skin tattoo positioning of several studies. Van Herk's formalism was used to calculate the mean, systematic and random error. Abbreviations: unknown (unk.) left-right (LR), superior-inferior (SI), anterior-posterior (AP), not determined (n.d.), electronic portal imaging device (EPID).

	Number of patients / scans	Measurement device (match based on)	Relative to skin tattoo or bony anatomy	Direction	Mean error (M) [mm]	Systematic error (∑) [mm]	Random error (σ) [mm]
Litzen-berg (2006) [50]	11 / unk.	EPID (gold fiducials in the prostate)	Skin tattoo	LR	0.1	2.2	3.4
				SI	0.05	3.1	3.3
				AP	0.6	1.5	5.2
Wong (2008) [51]	329 / 1870	kV CT (soft tissue matching of the prostate)	Skin tattoo	LR	n.d.	2.3	3.2
				SI	n.d.	1.7	2.3
				AP	n.d.	4.3	3.9
Snir (2011) [52]	17 / 449	kV CBCT (soft tissue matching of the prostate)	Skin tattoo	LR	-0.9	1.6	2.3
				SI	0.4	1.8	1.8
				AP	0.6	2.6	3.0
			Bony anatomy	LR	0.1	0.4	1.5
				SI	0.3	0.6	1.1
				AP	-0.2	0.7	2.0
Mayyas (2013) [53]	27 / 1100	kV CBCT (soft tissue matching of the prostate)	Skin tattoo	LR	1.1	2.4	2.5
				SI	0.2	1.4	2.2
				AP	-1.2	3.0	3.2
Mesías (2016) [54]	63 / 1615	kV CBCT (soft tissue matching of the prostate)	Skin tattoo	LR	0.3	2.6	3.9
				SI	-0.6	2.5	3.0
				AP	-1.1	2.9	3.9

Intrafraction prostate motion

The prediction of the intrafraction prostate motion is difficult because the motion is random, sporadic and patient-specific [55–57]. The intrafraction prostate motion has been measured continuously using different modalities, for example, electromagnetic tracking of transponders with the Calypso system, four-dimensional (4D) transperineal ultrasound (US), kilovoltage intrafraction monitoring (KIM), 4DCT or the electronic portal imaging device (EPID). From several studies followed that the likelihood of intrafraction prostate motion increased with elapsed time [22,58,59]. Table 3 summarizes the recorded real-time intrafraction prostate motion of several studies in LR, SI and AP direction. In these studies, Van Herk's formalism was used to determine the mean, systematic and random error [48,49]. In addition, the measured percentages of treatment time for which the 3D intrafraction prostate motion was >2, 3, 5, 7 and 10 mm are outlined in Table 4 for several studies.

Table 3: Intrafraction prostate motion using several measuring devices of several studies. Van Herk's formalism was used to calculate the mean, systematic and random error. Abbreviations: left-right (LR), superior-inferior (SI), anterior-posterior (AP), not determined (n.d.).

	Measurement device (measurement frequency)	Number of patients / fractions	Mean measure-ment time [min]	Direction	Mean error (μ) [mm]	Systematic error (∑) [mm]	Random error (σ) [mm]
Ng (2012) [60]	KIM (5-10 Hz)	10 / 268	2.5	LR	n.d.	0.23	0.53
				SI	n.d.	0.32	0.98
				AP	n.d.	0.26	1.04
Sihono (2018) [61]	4D US (2 Hz)	38 / 770	4.2	LR	0.01	0.30	0.59
				SI	0.15	0.23	0.64
				AP	-0.08	0.34	0.73

Table 4: Measured percentage of treatment time for which the 3D intrafraction prostate motion was >2, 3, 5, 7 or 10 mm of several studies. Abbreviation: not determined (n.d.).

	Measurement device (measurement frequency)	Number of patients / fractions	Mean Measure-ment time [min]	>1mm	>2mm	>3mm	>5mm	>7mm	>10mm
Langen (2008) [58]	Calypso (10 Hz)	17 / 550	10.0	n.d.	n.d.	13.6% of time	3.3% of time	n.d.	n.d.
Shah (2011) [62]	Calypso (10 Hz)	20 / 200	10.3	n.d.	n.d.	12.6% of time	2.9% of time	n.d.	n.d.
Ng (2012) [60]	KIM (5-10 Hz)	10 / 268	2.5	n.d.	n.d.	5.6% of time	2.2% of time	0.7% of time	0.4% of time
Wang (2012) [22]	Calypso (10 Hz)	29 / 1,061	6.0	57.0% of time	24.8% of time	11.7% of time	3.1% of time	n.d.	n.d.
Tong (2015) [59]	Calypso (10 Hz)	236 / 8,660	8.0	n.d.	27.8% of time	10.7% of time	1.6% of time	0.3% of time	n.d.

The main findings of the outlined studies are that the smallest intrafraction prostate motion was in the LR direction, whereas the magnitude of the intrafraction prostate motion in the SI and AP direction is much larger. Most of the intrafraction prostate motion was within a few millimetres. Besides intrafractional translations of the prostate, intrafractional rotations of the prostate may also be important. From Van de Water et al. (2014) followed that rotations around the LR axis are most important and required corrections for up to 5° when using a 3-mm margin to ensure 98% CTV coverage during stereotactic body radiotherapy (SBRT) [63].

1.3.7 Interplay effect

In PBS proton therapy, the pencil beam is scanned line-by-line and delivers spots to stationary coordinates of a virtual grid. When the required number of spots, as optimized during the treatment planning process, are delivered, the pencil beam moves to the next virtual grid position. For stationary targets, PBS enables the delivery of highly conformal doses to the tumour. However, when the target is moving during the delivery of PBS proton therapy, there is interference between target motion and dynamic radiation delivery. This so-called ''interplay effect'' between the dynamic radiation delivery and target motion adds an additional level of complexity to accurate radiation delivery. The result may be a deteriorated target dose distribution. Figure 4 visualizes the possible dosimetric impact of the interplay effect. [17] From several studies, it followed that the interplay effect may affect the coverage inside the prostate [16,64]. Whereas conventionally fractionated treatment delivery potentially mitigates the interplay effect, with the use of an extremely hypofractionated regimen, more attention should be paid to the interplay effect [17].

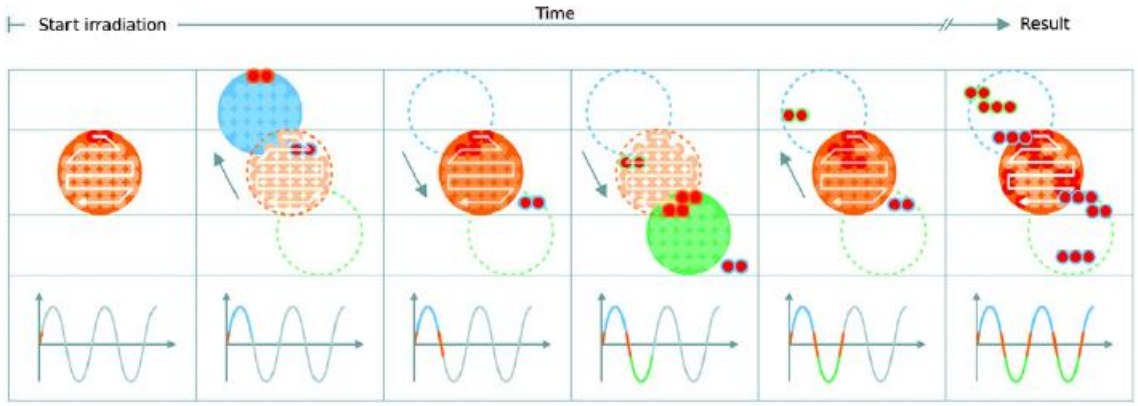

Figure 4: Possible dosimetric impact of the interplay effect. On the bottom, target motion is illustrated. At the start of irradiation, the target is accurately positioned, visualized in orange and the first spots are delivered in the right position. However, when the target moves up or down, indicated in blue and green respectively, spots are delivered to a wrong position within the target, or even outside the target. The result is a deterioration of the dose distribution in the target, as visualized on the right. [17]

1.3.8 Endorectal balloon

Since inter- and intrafraction prostate motion increase the radiation delivery uncertainty, the role of an ERB to decrease the inter- and intrafraction prostate motion was investigated. Interfraction prostate motion variations were not significantly reduced when using an ERB [20,21,65]. However, several studies reported that the intrafraction prostate motion was significantly reduced when an ERB was used [19–23]. Nonetheless, the necessity of an ERB needs further investigation. First, because of the opposing conclusions from studies about the dosimetric impact of an ERB. Xiang et al. (2017) performed a planning study on the dosimetric impact of an ERB during CyberKnife SBRT. They concluded that significant reductions in intermediate to high doses to the rectum with an ERB were observed [25]. Wong et al. (2015) performed also a planning study on the dosimetric impact of an ERB during SBRT. They found an increase in the volume of the rectum and rectal wall receiving a high dose, so they concluded that the use of an ERB resulted in an increased rectal dose and subsequent toxicity [24]. Second, the insertion of an ERB before every treatment delivery decreases patient comfort. At last, Jones et al. (2013) concluded that an error in the ERB position could result in prostate deformations and negatively affect the treatment [26].

1.4 Aim of this thesis and thesis outline

The aim of this thesis was to evaluate the dosimetric consequences of prostate motion with and without ERB during extremely hypofractionated proton therapy. For this purpose, we evaluated the impact of interfraction motion on target coverage and doses to the OARs, which is described in Chapter 2. In Chapter 3, we described a developed new methodology to simulate intrafraction motion measurements based on virtual CT scans. This enabled the evaluation of the combined effect of inter- and intrafraction motion and interplay effect on target coverage and doses to the OARs. Chapter 4 of this thesis covers the general discussion.

Chapter 2

Evaluation of the impact of interfraction prostate motion effects on target coverage and doses to the organs at risk

2.1 Abstract

Introduction: The combination of an extremely hypofractionated scheme and pencil beam scanning (PBS) proton therapy potentially results in an increased sensitivity to interfraction prostate motion. The aim of this study was to evaluate the dosimetric impact of interfraction prostate motion without endorectal balloon (ERB).

Materials and methods: Five conventionally treated prostate cancer patients, who underwent seven weekly repeated CTs (rCTs) were selected. PBS proton therapy plans were created using an extremely hypofractionated regimen of 5 fractions of 7.5 Gy (RBE), applying robust optimization using 5mm setup and 3% range uncertainty to fulfill V100%>95% for the prostate and V80%>95% for the proximal part of the seminal vesicles in the voxelwise minimal dose. In the first step, PBS proton plans were recalculated on all rCTs. In the second step, the first five rCTs were selected and the calculated fractional doses were projected to the planning CT (pCT) using deformable image registration (DIR). The deformed doses were accumulated on the pCT to simulate the complete treatment of five fractions with different anatomies (accumulated deformed doses). Target coverage and dose-volume constraints of the bladder (V70%<10.0mL and D0.01mL<39.8Gy), rectum (V105%<2.0mL and V95%<5.0mL), anterior rectal wall (D0.01mL<39.4Gy) and posterior rectal wall (D0.01mL<18.8Gy) were evaluated.

Results: The interfraction prostate motion did not negatively influence nominal target coverage of the prostate and proximal part of the seminal vesicles (accumulated deformed doses). Organ at risk (OAR) doses remained within protocol constraints, except for the bladder constraint V70%<10.0mL and posterior rectal wall dose constraint D0.01mL<18.8 Gy for 1/5 patients (accumulated deformed doses).

Conclusion: PBS proton treatment plans were robust to interfraction motion without the use of an ERB, without violating OAR dose constraints.

2.2 Introduction

To account for interfraction prostate motion and eliminate the daily setup error before radiation delivery, daily imaging can be used to reposition the patient. However, from several studies followed that this repositioning scheme might not be sufficient for residual anatomical variations, such as volume and shape changes of the targets and the surrounding organs at risk (OARs) [66,67]. These remaining anatomical variations potentially impact the daily delivered dose distribution.

In comparison with photons, protons have beneficial dose distribution properties, resulting in a larger potential of sparing healthy tissues [6,11,13]. However, since protons are more sensitive to tissue heterogeneities, proton therapy was expected to be more sensitive to interfraction prostate motion. Zhang et al. (2007) investigated the dosimetric impact of interfraction prostate motion on passively scattered proton therapy and intensity-modulated radiotherapy (IMRT). They recalculated the dose on eight daily CT images of ten patients and concluded that the dosimetric impact of interfraction prostate motion was similar for both modalities [68]. However, in this study, the dosimetric impact of interfraction prostate motion was not accumulated for the complete treatment. Therefore Wang et al. (2011) performed a study to quantify the dosimetric impact of interfraction prostate motion during the complete treatment [69]. 3D conformal proton plans were created for the planning CT (pCT) and recalculated on the daily CT images of three patients. The calculated dose on the daily CT images was warped on the pCT using deformable image registration (DIR). The results confirmed that target coverage was maintained in the presence of interfraction prostate motion. [69] Even though the studies of Zhang et al. (2007) and Wang et al. (2011) concluded that the dosimetric impact of interfraction prostate motion was similar for both photon and proton therapy, both studies used older techniques for proton beam delivery, including 3D conformal and passively scattered proton therapy.

Nowadays, pencil beam scanning (PBS) proton therapy enables the delivery of dose with higher conformity to the target because of the heterogeneous dose distributions of the fields compared to passively scattered proton therapy [6,11]. Therefore, it was expected that PBS proton therapy increases the sensitivity to interfraction prostate motion compared to passively scattered proton therapy. Soukup et al. (2009) studied the robustness of PBS proton therapy and IMRT against interfraction prostate motion. The treatment plans of four patients were recalculated on approximately sixteen CT images per patient. The authors concluded that the sensitivity of PBS and IMRT to the interfraction prostate motion were in the same order. [70]

Another factor that may increase the sensitivity to interfraction prostate motion is the use of a hypofractionated scheme. Because of the unique radiobiology and low α/β ratio of prostate cancer, the use of a hypofractionated scheme might increase the therapeutic ratio [8–10]. However, a decrease in the number of fractions might increase the motion-related dosimetric uncertainties, that otherwise canceled out in treatments with a larger number of fractions. In a study of Faasse-de Hoog et al. (2016), the dose to the OARs was evaluated for daily acquired repeated CTs (rCTs) during stereotactic body radiation therapy (SBRT) delivered in four fractions. The planned dose distributions were projected to the aligned rCTs. It was concluded that the planned mean dose was exceeded in the rCTs by on average 59±17%, 5±5% and 15±24% for the membranous urethra, rectum and anus, respectively [71]. So the dosimetric impact of interfraction prostate motion seems clinically relevant in hypofractionated photon therapy. Wang et al. (2013) studied the dosimetric impact of

interfraction prostate motion by recomputing the 3D conformal proton plan on the acquired daily CT images of three patients and renormalizing the plans for different hypofractionated schemes. It was found that the dosimetric impact of interfraction prostate motion was largest in the peripheral 5% of the target, whereas the dosimetric impact was small for the central 95% of the target. Moreover, the target equivalent dose increased when shortening the treatment from 28 to 5 fractions. However, because of the decreased averaging of interfraction prostate motion effects, the uncertainty in target coverage increased. [72]

The first study that evaluated the combined effect of a hypofractionated scheme and PBS proton therapy was conducted by Moteabbed et al. (2018). They have evaluated the dosimetric impact of interfraction prostate motion with endorectal balloon (ERB) on hypofractionated PBS proton therapy for six patients. They recomputed the plans on the weekly CT images and concluded that the delivered target dose and OAR doses remained within clinical tolerance. [73]

The aim of this study was to evaluate the impact of interfraction prostate motion effects without ERB on target coverage and doses to the OARs in extremely hypofractionated PBS proton therapy.

2.3 Materials and methods

2.3.1 Study population and image acquisition

Five prostate cancer patients who were conventionally treated at our department in 35 fractions of 2.2 Gy were randomly selected. Three gold fiducials were implanted in the prostate before treatment to facilitate setup using orthogonal kilovoltage (kV) images. All patients underwent a pCT acquisition in the treatment position using a CT scanner with an axial resolution of 0.977x0.977 mm and a slice thickness of 2 mm (Siemens SOMATOM Definition AS, Siemens Healthineers, Erlangen, Germany). In addition, all patients underwent seven weekly rCTs in the treatment position within half an hour of the treatment fraction. The rCTs of the first patient were acquired using the Siemens SOMATOM CT scanner, whereas the rCTs of patients 2-5 were acquired using a CT scanner with an axial resolution of 0.998x0.998 mm and a slice thickness of 2.5 mm (GE MEDICAL SYSTEMS Optima CT580, GE Healthcare, Chicago, Illinois). All scans were acquired without ERB.

2.3.2 Structure contouring and registration

Two clinical target volumes (CTVs) were manually delineated in the transverse slice direction on the pCT and all rCTs, including the prostate and the proximal part of the seminal vesicles. The proximal part of the seminal vesicles was included, given that microscopic spread from the prostate to the seminal vesicles is most likely confined to the proximal part of the seminal vesicles [74,75]. The delineation was done by an experienced radiation oncologist, using RayStation 7.99 Research (RaySearch Laboratories, Stockholm, Sweden). The MRI image was used to check the delineation boundaries. Second, the gold fiducials and different OARs were delineated on both pCT and rCTs by a radiation therapist (RTT) student and a technical medicine student, under the supervision of the radiation oncologist. The pCT and rCTs were rigidly registered, using a region of interest (ROI) based registration to the gold fiducials, taken into account both translations and rotations. Next, DIR was performed, using the ANACONDA algorithm, which is based on image intensity and anatomical information [76]. The prostate, seminal vesicles, bladder, anorectum and pelvic bones were used as controlling ROIs.

2.3.3 Quantification of displacement and bladder and rectum volumes

Interfraction prostate motion relative to the pelvic bones was determined by the difference between the center of mass of the pelvic bones (pb) and the prostate (pros), respectively. The pelvic bones include the symphysis and the femoral heads. The distance between the two centers of mass was calculated using the following equation:

$$Distance = \sqrt{(x_{pros} - x_{pb})^2 + (y_{pros} - y_{pb})^2 + (z_{pros} - z_{pb})^2} \quad (2)$$

In addition, volumes of the bladder and rectum were quantified for the pCT and all rCTs.

2.3.4 Pencil beam scanning proton treatment planning

Patients were virtually planned for PBS proton therapy using RayStation 7.99 Research (RaySearch Laboratories, Stockholm, Sweden). First, a template for PBS proton planning was created by an RTT and two experienced medical physicists. The virtual plans have to consist of an extremely hypofractionated regimen of 5 fractions of 7.5 Gy (RBE), applying robust optimization using 5mm setup and 3% range uncertainty to fulfill V100%>95% for the prostate and V80%>95% for the proximal part of the seminal vesicles. In addition, different dose-volume constraints for the OARs, prepared by the radiation oncologist, were taken into account, which are added in Appendix A. The proton plans consisted of two opposing lateral beams from 90 and 270 degrees. The defined dose grid size was 2x2x2 mm^3. During plan optimization, target coverage and dose-volume constraints of the rectum, anorectum and anal canal were prioritized. The developed objective lists for all patients are added in Appendix B. All proton plans were clinically accepted by an experienced radiation oncologist and medical physicist.

2.3.5 Dosimetric evaluation

The assessment of the dosimetric impact of interfractional anatomical variation was twofold. In the first step, the virtual proton plans were recalculated on all matched rCTs. In the second step, the calculated doses on these rCTs were considered as single fraction doses and projected to the pCT using DIR. The deformed doses of the five rCTs were accumulated to simulate the robustness for the complete treatment of five fractions with five different interfraction motions (accumulated deformed dose). The target coverage and doses to the rectum and bladder were evaluated for all rCTs separately and for the accumulated deformed dose on the pCT. In addition, the accumulated deformed dose was compared to the planned dose on the pCT.

2.3.6 Robustness evaluation

The dose calculation of the proton plans on the rCTs was evaluated under 14 symmetrically perturbed setup scenarios of 5.0 mm and 2.0 mm for the pCT and rCTs, respectively. For determining the setup error of 2.0 mm for the rCT, Van Herk's formula was used and included errors were the difference between the proton isocenter and the imaging center, the patient (re-)positioning accuracy and the intrafraction variation of the patient [48]. In addition, the range uncertainty was implemented for all setup scenarios by scaling the Hounsfield Units of the CT by ±3%, resulting in 28 scenarios. Target coverage was assessed for the constructed voxelwise minimal dose distribution from the 28 scenarios.

2.4 Results

2.4.1 Patient characteristics

The patient population consisted of five men. Mean age of the patients was 74 ± 2.24 year (range: 71-77 year). TNM stage, initial PSA and Gleason Score are described in Table 5 for all patients.

Table 5: Patient characteristics, including Tumour-Node-Metastases (TNM) stage, initial PSA (iPSA) and Gleason Score for all patients.

	TNM stage	iPSA (ng/mL)	Gleason Score
Patient 1	cT1cNxMx	6.5	3+4=7
Patient 2	pT2cN0M0	6.3	4+4=8
Patient 3	cT1cNxMx	7.5	3+4=7
Patient 4	cT2aNxMx	13	3+4=7
Patient 5	cT2NxMx	6.2	4+3=7

2.4.2 Quantification of interfraction prostate motion relative to pelvic bones

The absolute interfraction prostate motion relative to the pelvic bones on the rCTs compared to the pCT are visualized in Figure 5 for all patients. Interfraction prostate motion relative to the pelvic bones increased or decreased with 0-0.25 cm for 82.9%, 0.25-0.5 cm for 17.1% and >0.5 cm for 5.7% of the rCTs compared to the pCT, respectively.

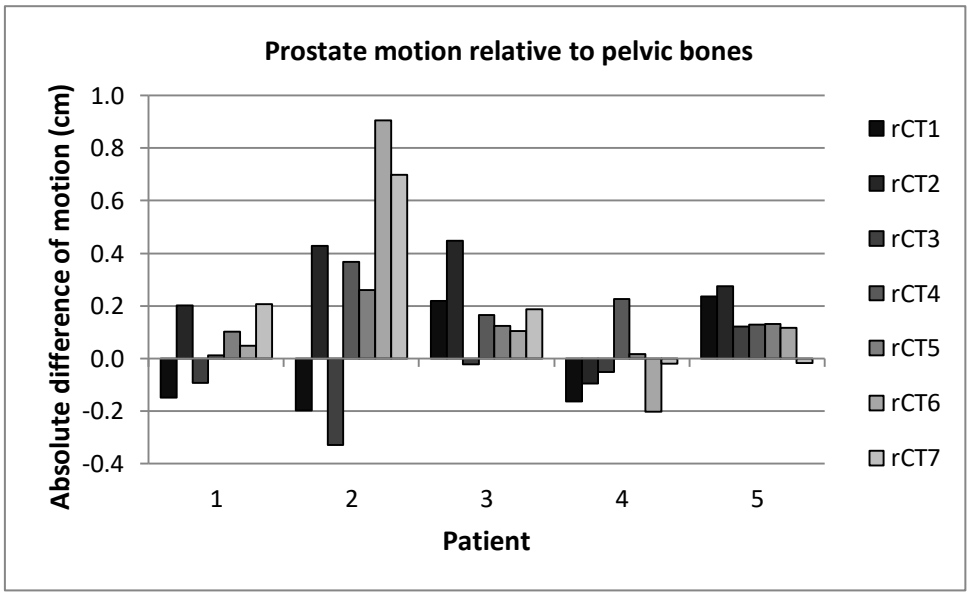

Figure 5: Absolute interfraction prostate motion relative to pelvic bones on the rCTs compared to the pCT for all patients. Abbreviations: repeated CT (rCT).

2.4.3 Quantification of bladder and rectum volume

Bladder and rectum volumes were determined for the pCT and all rCTs. The variability of the volumes is summarized in Table 6.

Table 6: Variability of bladder and rectum volume (mL) for all patients.

	Bladder volume (mL)	Rectum volume (mL)
Patient 1	156.30 ± 43.53 (range: 109.12 – 252.24)	73.42 ± 28.48 (range: 50.30 – 131.25)
Patient 2	575.73 ± 111.83 (range: 430.98 – 751.27)	93.43 ± 21.00 (range: 64.52 – 127.14)
Patient 3	133.48 ± 61.31 (range: 74.84 – 233.87)	53.29 ± 10.38 (range: 40.84 – 68.15)
Patient 4	92.00 ± 33.57 (range: 59.73 – 154.46)	73.85 ± 17.70 (range: 55.00 – 101.62)
Patient 5	195.85 ± 60.58 (range: 117.09 – 284.75)	128.84 ± 36.52 (range: 86.92 – 183.82)

The relative differences of the bladder and rectum volumes on the rCTs compared to the pCT are visualized in Figure 6. Bladder volume increased or decreased with 0-50% for 74.3%, 50-100% for 14.3% and >100% for 11.4% of rCTs compared to the pCT, respectively. Rectum volume increased or decreased with 0-50% for 80.0%, 50-100% for 17.1% and >100% for 2.9% of rCTs compared to the pCT, respectively.

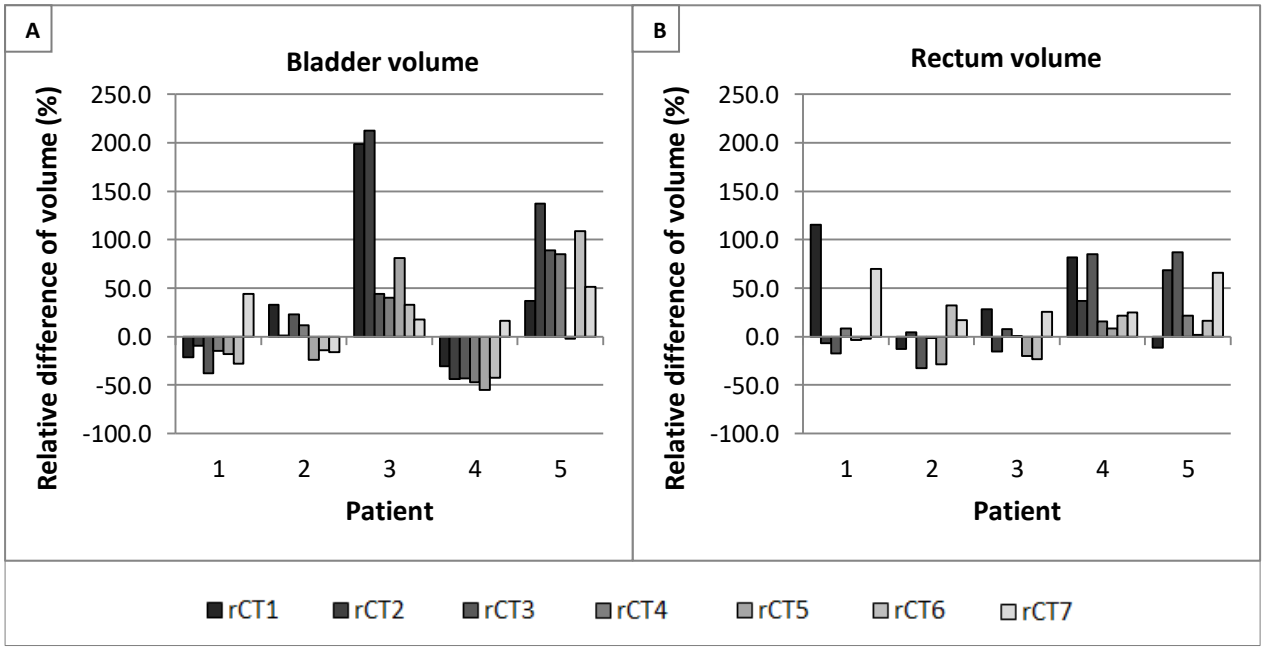

Figure 6: Relative differences of the bladder (A) and rectum volume (B) of all rCTs compared to pCT for all patients.

2.4.4 Dosimetric effects of interfraction prostate motion of all repeated CTs

The D95 of the nominal and voxelwise minimal dose of the prostate and proximal part of the seminal vesicles are visualized in Figure 7 for the pCT and rCTs of all patients. The V100 of the nominal and voxelwise minimal doses of the prostate and proximal part of the seminal vesicles are added in Appendix C. The aim for D95 was 37.5 Gy for the prostate and 30.0 Gy for the proximal part of the seminal vesicles, respectively. For the nominal dose, D95 of the prostate was above the aim for 100% of pCTs and rCTs. However, for the voxelwise minimal dose, D95 of the prostate was below the aim for 60% of pCTs (mean decrease below the aim was 0.2±0.01 Gy, range: 0.1-0.3 Gy) and below the aim for 51.4% of rCTs (mean decrease below the aim was 0.7±0.7 Gy, range: 0.0-2.7 Gy). For the nominal dose, D95 of the proximal part of the seminal vesicles was above the aim for 100% of pCTs and was below the aim for 11.4% of rCTs (mean decrease below the aim was 1.0±1.0 Gy, range: 0.1-1.9 Gy). When evaluating the voxelwise minimal dose, D95 of the proximal part of the seminal vesicles was below the aim for 20% of pCTs (decrease below the aim was 5.6 Gy) and was below the aim for 37.1% of rCTs (mean decrease below the aim was 2.4±2.3 Gy, range 0.1-7.7 Gy).

In Figure 8, the clinical goals for the bladder, rectum, anterior rectal wall and posterior rectal wall are visualized. Dose-volume histograms of the bladder and rectum are added in Appendix C. For the volume constraint V70%<10.0mL of the bladder, visualized in A, 100% of pCTs was above the constraint (mean increase above the constraint was 22.5±14.6 Gy, range 6.9-46.0 Gy) and 97.1% of rCTs were above the constraint (mean increase above the constraint was 16.2±9.6 Gy, range 2.1-36.2 Gy). For the dose constraint D0.01mL<39.8Gy for the bladder, visualized in B, 40% of pCTs were above the constraint (mean increase above the constraint was 0.1±0.2 Gy, range 0.0-0.2 Gy) and 42.9% of rCTs were above the constraint (mean increase above the constraint was 0.3±0.2 Gy (range: 0.1-0.7 Gy). For the volume constraint V105%<2.0mL of the rectum, visualized in C, 100% of pCTs and rCTs were below the constraint. For the volume constraint V95%<5.0mL of the rectum, visualized in D, 100% of pCTs was below the constraint and 14.3% of rCTs was above the constraint (mean increase above the constraint was 0.5±0.7 Gy, range 0.0-1.8 Gy). For the dose constraint D0.01mL<39.4Gy of the anterior rectal wall, visualized in E, 40% of pCTs was above the constraint (mean increase above the constraint was 0.1±0.1 Gy, range 0.0-0.2 Gy) and 57.1% of rCTs were above the constraint (mean increase above the constraint was 0.4±0.2 Gy, range: 0.0-1.0 Gy). For the dose constraint D0.01mL<18.8Gy of the posterior rectal wall, visualized in F, 20% of pCTs was above the constraint (increase above the constraint was 0.4 Gy) and 77.1% of rCTs was above the constraint (mean increase above the constraint was 4.9±4.1 Gy, range: 0.7-12.6 Gy).

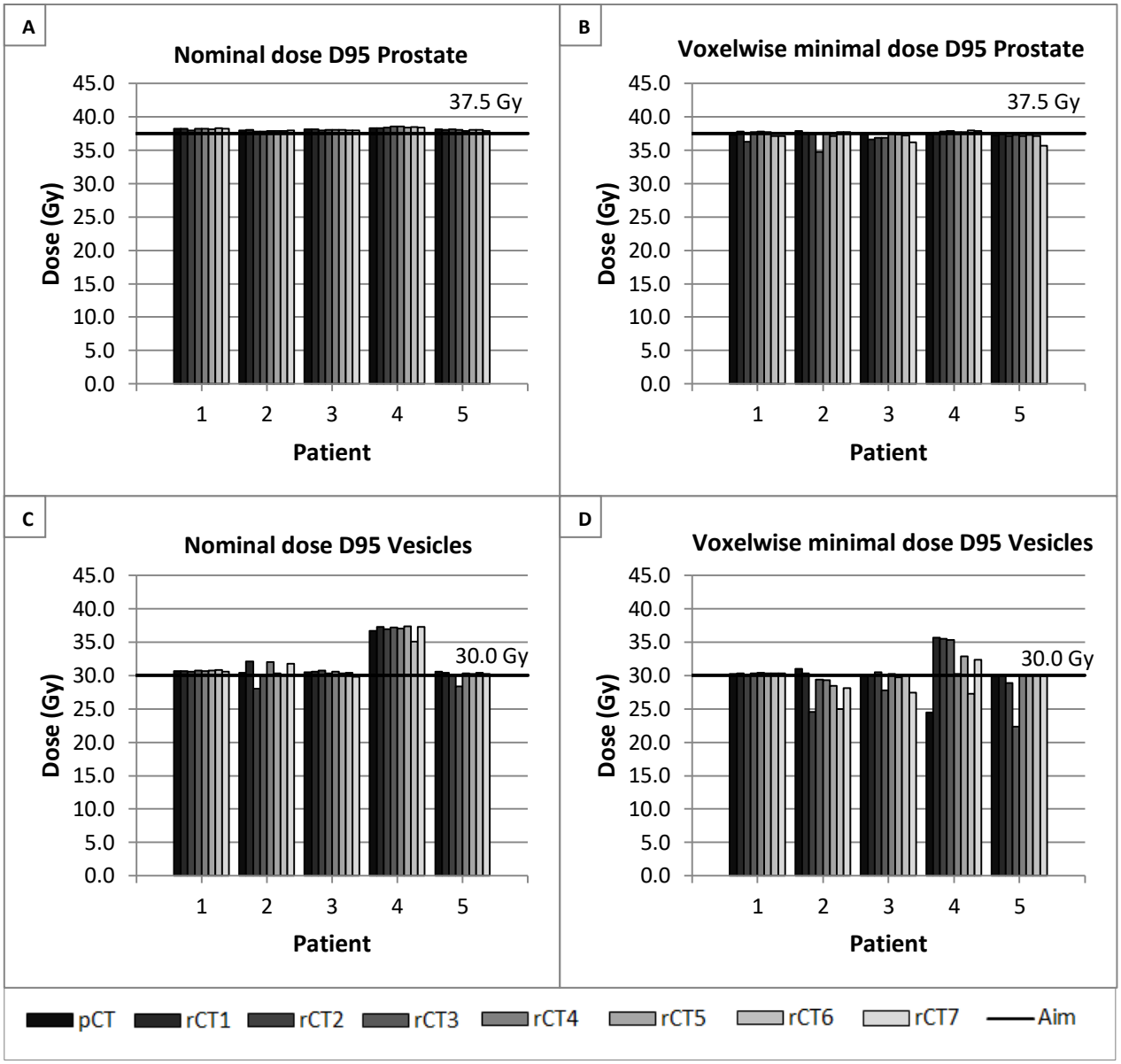

Figure 7: D95 of the nominal (A and C) and voxelwise minimal doses (B and D) of the prostate (A and B) and the proximal part of the seminal vesicles (C and D) for the pCT and rCTs of all patients. The black lines indicate the aims of the prostate (37.5 Gy) and proximal part of the seminal vesicles (30.0 Gy).

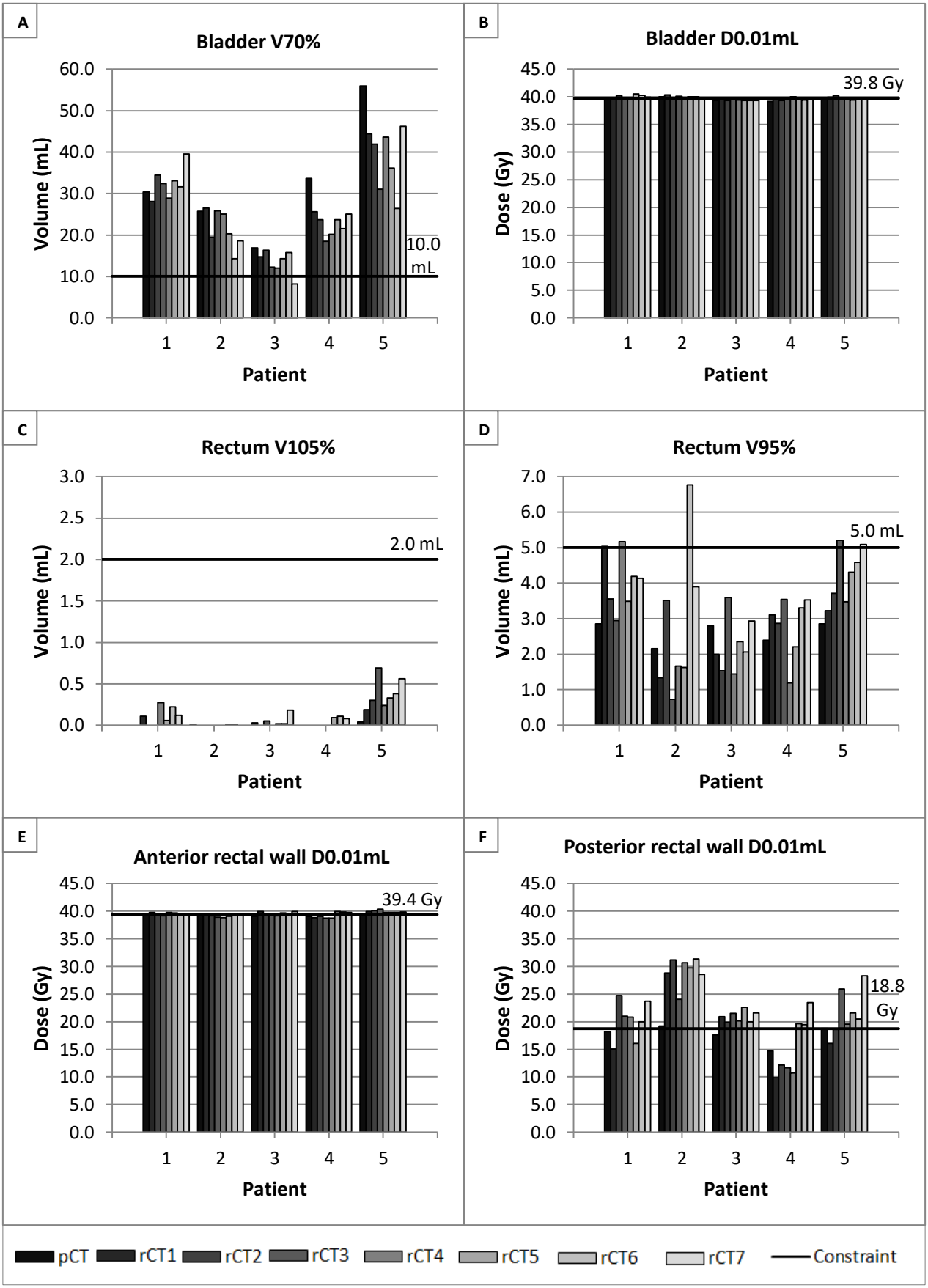

Figure 8: Clinical goals for the bladder (A and B), rectum (C and D), anterior rectal wall (E) and posterior rectal wall (F). The constraints of the clinical goals are indicated by the black line and values are written above the black line.

2.4.5 Dosimetric effects of interfraction prostate motion for complete treatment of 5 fractions

Figure 9 visualizes the D95 of the nominal and voxelwise minimal dose of the prostate and proximal part of the seminal vesicles for the planned and accumulated deformed doses of the first five weekly rCTs on the pCT. The V100 of the nominal and voxelwise minimal doses of the prostate and proximal part of the seminal vesicles are added in Appendix C. For the nominal dose, D95 of the prostate and proximal part of the seminal vesicles was above the aim for 100% of accumulated deformed doses. However, for the voxelwise minimal dose, D95 of the prostate was below the aim for 60% of accumulated deformed doses (mean decrease below the aim was 0.2±0.2 Gy, range 0.0-0.4 Gy) and D95 of the proximal part of the seminal vesicles was below the aim for 40% of accumulated deformed doses (mean decrease below the aim was 0.7±0.5 Gy, range: 0.3-1.1 Gy).

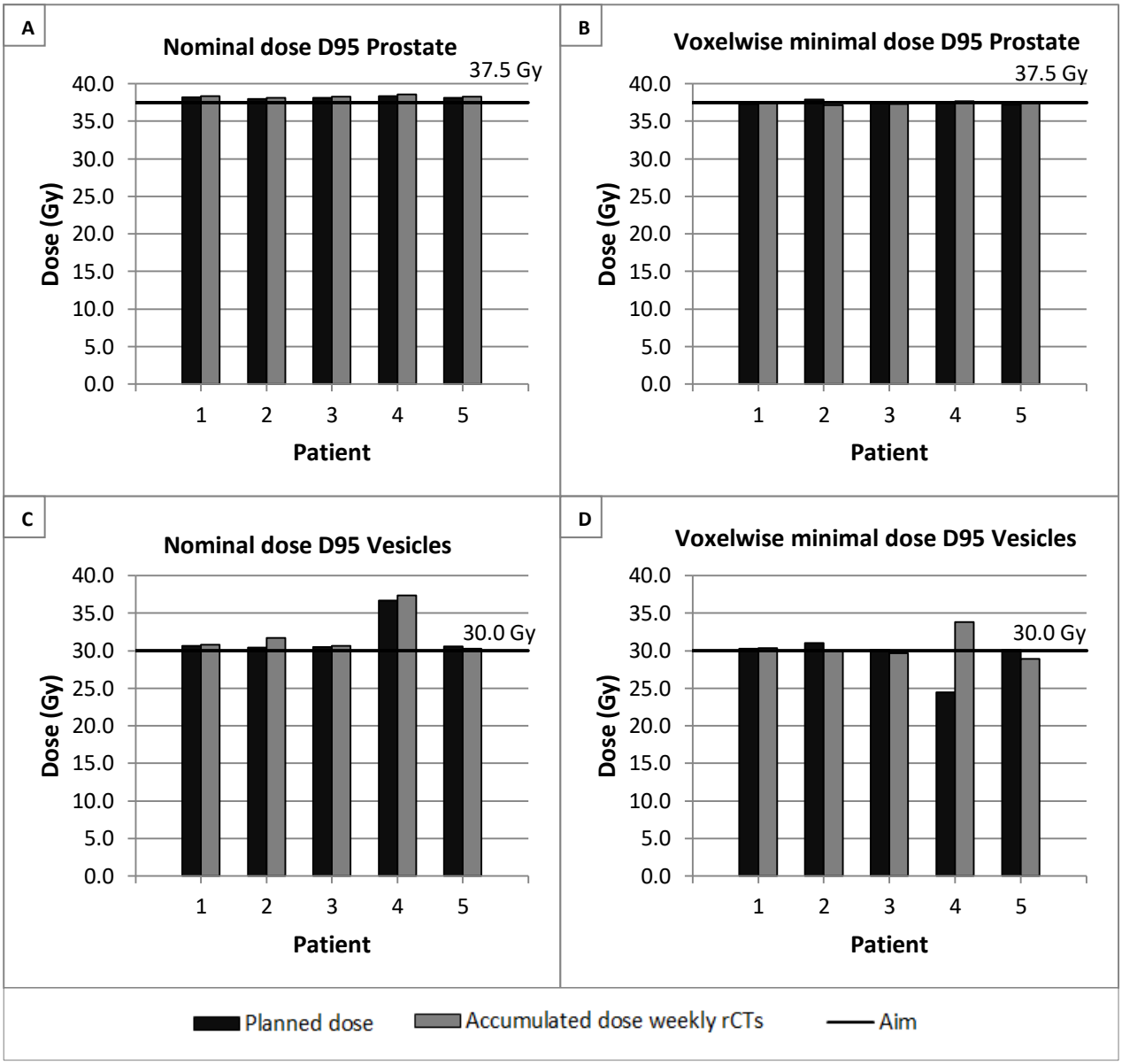

Figure 9: D95 of the nominal (A and C) and voxelwise minimal doses (B and D) of the prostate (A and B) and proximal part of the seminal vesicles (C and D) for the planned dose and the accumulated deformed dose of the first five weekly rCTs on the pCT. The black lines indicate the aims of the prostate (37.5 Gy) and proximal part of the seminal vesicles (30.0 Gy).

In Figure 10, the clinical goals for the bladder, rectum, anterior and posterior rectal wall are visualized. Dose-volume histograms of the bladder and rectum are added in Appendix C. For the volume constraint V70%<10.0mL of the bladder, visualized in A, 100% of accumulated deformed doses was above the constraint (mean increase above the constraint was 27.2±22.1 Gy, range: 5.3-63.3 Gy). For the dose constraint D0.01mL<39.8Gy of the bladder, volume constraints V105%<2.0mL and V95%<5.0mL of the rectum, visualized in B-D, 100% of accumulated deformed doses were below the constraint. For the anterior rectal wall dose constraint D0.01mL<39.4Gy, visualized in E, 20% of deformed accumulated doses was above the constraint (increase above the constraint was 0.2 Gy). For the posterior rectal wall dose constraint D0.01mL<18.8 Gy, visualized in F, 20% of accumulated deformed doses was above the constraint (increase above the constraint was 7.6 Gy).

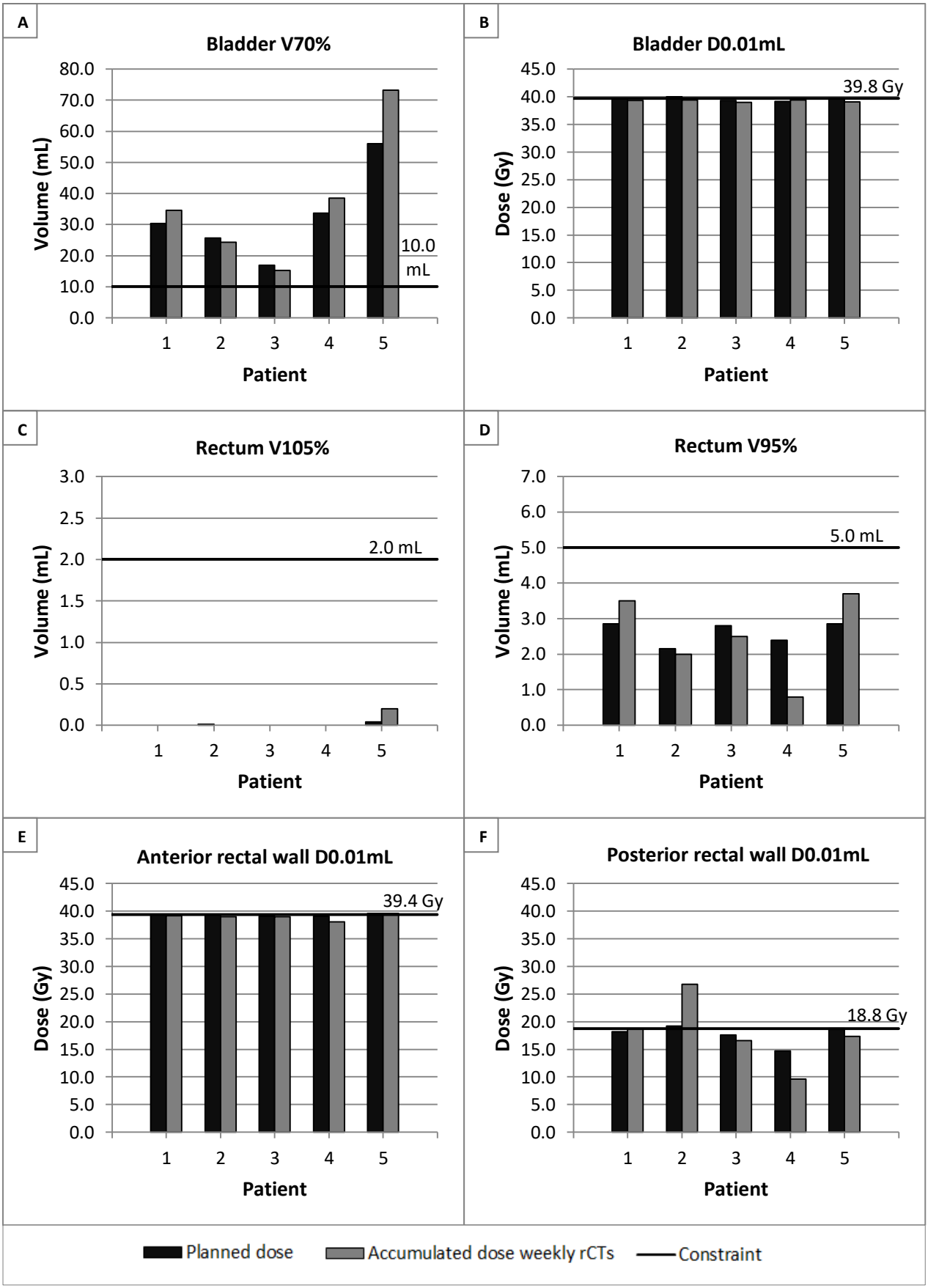

Figure 10: Clinical goals for the bladder (A and B), rectum (C and D), anterior rectal wall (E) and the posterior rectal wall (F). The constraints of the clinical goals are indicated by the black lines and values are written above the black line.

2.5 Discussion

In this study, we have evaluated the impact of interfraction prostate motion effects without ERB on target coverage and doses to the OARs in extremely hypofractionated PBS proton therapy. The interfraction prostate motion did not negatively influence nominal target coverage of the prostate and proximal part of the seminal vesicles (accumulated deformed doses). These results are in line with the literature on the dosimetric impact of interfraction prostate motion for conventionally fractionated 3D conformal proton therapy [69]. A recently published study that evaluated the influence of interfraction prostate motion for extremely hypofractionated PBS proton therapy confirmed our conclusion on target coverage as well [73]. Moteabbed et al. (2018) investigated the robustness for PBS proton plans consisting of five fractions to interfraction prostate motion. They showed that the median delivered D98 to the prostate was only 0.13 Gy lower than the planned dose and remained within the clinical protocol tolerance. [73] In contrast to the study of Moteabbed et al., our proton plans were robustly optimized and we simulated interfraction prostate motion without ERB (five patients), whereas Moteabbed et al. simulated interfraction prostate motion with ERB (six patients).

Our results showed that OAR doses also remained within protocol constraints (except for the bladder constraint V70%<10.0mL). The posterior rectal wall dose constraint D0.01mL<18.8Gy was not met in 1/5 patients (accumulated deformed doses). The study on conventional fractionation confirmed our results (max bladder dose) [69]. Our results regarding the maintenance of maximum bladder and anterior rectal wall doses within protocol constraints, were in line with the study of Moteabbed et al. [73]. However, an important difference in constraints is that we used D0.01mL, whereas they used D2%.

While fractional doses did not meet all protocol constraints, accumulated deformed dose did, which is consistent with the previous study on the dosimetric impact of interfraction motion on conventionally fractionated 3D conformal proton therapy [69]. Since protocol constraints are intended for the total dose rather than the fractional dose, only the total dose is of clinical relevance. The results showed that it was hard to meet the defined bladder volume constraint V70%<10.0mL for both planned and accumulated deformed doses. This constraint was introduced to keep bladder dose low in this experimental setting (in daily clinic we are using V70%<50%). We think that this constraint should be relaxed to V70%<30%.

We found a limited association between bladder and rectum dose and organ volume, whereas no specific dietary guidelines or instructions to ensure an empty rectum were used. Compared to the pCT, bladder volume varied between -55.0% and 212.5% for the rCTs, whereas maximum bladder dose varied between -0.8% and 2.0%. In addition, rectum volume varied between -32.8% and 115.3% for the rCTs compared to the pCT, whereas anterior rectal wall dose varied between -1.5% and 2.3% for the rCTs compared to the pCT. In conventionally fractionated 3D conformal proton therapy, decreased bladder volumes resulted in increased fractional bladder dose in two patients. Moreover, increased rectum volume resulted in increased fractional dose to the anterior rectal wall. However, they did not quantify the relationship between bladder- and rectum volumes and bladder- and rectum doses. [69]

Several limitations of the study should be recognized. First, uncertainties in DIR, used for dose deformation and accumulation, could influence the results. However, we tried to limit this effect by

delineating the CTVs and OARs in all rCTs. Furthermore, we used controlling ROIs for DIR. Second, weekly rCTs of patients who were conventionally treated were included in this study, which is different than the extremely hypofractionated scheme of one fraction every other day. However, it was not possible yet to include rCTs of these patients, since the extremely hypofractionated scheme is not used in our clinical practice yet. At last, because of the limited number of patients included in this study, a meaningful statistical analysis was not allowed and evaluations were performed patient-specifically.

In future research, the following recommendations have to be taken into account. First, more representative patients that meet the inclusion criteria of hypofractionated proton therapy (prostate volume <90cc and without benign prostatic hyperplasia) have to be included [77]. Second, in this study a robust optimization using a 5mm setup was sufficient to account for interfraction prostate motion. Therefore, in future research it is worthy to investigate the influence of a 3mm setup margin on target coverage and OAR doses.

2.6 Conclusion

PBS proton treatment plans were robust to interfraction motion without the use of an ERB, without violating OAR dose constraints.

Chapter 3

Virtual CTs to evaluate inter- and intrafraction prostate motion and the interplay effect

3.1 Abstract

Introduction: Pencil beam scanning (PBS) proton therapy using an extremely hypofractionated scheme is an attractive treatment option for prostate cancer. However, a major challenge is the increased sensitivity to intrafraction prostate motion and the interplay effect. The aim of this study was to evaluate the combined effect of worst-case inter- and intrafraction prostate motion with and without endorectal balloon (ERB) and the interplay effect.

Materials and methods: For interfraction prostate motion evaluation, five repeated CTs (rCTs) of two prostate cancer patients conventionally treated at our institution were available. Two clinical target volumes (CTVs) were delineated, including the prostate and the proximal part of the seminal vesicles. The patients were virtually planned for PBS proton therapy using RayStation 7.99 Research (RaySearch Laboratories Inc., Stockholm, Sweden). Intrafraction prostate motion measurements were available from 54 patients treated in ≥10 fractions in the department of radiation oncology of the University of Pennsylvania. 52% of these patients were treated with ERB, whereas 48% were treated without ERB. Motion was recorded in three degrees of freedom using a real-time electromagnetic tracking system. To select worst-case intrafraction motion, the area under the curve (AUC) of the 3D motion was calculated for time intervals of fifteen seconds. Ten worst-case intrafraction motions of the worst-case patients treated with ERB and without ERB were selected and applied on the rCTs of the UMCG patients, to create virtual CTs (vCTs) using deformable image registration (DIR). To simulate the interplay effect, proton treatment plans were split into subplans of one second. These subplans were calculated on the corresponding vCTs. Doses were deformed and summed from the vCTs to the corresponding rCTs and in the end to the corresponding planning CT (pCT) using DIR (4D accumulated dose). Moreover, doses on the rCTs without motion were deformed and summed to the pCT using DIR (accumulated deformed dose). Target coverage of the prostate and proximal part of the seminal vesicles and bladder and rectum constraints were evaluated for both accumulated deformed and 4D accumulated doses.

Results: Interfraction prostate motion (accumulated deformed dose) and combined worst-case prostate motion with ERB (4D accumulated dose) resulted in maintenance of target coverage of the prostate and proximal part of the seminal vesicles. However, for the combined worst-case prostate motion without ERB, target coverage (4D accumulated dose) of the prostate and proximal part of the seminal vesicles was degraded on average 8.3±0.1 and 7.0±8.4Gy below the protocol limits, respectively. For interfraction prostate motion (accumulated deformed dose) and the combined worst-case prostate motion with ERB (4D accumulated dose), bladder and rectum doses were within the protocol limits for 2/4 and 6/8 constraints, respectively. However, for the combined worst-case prostate motion without ERB (4D accumulated dose), bladder and rectum doses were within the protocol limits for 4/4 and 3/8 constraints.

Conclusion: Extremely hypofractionated proton plans were robust to interfraction prostate motion and combined worst-case prostate motion with ERB, without violating rectum and bladder dose constraints. For combined worst-case prostate motion without ERB, large concessions had to be made for target coverage and rectal doses. In future research, a more probabilistic description of intrafraction prostate motion is necessary to estimate the actually given dose for the combined motion with and without ERB more realistically.

3.2 Introduction

The use of an extremely hypofractionated scheme for prostate cancer is attractive because of the unique radiobiology and low α/β ratio of prostate cancer [8–10]. When delivering higher doses per fraction in a smaller amount of fractions, the sparing of healthy tissues is of greater importance. Protons have beneficial dose distribution properties and therefore a larger potential of sparing healthy tissues compared to photons [6,11–13]. In proton pencil beam scanning (PBS) technology, a pencil beam is scanned using magnetic fields, enabling highly conformal dose delivery to the target [6,11,13]. However, a major challenge in extremely hypofractionated PBS proton therapy is the increased sensitivity to inter- and intrafraction prostate motion and the interplay effect [17]. The intrafraction prostate motion causes interference between the dynamic delivery of the PBS proton beam delivery and intrafraction prostate motion (interplay), possibly resulting in a heterogeneous dose coverage inside the target.

Tang et al. (2013) investigated the dosimetric impact caused by the interplay effect between intrafraction prostate motion and the intermittent delivery of a conventionally fractionated PBS proton therapy plan. They synchronized intrafraction prostate motion with endorectal balloon (ERB), obtained using the Calypso real-time tracking system, and the PBS beam delivery sequence. The results showed that clinical target volume (CTV) coverage was degraded <2% when averaged over the complete treatment, but CTV coverage degraded >10% for the worst-case fraction [64]. A limitation of this study was the assumption that the intrafraction prostate motion did not affect the range of the beam, because of the assumption of small differences between Hounsfield units of the prostate and the surrounding tissues. In addition, organs at risk (OARs) doses were not evaluated and only intrafraction prostate motion with ERB was included. However, the necessity of an ERB needs further investigation, because of opposing conclusions from studies about the dosimetric impact of an ERB, the possible deformation of the prostate when an ERB is positioned wrongly and the decrease of patient comfort when an ERB is inserted before every treatment delivery [24–26].

In addition, several studies have reported on the dosimetric changes associated with intrafraction prostate motion in extremely hypofractionated photon therapy [78,79]. Zhang et al. (2011) simulated the real-time monitored intrafraction motion without ERB in volumetric-modulated arc therapy (VMAT) plans with prescription doses of 32.5 and 42.5 Gy in five fractions. The beam isocenter at each beam was displaced to simulate intrafraction prostate motion in the plan, assuming rigid organ motion. They concluded that the CTV coverage was only marginally affected. The limitations of this study are the assumption of rigid motion and displacement of the beam isocenter only [78]. Koike et al. (2018) measured intrafraction prostate motion with an orthogonal kV image frequency of approximately 70s for 16 patients. These patients underwent CyberKnife treatment with a prescription dose of 35 Gy delivered in 5 fractions. They simulated the measured intrafraction prostate motion by shifting the DICOM structures according to the corresponding beam offset. The dosimetric impact of intrafraction motion was assessed by comparing the dose-volume indices of the simulated plan with the original plan. They found that the relative differences were mostly less than 1% and absolute dose differences were <0.1 Gy compared with the planned dose. The limitation of the study of Koike et al. (2018) is that the intrafraction motion was not monitored in real-time [79].

Despite the studies of Tang et al. (2013), Zhang et al. (2011) and Koike et al. (2018), a methodology to study the dosimetric effect of the combined inter- and intrafraction prostate motion and the interplay effect has not been presented yet. Therefore, the aim of this study was to evaluate the combined effect of worst-case inter- and intrafraction prostate motion with and without ERB and the interplay effect.

3.3 Design of methodology

To develop a new methodology to evaluate the dosimetric impact of inter- and intrafraction prostate motion and the interplay effect, a specification of requirements was made. The requirements were assigned to different purposes:

- Simulation of the combined motion effect for the complete treatment of five fractions.
- Selection of interfraction prostate motion.
- Selection of worst-case intrafraction prostate motion with and without ERB.
- Simulation of the interplay effect.
- Application of intrafraction prostate motion to create virtual CTs.

In the following subparagraphs 3.3.1 – 3.3.5 the considerations regarding the different purposes are outlined.

3.3.1 Simulation of the combined motion effect for the complete treatment of five fractions

To simulate the combined worst-case motion effect for the complete treatment of five fractions, different steps were undertaken. First, the image guidance and treatment workflow to irradiate prostate cancer patients using protons in an extremely hypofractionated scheme was developed. Discussions with experts in the clinic, including a radiation oncologist, medical physicist and radiation therapists (RTTs) specialized in patient position verification were conducted. As a result, a concept workflow was suggested, visualized in Figure 11.

Next, a phantom with fiducial markers was used to measure the time interval between daily image acquisition for position verification and proton beam delivery. The measured time interval between daily image acquisition for patient positioning and proton beam delivery was approximately four minutes. In this time interval, a possible delay between patient positioning and proton beam delivery, including one minute to wait for the beam, was taken into account. The proton treatment plan consisted of two lateral opposed beams. From the literature followed that intrafraction prostate motion increased with elapsed time [22,58,59]. Therefore, position verification (2DkV to check marker position) before the delivery of every beam is recommended. The actual beam-delivery time per beam was approximately fifteen seconds for ~15 energy layers.

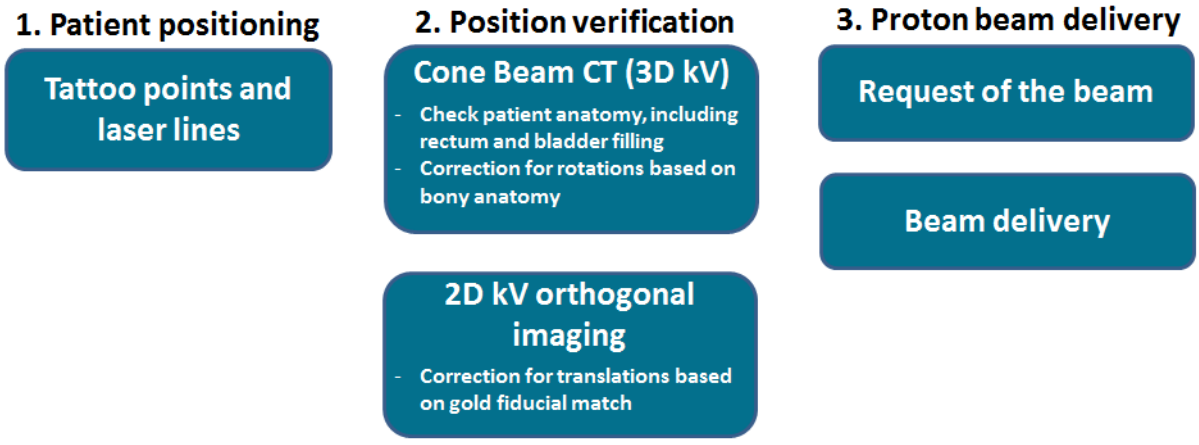

Figure 11: Concept workflow of irradiation of prostate cancer patients using protons in an extremely hypofractionated scheme. Abbreviations: kilovoltage (kV).

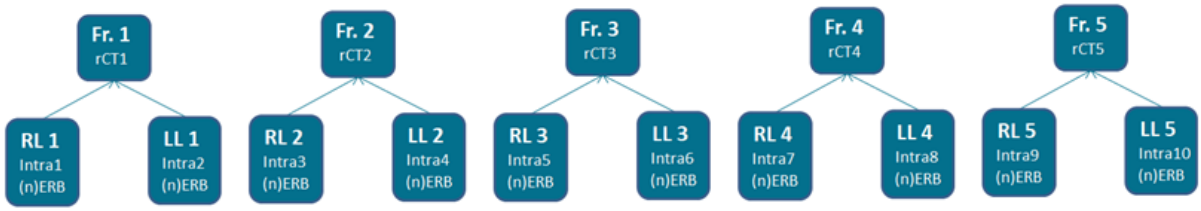

Figure 12: Methodology to simulate the combined worst-case prostate motion effect (inter- and intrafraction motion and the interplay effect) for the whole treatment of five fractions. Abbreviations: fraction (fr.), right lateral beam (RL), left lateral beam (LL), intrafraction prostate motion (intra), with endorectal balloon (ERB), without endorectal balloon (nERB).

Different designs have been considered, regarding the simulation of inter- and intrafraction prostate motion. Because a treatment fraction consists of two lateral opposing beams, it was decided to simulate ten different intrafraction prostate motions, so for every beam one different intrafraction prostate motion. Moreover, it was decided to simulate five different interfraction prostate motions, so for every treatment fraction one interfraction prostate motion. The chosen methodology is visualized in Figure 12.

3.3.2 Selection of interfraction prostate motion

For interfraction prostate motion, seven weekly rCTs were available of five UMCG patients. For the selection of interfraction prostate motion, the following requirements have to be met:

1. Selection of two representative UMCG patients.
2. Selection of five rCTs of each UMCG patient.

To meet requirement 1, exclusion criteria related to patient anatomy were formulated, including patients with median lobe hyperplasia of the prostate and/or protrusion of the prostate into the bladder. Patients 1, 4 and 5 had median lobe hyperplasia or protrusion of the prostate into the bladder, so therefore these patients were excluded. As a result, UMCG patients 2 and 3 were included. For requirement 2, different options were considered. The first option that was considered was to select the five worst-case fractions, based on motion of the prostate relative to the pelvic bones. The second option that was taken into consideration was to select the first five rCTs chronologically. Since we wanted to evaluate the combined effect of worst-case motion, the first option seems beneficial. However, from a study of Moteabbed et al. (2018) followed that the worst-case scenario was only slightly inferior to the random scenario [73]. Moreover, since the extremely hypofractionated scheme is given in a shorter time (two weeks instead of seven weeks), it was decided to choose the second and select the first five consecutive rCTs of the two selected UMCG patients.

3.3.3 Selection of worst-case intrafraction prostate motion with and without endorectal balloon

The intrafraction prostate motion was available from 54 prostate cancer patients treated in ≥10 fractions for whom the prostate motion was measured using the Calypso real-time tracking system. 28 patients were treated with ERB and 26 patients were treated without ERB. For each patient, the 3D motion was selected. Before the design of a methodology regarding the selection of worst-case intrafraction prostate motion with and without ERB, a specification of requirements was made:

1. The intrafraction prostate motion has to be measured within the measured time interval between daily image acquisition for patient positioning and proton beam delivery.

2. The intrafraction prostate motion has to be selected for time intervals equal to the actual beam-delivery time.
3. The selection of ten worst-case intrafraction prostate motions with and without ERB has to be unbiased.

The measured time interval between daily image acquisition for patient positioning and proton beam delivery was four minutes (as found from the fiducial marker dry run). Therefore, to meet requirement 1, a time interval up to four minutes of Calypso data of all fractions of the patients were selected. The actual beam-delivery time was fifteen seconds. Therefore, for requirement 2, the selected time interval, was divided into consecutive time intervals of fifteen seconds, every time interval starts ~0.1s after the previous one, equivalent to the measurement frequency of the Calypso system.

To meet requirement 3, first, the 54 prostate cancer patients were subdivided into patients treated with ERB and patients treated without ERB. Second, different methods were considered. The first method that was considered was the selection of worst-case intrafraction prostate motion by selecting peaks of the 3D motion of the different time intervals of fifteen seconds for the different fractions and patients. The other considered method was the selection of worst-case intrafraction prostate motion by calculating the area under the curve (AUC) for the different time intervals of fifteen seconds and selecting the time interval of fifteen seconds with the largest AUC for every fraction and every patient. In the end, the AUC methodology was chosen because it was expected that the influence of a broader peak, so a larger AUC and motion trend, will have a larger influence on the OAR doses, instead of small and higher peaks. The third requirement was to select ten worst-case intrafraction prostate motions with and without ERB in an unbiased way. Therefore, different options were considered. The first considered option was to select ten worst-case intrafraction prostate motion of different fractions of different patients with and without ERB. However, this option was not chosen, because of the introduction of bias when selecting time intervals of fractions of different patients. The second option that was taken into consideration and was chosen was the selection of ten fractions of the worst-case patient with ERB and ten fractions of the worst-case patient without ERB.

3.3.4 Simulation of the interplay effect

Before the development of a methodology to simulate the interplay effect, a list of requirements was made:

1. Proton treatment plans have to be divided into subplans using a time interval that represents the Calypso signal well.
2. The selected worst-case intrafraction prostate motion has to be divided into the x-,y-,z-coordinates for motion at the defined time interval of requirement 1.

Each proton treatment plan consists of a right lateral beam and a left lateral beam. The time to deliver one spot was ~15ms and the layer switching time was ~1.0s. The total delivery time of one beam that consists of ~15 layers was approximately fifteen seconds. The Calypso signal was represented well when a time interval of one second was used. To fulfill requirement 2, we have to divide the selected worst-case intrafraction prostate motion into x-, y- and z-coordinates at 0-15 seconds. So we will simulate the intrafraction prostate motion at every second during a time interval

of 0-15 seconds, which means a simulation of 16 intrafraction prostate motions on one rCT for every beam.

3.3.5 Application of intrafraction prostate motion to repeated CTs to create virtual CTs

To apply the intrafraction prostate motion to the rCTs, we have to create virtual CTs (vCTs). Before the development of a methodology to create the vCTs, we made a list of requirements:

1. Translation of the CTVs including the prostate and proximal part of the seminal vesicles according to the calculated intrafraction prostate motion.
2. Pelvic bones including symphysis and femoral heads have to be fixed.
3. Surrounding structures such as bladder and rectum have to be mapped deformably according to the calculated 3D prostate intrafraction prostate motion.
4. Creation of one vCT for every second, to simulate 16 intrafraction prostate motions and interplay on one rCT for every beam.

In an attempt to meet requirements 1-3, first RayStation 7.99 Research (RaySearch Laboratories Inc., Stockholm, Sweden) was used and a manual methodology was developed. In the end, it turned out that the methodology developed in RayStation meets all requirements. An user manual for the creation of vCTs in RayStation 7.99 Research is added in Appendix D.

To meet requirement 4, 16 intrafraction prostate motions have to be simulated on one rCT for every beam. In total, ten intrafraction prostate motions and five rCTs were selected, to simulate the combined motion effect for the complete treatment of five fractions. Therefore, 16*10 = 160 vCTs have to be created for one UMCG patient for the simulation of intrafraction prostate motion with ERB. We aimed to evaluate the combined motion effect for both intrafraction prostate motion with and without ERB and for two UMCG patients, so in total 160*2*2=640 vCTs have to be created.

3.4 Materials and methods

In this paragraph, the eventually developed methodology is described.

3.4.1 Selected repeated CTs for interfraction prostate motion

pCTs and rCTs were available from two prostate cancer patients who were conventionally treated at our department in 35 fractions of 2.2 Gy. Three gold fiducials were implanted in the prostate before treatment and a pCT acquisition was performed in the treatment position using a CT scanner with an axial resolution of 0.977x0.977 mm and a slice thickness of 2 mm (Siemens SOMATOM Definition AS, Siemens Healthineers, Erlangen, Germany). In addition, both patients underwent seven weekly rCTs in the treatment position without ERB using a CT scanner with an axial resolution of 0.998x0.998 mm and a slice thickness of 2.5 mm (GE MEDICAL SYSTEMS Optima CT580, GE Healthcare, Chicago, Illinois). Two CTVs were manually delineated in the transverse slice direction on the pCT and rCTs, including the prostate and the proximal part of the seminal vesicles. This was done by an experienced radiation oncologist, using RayStation 7.99 Research (RaySearch Laboratories, Stockholm, Sweden). Moreover, gold fiducials and different OARs were delineated on the rCTs by an RTT student and a technical medicine student, under the supervision of the radiation oncologist.

3.4.2 Pencil beam scanning proton treatment planning

Patients were virtually planned for PBS proton therapy using RayStation 7.99 Research (RaySearch Laboratories, Stockholm, Sweden). The virtual plans consisted of a regimen of 5 fractions of 7.5 Gy (RBE), applying robust optimization using 5mm setup and 3% range uncertainty to fulfill V100%>95% for the prostate and V80%>95% for the proximal part of the seminal vesicles. The dose-volume constraints that were taken into account are added in Appendix A. The proton plans consisted of two opposing lateral beams from 90 and 270 degrees. The defined dose grid size was 2x2x2 mm^3. During plan optimization, target coverage and dose-volume constraints of the rectum, anorectum and anal canal were prioritized. The developed objective lists for all patients are added in Appendix B. All proton plans were clinically accepted by an experienced radiation oncologist and medical physicist.

3.4.3 Intrafraction prostate motion measurements

Intrafraction prostate motion measurements were available from 54 patients treated in ≥10 fractions in the department of radiation oncology of the University of Pennsylvania. 28 of 54 patients (52%) were treated with ERB and 26 patients were treated without ERB. The motion was recorded in real-time at a frequency of 10 Hz in three degrees of freedom using the Calypso 4-dimensional tracking system (Calypso Medical Technologies, Seattle, WA). The x-axes specified prostate motion in the lateral direction, the y-axes in the superior-inferior direction and the z-axes in the anterior-posterior direction (see Figure 13).

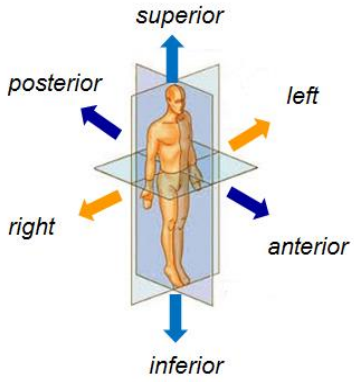

Figure 13: Prostate motion in three degrees of freedom

3.4.4 Selection of worst-case intrafraction prostate motion with and without endorectal balloon

The intrafraction prostate motion data of the 54 patients were imported into MATLAB R2018A (The Mathworks, Inc., United States) for analysis. The 3D motion was plotted against tracking time in seconds for time intervals of 0-4 minutes for every fraction of every patient. Next, the 0-4 minutes time interval was split into different time intervals of 15 seconds and the AUC of these small time intervals was determined. For every fraction of every patient, the time interval of 15 seconds with the largest AUC was selected. Subsequently, the ten fractions for every patient with the largest AUCs were selected. The mean AUCs of this selection were calculated and based on this, the patient treated with ERB and the patient treated without ERB with the worst-case intrafraction prostate motion were selected. The x-, y- and z-coordinates of the selected AUCs were determined. The MATLAB script for selecting the time intervals of 15 seconds of the ten fractions of the worst-case patients is added in Appendix E. In addition, the selected time intervals of 15 seconds are added in

Appendix F for the selected worst-case intrafraction motion of the patient treated with ERB and in Appendix G of the patient treated without ERB.

3.4.5 Creation of virtual CTs

The selected time intervals of 15 seconds of the worst-case intrafraction prostate motion were split into intrafraction prostate motions for every second. The regions of interest (ROIs) of the prostate and proximal part of the seminal vesicles were manually displaced in the copied rCTs using the calculated worst-case intrafraction prostate motion. The first two fractions were applied to the first rCT, the second two fractions to the second rCTs and so on. Next, a deformation vector field (DVF) was created between the reference rCT and the copied rCT with the displaced CTVs using RayStation 7.99 Research (RaySearch Laboratories Inc., Stockholm, Sweden). Controlling ROIs were the prostate, proximal part of the seminal vesicles and pelvic bones. In this way, vCTs were created. The user manual for creating vCTs in RayStation 7.99 Research is added in Appendix D. 160 vCTs were created for evaluation of intrafraction prostate motion with ERB for one UMCG patient, so in order to evaluate the impact of both intrafraction prostate motion with and without ERB for two UMCG patients, we have created 640 vCTs in total.

3.4.6 Simulation of the interplay effect

Each proton plan was irradiated and the PBS sequence was extracted from the treatment log files. To simulate a treatment delivery during intrafraction prostate motion, each proton plan was split into subplans with a delivery duration of one second.

3.4.7 (4D) dose calculation

Each subplan was recalculated on the corresponding vCT. Next, deformable image registration (DIR) was used to warp the calculated dose on the vCTs to the corresponding rCT, resulting in the 4D dose. To analyze the combined dosimetric effect of inter- and intrafraction prostate motion and the interplay effect, the 4D dose on the five rCTs was warped on the pCT using DIR between the rCTs and the pCT, resulting in the 4D accumulated dose. In Figure 14, a flowchart visualizes the method used for 4D dose calculation. Moreover, doses on the rCTs without motion were deformed and summed to the pCT using DIR (accumulated deformed dose). Target coverage of the prostate and proximal part of the seminal vesicles and bladder and rectum constraints were evaluated for both accumulated deformed and 4D accumulated doses.

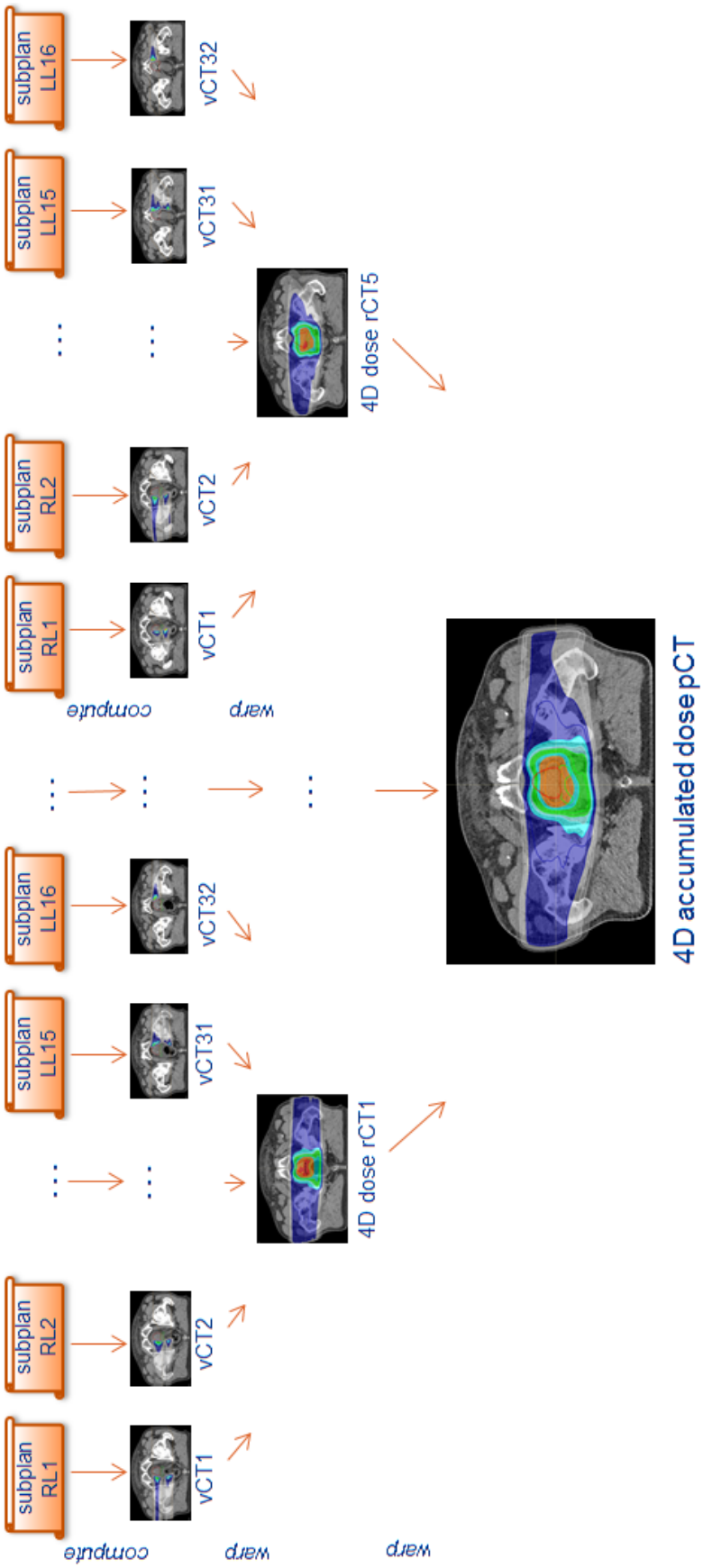

Figure 14: Flowchart of 4D dose calculation. Abbreviations: right lateral beam (RL), left lateral beam (LL), virtual CT (vCT), repeated CT (rCT), planning CT (pCT).

3.5 Results

3.5.1 Evaluation of intrafraction prostate motion with and without endorectal balloon and the interplay effect on the different repeated CTs

Figure 15 visualizes the D95 of the prostate and proximal part of the seminal vesicles for the pCTs and rCTs without motion, rCTs with ERB (wERB) motion and rCTs without ERB (nERB) motion of patients 2 and 3. The V100 of the prostate and proximal part of the seminal vesicles are added in Appendix H. The aim for D95 of the prostate and proximal part of the seminal vesicles were 7.5 and 6.0 Gy, respectively. D95 of the prostate was above the aim for 100% of pCTs and rCTs without motion. However, D95 of the prostate was below the aim for 20% of rCTs with wERB motion (mean decrease below the aim was 0.1±0.0 Gy, range: 0.1-0.1 Gy) and was below the aim for 100% of rCTs with nERB motion (mean decrease was 1.7±0.8 Gy, range: 1.0-3.2 Gy). D95 of the proximal part of the seminal vesicles was above the aim for 100% of pCTs without motion and was below the aim for 20% of rCTs without motion (mean decrease below the aim was 0.2±0.3 Gy, range: 0.0-0.4 Gy). D95 of the proximal part of the seminal vesicles was below the aim for 60% of rCTs with wERB motion (mean decrease below the aim was 0.4±0.2 Gy, range: 0.2-0.7 Gy) and was below the aim for 80% of rCTs with nERB motion (mean decrease below the aim was 2.3±1.2 Gy, range: 0.7-4.8 Gy).

In Figure 16 and 17, the clinical goals for the bladder, rectum, anterior rectal wall and posterior rectal wall are visualized. For the volume constraint V70%<10.0mL of the bladder, visualized in 16A, 100% of pCTs without motion was above the constraint (mean increase above the constraint was 11.3±6.2 Gy, range 6.9-15.7 Gy) and 100% of rCTs without motion was above the constraint (mean increase above the constraint was 8.7±5.6 Gy, range 2.1-16.5 Gy). In addition, 80% of rCTs with wERB motion was above the constraint (mean increase above the constraint was 8.1±4.8 Gy, range 3.3-18.2 Gy) and 10% of rCTs with nERB motion was above the constraint (increase above the constraint was 1.0 Gy). For the volume constraint V105%<2.0mL of the rectum, visualized in 16B, 100% of pCTs and rCTs without motion were below the constraint. Moreover, 100% of rCTs with wERB motion were below the constraint and 10% of rCTs with nERB motion was above the constraint (increase above the constraint was 0.1 Gy). For the volume constraint V95%<5.0mL of the rectum, visualized in 16C, 100% of pCTs and rCTs without motion were below the constraint. In addition, 100% of rCTs with wERB motion were below the constraint and 70% of rCTs with nERB motion was above the constraint (mean increase above the constraint was 2.2±1.5 Gy, range 0.1-4.3 Gy).

For the dose constraint D0.01mL<8.0Gy for the bladder, visualized in 17A, 50% of pCTs without motion was above the constraint (increase above the constraint was 0.0 Gy) and 50% of rCTs without motion was above the constraint (mean increase above the constraint was 0.1±0.1 Gy, range 0.0-0.2 Gy). In addition, 100% of rCTs with wERB and nERB motion were below the constraint. For the dose constraint D0.01mL<7.9Gy of the anterior rectal wall, visualized in 18B, 50% of pCTs without motion was above the constraint (increase above the constraint was 0.0 Gy) and 30% of rCTs without motion was above the constraint (mean increase above the constraint was 0.1±0.0 Gy, range 0.0-0.1 Gy). In addition, 10% of rCTs with wERB motion was above the constraint (increase above the constraint was 0.1 Gy) and 30% of rCTs with nERB motion was above the constraint (increase above the constraint was 0.3±0.3 Gy, range 0.0-0.5 Gy). For the dose constraint D0.01mL<3.8Gy of the posterior rectal wall, visualized in 17C, 50% of pCTs without motion was above the constraint (increase above the constraint was 0.1 Gy) and 100% of rCTs without motion was above the constraint (mean increase

above the constraint was 1.2±0.9 Gy, range 0.2-2.5 Gy). In addition, 70% of rCTs with wERB motion was above the constraint (mean increase above the constraint was 1.5±0.4 Gy, range 0.7-1.9 Gy) and 90% of rCTs with nERB motion was above the constraint (mean increase above the constraint was 2.9±0.5 Gy, range 2.1-3.4 Gy).

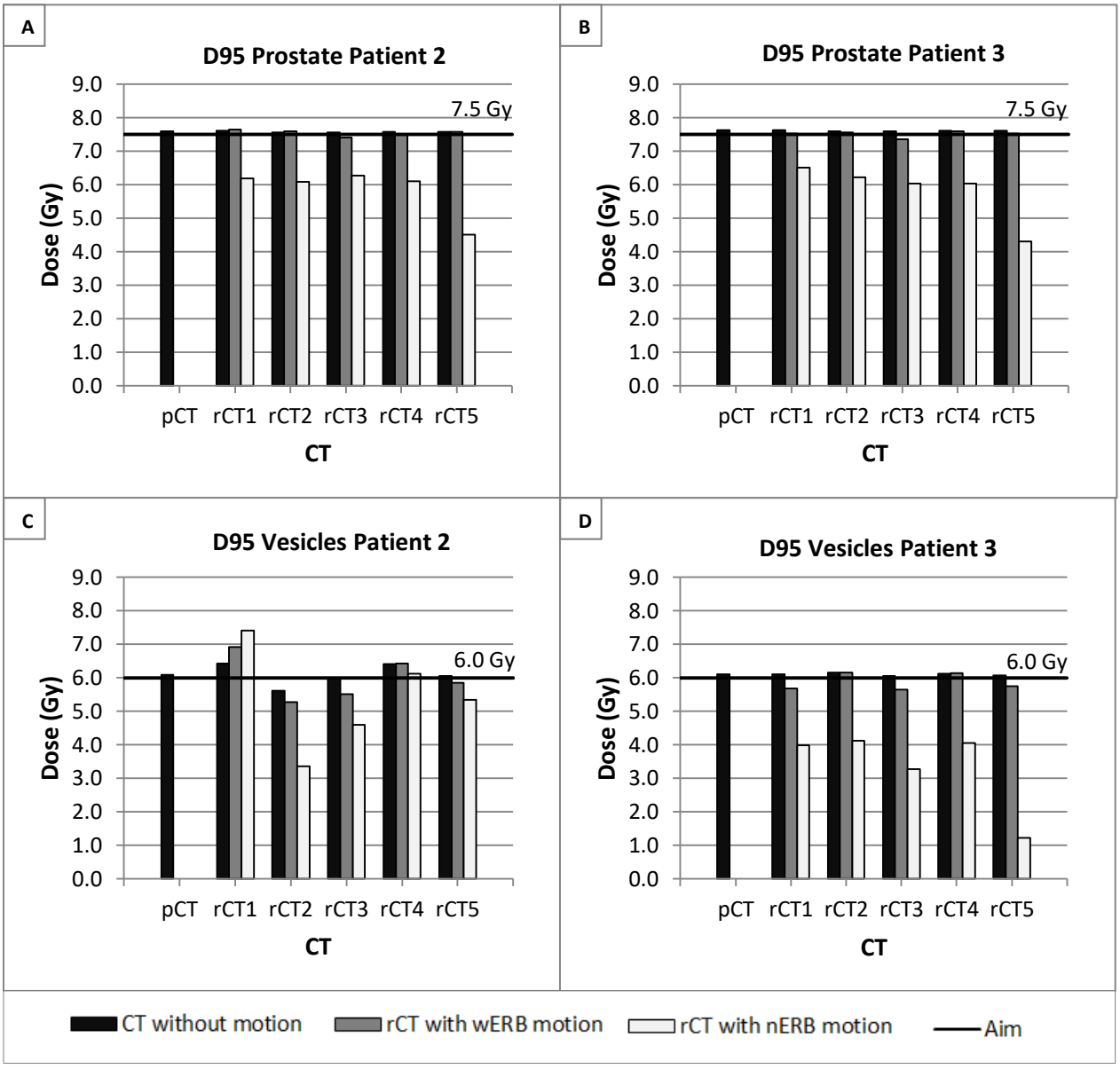

Figure 15: D95 of the 4D dose for the prostate (A and B) and proximal part of the seminal vesicles (C and D) for patient 2 (A and C) and patient 3 (B and D). The aim of D95 was 7.5 Gy for the prostate and 6.0 Gy for the proximal part of the seminal vesicles, respectively. Abbreviations: with endorectal balloon (wERB) and without endorectal balloon (nERB).

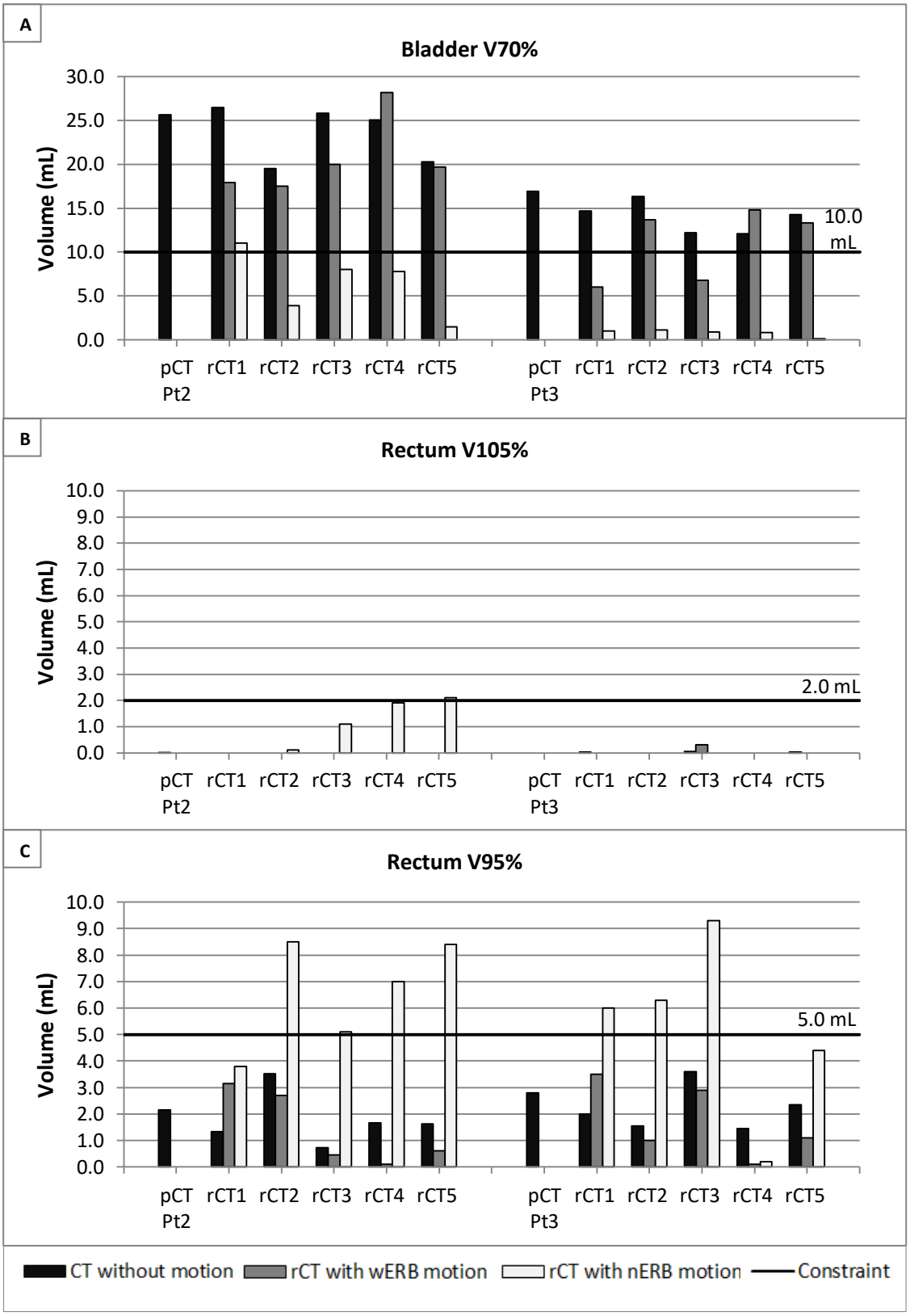

Figure 16: Clinical goals of the 4D fractional dose for the bladder (A) and rectum (B and C). The constraints of the clinical goals are indicated by the black lines and values are written above the black line. Abbreviations: patient (pt), with endorectal balloon (wERB) and without endorectal balloon (nERB).

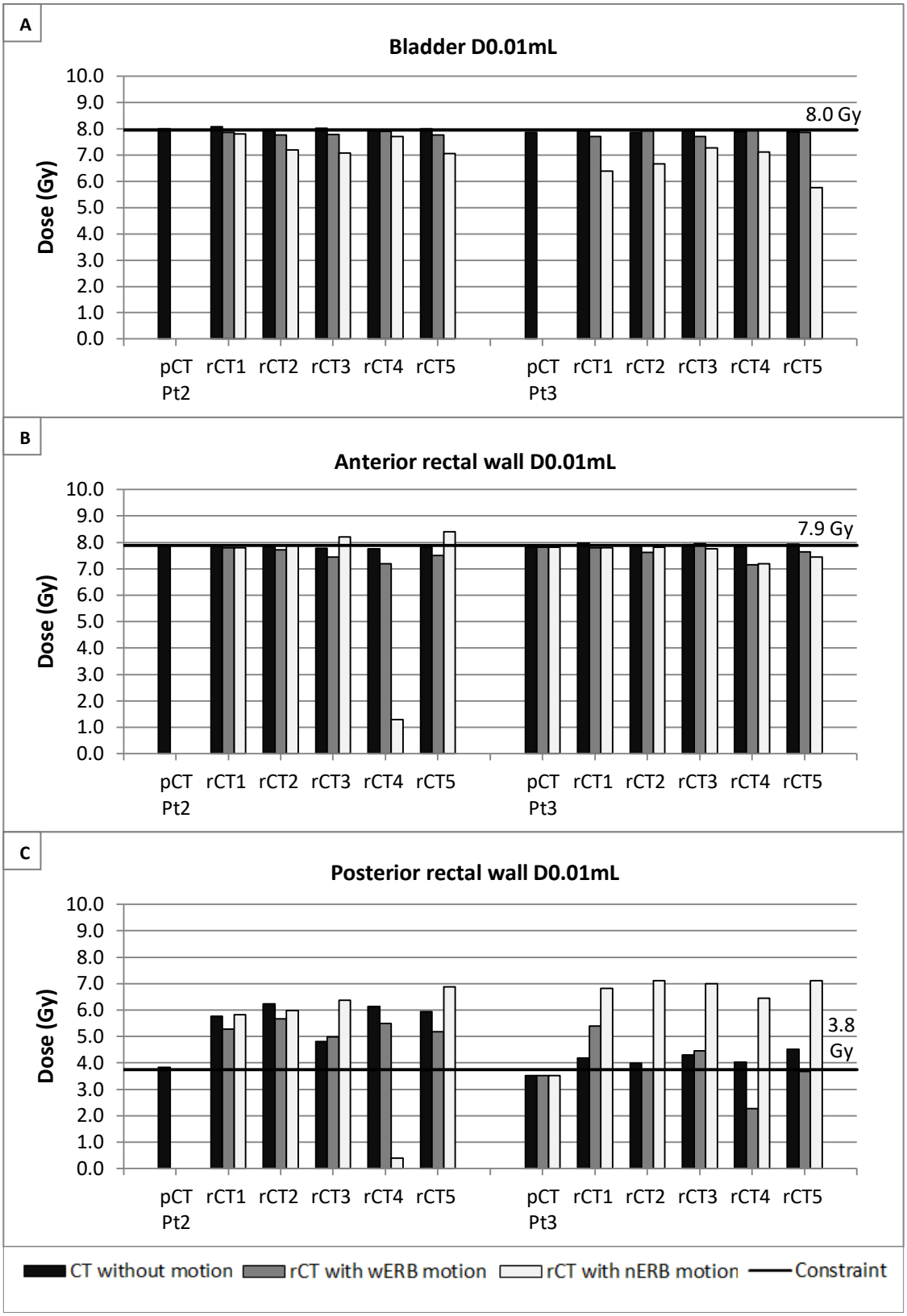

Figure 17: Clinical goals of the 4D fractional dose for the bladder (A), anterior rectal wall (B) and posterior rectal wall (C). The constraints of the clinical goals are indicated by the black lines and values are written above the black line. Abbreviations: patient (pt), with endorectal balloon (wERB) and without endorectal balloon (nERB).

3.5.2 Evaluation of the combined effect of inter- and intrafraction prostate motion and the interplay effect

Figure 18 visualizes the D95 of the prostate and proximal part of the seminal vesicles for the planned dose, accumulated dose of rCTs without motion and 4D accumulated doses of the rCTs with wERB and nERB motion. The V100 of the prostate and proximal part of the seminal vesicles are added in Appendix H. The aim for D95 of the prostate and proximal part of the seminal vesicles were 37.5 and 30.0 Gy, respectively. D95 of the prostate was above the aim for 100% of the planned doses, accumulated doses of rCTs without motion and 4D accumulated doses of rCTs with wERB motion. However, D95 of the prostate was below the aim for 100% of accumulated doses of rCTs with nERB motion (mean decrease below the aim was 8.3±0.1 Gy, range 8.2-8.3 Gy). D95 of the proximal part of the seminal vesicles was above the aim for 100% of the planned doses and accumulated doses of rCTs without motion. However, D95 of the proximal part of the seminal vesicles was below the aim for 50% of 4D accumulated doses of rCTs with wERB motion (decrease below the aim was 0.5 Gy) and was below the aim for 100% of 4D accumulated doses of rCTs with nERB motion (mean decrease below the aim was 7.0±8.4 Gy, range 1.0-13.0 Gy).

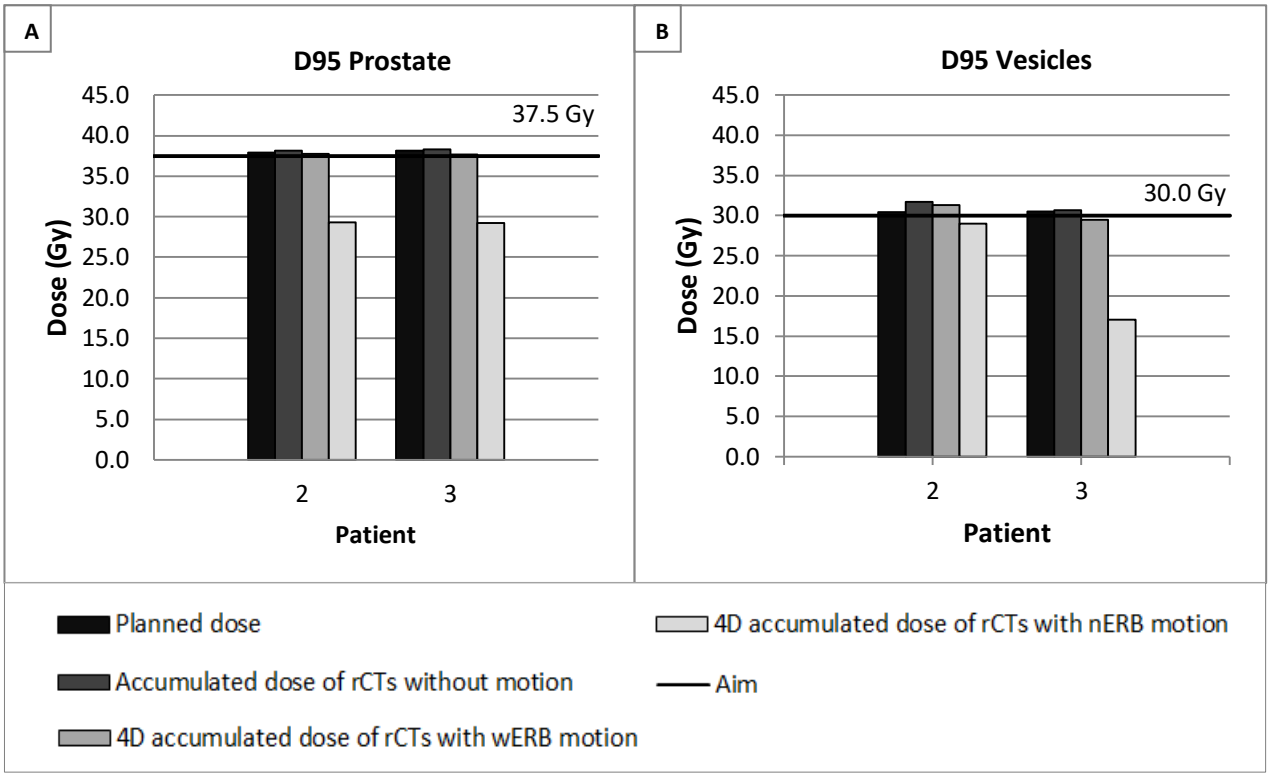

Figure 18: D95 of the prostate (A) and proximal part of the seminal vesicles (B) for the planned dose, accumulated dose of rCTs without motion and the 4D accumulated doses of rCTs with wERB and nERB motion. The black lines indicate the aims of the prostate (37.5 Gy) and proximal part of the seminal vesicles (30.0 Gy). Abbreviations: repeated CT (rCT), with endorectal balloon (wERB), without endorectal balloon (nERB).

In Figure 19, the clinical goals for the bladder, rectum, anterior and posterior rectal wall are visualized for the planned dose, accumulated dose of rCTs without motion and 4D accumulated doses of rCTs with wERB and nERB motion. The dose-volume histograms of the bladder and rectum are added in Appendix H. For the volume constraint V70%<10.0mL of the bladder, visualized in A, 100% of planned doses were above the constraint (mean increase above the constraint was 11.3±6.2 Gy, range 6.9-16.0 Gy) and 100% of accumulated doses of rCTs without motion were above the constraint (mean increase above the constraint was 9.9±6.4 Gy, range: 5.3-14.4 Gy). In addition, 100% of 4D accumulated doses of rCTs with wERB motion were above the constraint (mean increase above the constraint was 7.3±6.0 Gy, range 3.0-11.5 Gy) and 100% of 4D accumulated doses of rCTs with nERB motion were below the constraint.

For the dose constraint D0.01mL<39.8Gy of the bladder, visualized in B, 50% of planned doses were above the constraint (increase above the constraint was 0.2 Gy) and 100% of accumulated doses of rCTs without motion, 4D accumulated doses of rCTs with wERB and nERB motion were below the constraint.

For the volume constraint V105%<2.0mL of the rectum, visualized in C, 100% of planned, accumulated doses of rCTs without motion and 4D accumulated doses of rCTs with wERB and nERB motion were below the constraint. For the volume constraint V95%<5.0mL of the rectum, visualized in D, 100% of planned, accumulated doses of rCTs without motion and 4D accumulated doses of rCTs with wERB motion were below the constraint. In addition, 100% of 4D accumulated doses of rCTs with nERB motion was above the constraint (mean increase above the constraint was 1.5±0.3 Gy, range 1.3-1.7 Gy).

For the dose constraint D0.01mL<39.4Gy of the anterior rectal wall, visualized in E, 50% of planned doses was above the constraint (increase above the constraint was 0.0 Gy). In addition, 100% of accumulated doses of rCTs without motion and 4D accumulated doses of rCTs with wERB motion was below the constraint. Moreover, 50% of 4D accumulated doses of rCTs with nERB motion was above the constraint (increase above the constraint was 1.1 Gy).

For the dose constraint D0.01mL<18.8Gy of the posterior rectal wall, visualized in F, 50% of planned doses was above the constraint (increase above the constraint was 0.4 Gy) and 50% of accumulated doses of rCTs without motion was above the constraint (increase above the constraint was 8.1 Gy). In addition, 100% of 4D accumulated doses of rCTs with wERB motion was above the constraint (mean increase above the constraint was 3.3±4.5 Gy, range 0.2-6.5 Gy) and 100% of accumulated doses of rCTs with nERB motion was above the constraint (mean increase above the constraint was 12.9±2.4 Gy, range 11.2-14.6 Gy).

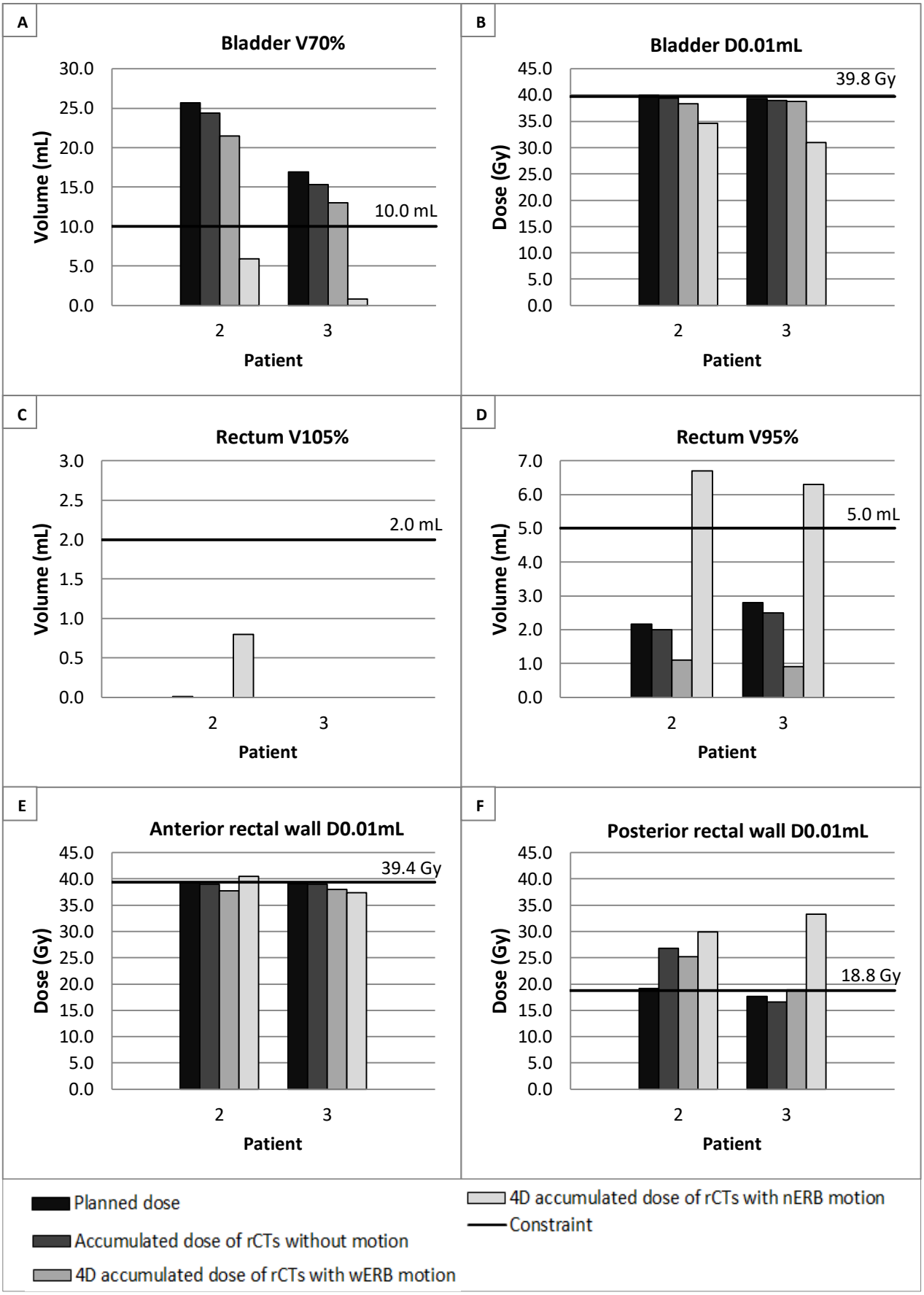

Figure 19: Clinical goals for the bladder (A and B), rectum (C and D), anterior rectal wall (E) and posterior rectal wall (F) for the planned, accumulated dose of rCTs without motion and the 4D accumulated doses of rCTs with wERB and nERB motion. Abbreviations: repeated CT (rCT), with endorectal balloon (wERB) and without endorectal balloon (nERB).

3.6 Discussion

The aim of this study was to evaluate the combined dosimetric impact of worst-case inter- and intrafraction prostate motion with and without ERB and the interplay effect. Interfraction prostate motion (accumulated deformed dose) and combined worst-case prostate motion with ERB (4D accumulated dose) resulted in maintenance of target coverage of the prostate and proximal part of the seminal vesicles. However, for the combined worst-case motion without ERB, target coverage (4D accumulated dose) of the prostate and proximal part of the seminal vesicles was on average 8.3±0.1Gy and 7.0±8.4Gy lower than protocol limits, respectively. Furthermore, simulated 3D worst-case intrafraction prostate motion without ERB was maximal 8.8 mm larger compared to simulated 3D worst-case intrafraction prostate motion with ERB. This finding is in line with published data that reported a reduced intrafraction motion with ERB compared to intrafraction motion without ERB [19,21,22]. In these studies, they reported a reduction of transient movements (probably caused by moving rectal gas). Another important finding in these studies was the reduction of the intrafraction motion trend over time when an ERB was used. Our results on target coverage were in line with a recently published study that reported that the combined motion effect with ERB decreased CTV coverage by approximately 2-3% [80]. They investigated the combined worst-case inter- and intrafraction prostate motion and the interplay effect (with ERB) for conventionally fractionated PBS proton therapy [80]. They found more influence of intrafraction motion (with ERB) on target coverage of the prostate than interfraction prostate motion (with ERB). In the former study, the prostate motion without ERB was not investigated.

Bladder doses were lower than protocol constraints while rectum doses increased above the protocol constraints for the combined worst-case prostate motion without ERB. This could be due to the 3D simulated motion without ERB, for which motion was largest in the superior and anterior motion direction. As a result bladder and rectum moved also in superior and anterior direction.

The dosimetric influence of the combined motion is the most relevant to be investigated in clinical practice. Previous studies used different methods to evaluate intrafraction prostate motion [78–80]. However, the used methods had several limitations, including the displacement of the beam isocenter and structure sets according to the beam offset and the assumption of small differences between Hounsfield units of the prostate and surrounding tissues. To compensate for above mentioned shortcomings of the methods, in our study 3D vCTs were created and deformable mapping of surrounding structures was applied according to the intrafraction prostate motion.

One limitation of our study is the simulation of worst-case intrafraction prostate motion only. This worst-case motion was reported sporadically in a very short time of the total treatment time. In the literature, the measured percentage of treatment time for which the 3D intrafraction prostate motion was >5mm (beyond the setup margin in our study) varied from 1.6-3.3% of time, whereas treatment time varied from 2.5-10.3min [22,58–60,62]. Therefore, in future research, a more probabilistic intrafraction prostate motion has to be simulated, for example by estimating the intrafraction prostate motion using a random walk model [55,56].

The creation of vCTs is associated with several limitations related to the available measurements of prostate intrafraction motion only. First, the proximal part of the seminal vesicles was displaced rigidly relative to the prostate, according to the measured prostate motion. However, from several studies followed that the prostate and the seminal vesicles do not move rigidly relative to each other

[81,82]. Moreover, only translations of the prostate have been measured, whereas rotations of the prostate may also be important [63]. At last, bladder and rectum were deformed according to the prostate motion, whereas prostate motion is effected by bladder and rectum volume. Therefore, in future research, it is important to measure both prostate and seminal vesicle motion using e.g. cine MRI. In addition, the measured motion in the cine MRI have to be simulated on the rCTs to create vCTs, or cine MRI has to be made suitable for dose calculation using synthetic CTs.

3.7 Conclusion

Extremely hypofractionated proton plans were robust to interfraction prostate motion and combined worst-case prostate motion with ERB, without violating rectum and bladder dose constraints. For combined worst-case prostate motion without ERB, large concessions had to be made for target coverage and rectal doses. In future research, a more probabilistic description of intrafraction prostate motion is necessary to estimate the actually given dose for the combined motion with and without ERB more realistically.

Chapter 4

General discussion

The aim of this thesis was to evaluate the dosimetric consequences of prostate motion in extremely hypofractionated proton therapy. For this purpose, two studies have been performed. In the first study, the impact of interfraction prostate motion on target coverage and doses to the organs at risk (OARs) has been evaluated. In the second study, the combined effect of inter- and intrafraction motion and the interplay effect has been evaluated for prostate motion with and without endorectal balloon (ERB).

Inter- and intrafraction prostate motion lead to geometrical uncertainties, which may result in lower coverage of the target and higher doses to the OARs. The severity and frequency of late rectum toxicities has been shown to be directly related to the irradiated volume of the rectum or rectal wall [38–40]. The introduction of image-guided radiotherapy contributed to a significant reduction of urinary and gastrointestinal toxicity rates and improvement of biochemical tumour control [83–85]. In our study, image-guided patient positioning, based on fiducial-based registration of the kV orthogonal images, was used without ERB. Our results reported no influence of interfraction prostate motion on target coverage and OAR doses in extremely hypofractionated PBS proton plans, using setup margins as in our conventionally fractionated photon treatment.

Several studies investigated the use of an ERB to limit intrafraction prostate motion and reported a significant reduction [21,22]. Results of our second study on the combined effect of inter- and intrafraction prostate motion and the interplay effect, showed that the use of an ERB resulted in maintenance of target coverage and rectal doses within the protocol limits, compared to a lower target coverage and higher rectal doses above the protocol constraints without the use of an ERB. However, in our study, worst-case intrafraction prostate motion was simulated, which represents an extreme scenario in a very limited time of the total treatment time. Moreover, intrafraction prostate motion was simulated using motion data of patients who were conventionally treated with photons. These data is not fully representative for extremely hypofractionated pencil beam scanning (PBS) proton therapy. Therefore, future research using motion data of patients already treated with this regimen is essential for an accurate evaluation of intrafraction prostate motion before drawing definite conclusions regarding the use of an ERB during extremely hypofractionated PBS proton therapy.

Our developed methodology is manual and hence time consuming. To facilitate further research using data of more patients (we used only 2 patients), it is desirable to automate the steps to simulate the motion. Furthermore, to simulate a more probabilistic intrafraction prostate motion, cine MRI and random walk models can be used to measure and estimate a more probabilistic intrafraction motion to define a safe and effective treatment strategy.

References

[1] Nederlandse Kanker Registratie. Het vóórkomen van prostaatkanker 2018. 2019. https://www.volksgezondheidenzorg.info/onderwerp/prostaatkanker/cijfers-context/huidige-situatie (accessed April 23, 2019).

[2] Integraal Kankercentrum Nederland. Incidentie prostaat 2018. 2018. https://www.cijfersoverkanker.nl/selecties/incidentie_prostaat/img568b9b5b8749f (accessed March 12, 2018).

[3] Meulepas M, Kiemeney LALM. Kanker in Nederland tot 2020: Trends en prognoses. 2011. https://www.kwf.nl/SiteCollectionDocuments/rapport-Kanker-in-Nederland-tot-2020.pdf (accessed October 17, 2018).

[4] Vanneste BG, Van Limbergen EJ, Van Lin EN, Van Roermund JGH, Lambin P. Prostate Cancer Radiation Therapy: What Do Clinicians Have to Know? Biomed Res Int 2016;2016. doi:10.1155/2016/6829875.

[5] Nederlandse vereniging voor urologie. Prostaatcarcinoom Landelijke richtlijn, Versie 2.1. Oncoline 2016. https://www.oncoline.nl/prostaatcarcinoom (accessed October 17, 2018).

[6] Wisenbaugh ES, Andrews PE, Ferrigni RG, Schild SE, Keole SR, Wong WW, et al. Proton beam therapy for localized prostate cancer 101: basics, controversies, and facts. Rev Urol 2014;16:67–75. doi:10.3909/riu0601.

[7] Schaake W, Wiegman EM, De Groot M, Van Der Laan HP, Van Der Schans CP, Van Den Bergh ACM, et al. The impact of gastrointestinal and genitourinary toxicity on health related quality of life among irradiated prostate cancer patients. Radiother Oncol 2014;110:284–90. doi:10.1016/j.radonc.2013.11.011.

[8] Tiberi D, Vavassis P, Nguyen D, Yassa M. Hypofractionation for prostate cancer: an update. Expert Rev Endocrinol Metab 2017;12:199–205. doi:10.1080/17446651.2017.1324294.

[9] Koontz BF, Bossi A, Cozzarini C, Wiegel T, D'Amico A. A systematic review of hypofractionation for primary management of prostate cancer. Eur Urol 2015;68:683–91. doi:10.1016/j.eururo.2014.08.009.

[10] Cabrera AR, Lee WR. Hypofractionation for clinically localized prostate cancer. Semin Radiat Oncol 2013;23:191–7. doi:10.1016/j.semradonc.2013.01.005.

[11] Mouw KW, Trofimov A, Zietman AL, Efstathiou JA. Clinical Controversies: Proton Therapy for Prostate Cancer. Semin Radiat Oncol 2018;23:109–14. doi:10.1016/j.semradonc.2012.11.009.

[12] Efstathiou JA, Trofimov A V., Zietman AL. Life, liberty, and the pursuit of protons: An evidence-based review of the role of particle therapy in the treatment of prostate cancer. Cancer J 2009;15:312–8. doi:10.1097/PPO.0b013e3181b14ec0.

[13] DeLaney TF. Proton Therapy in the clinic. Front Radiat Ther Oncol 2011;43:465–85. doi:10.1159/000322511.

[14] Höcht S, Aebersold DM, Albrecht C, Böhmer D, Flentje M, Ganswindt U, et al. Hypofractionated radiotherapy for localized prostate cancer. Strahlentherapie Und Onkol 2017;193:1–12. doi:10.1007/s00066-016-1041-5.

[15] Tang S, Deville C, McDonough J, Tochner Z, Wang K, Vapiwala N, et al. A Quantitative Assessment of the Interplay Effect of Prostate Intrafraction Motion in Proton Pencil Beam Scanning. Int J Radiat Oncol 2013;87:S739–40. doi:10.1016/j.ijrobp.2013.06.1959.

[16] Ammazzalorso F, Jelen U. A 4D dose computation method to investigate motion interplay effects in scanned ion beam prostate therapy. Phys Med Biol 2014;59. doi:10.1088/0031-9155/59/11/N91.

[17] Bert C, Grözinger SO, Rietzel E. Quantification of interplay effects of scanned particle beams and moving targets. Phys Med Biol 2008;53:2253–65. doi:10.1088/0031-9155/53/9/003.

[18] Mancosu P, Clemente S, Landoni V, Ruggieri R, Alongi F, Scorsetti M, et al. SBRT for prostate cancer: Challenges and features from a physicist prospective. Phys Medica 2016;32:479–84. doi:10.1016/j.ejmp.2016.03.011.

[19] Vargas C, Saito AI, Hsi WC, Indelicato D, Falchook A, Zengm Q, et al. Cine-magnetic resonance imaging assessment of intrafraction motion for prostate cancer patients supine or prone with and without a rectal balloon. Am J Clin Oncol Cancer Clin Trials 2010;33:11–6. doi:10.1097/COC.0b013e31819fdf7c.

[20] Smeenk RJ, Teh BS, Butler EB, van Lin ENJT, Kaanders JHAM. Is there a role for endorectal balloons in prostate radiotherapy? A systematic review. Radiother Oncol 2010;95:277–82. doi:10.1016/j.radonc.2010.04.016.

[21] Smeenk RJ, Louwe RJW, Langen KM, Shah AP, Kupelian PA, Van Lin ENJT, et al. An endorectal balloon reduces intrafraction prostate motion during radiotherapy. Int J Radiat Oncol Biol Phys 2012;83:661–9. doi:10.1016/j.ijrobp.2011.07.028.

[22] Wang K, Vapiwala N, Deville C, Plastaras J, Scheuermann R, Lin H, et al. A Study to Quantify the Effectiveness of Daily Endorectal Balloon (ERB) for Prostate Intrafraction Motion Management. Int J Radiat Oncol Biol Phys 2012;83:1055–63. doi:10.1118/1.3611913.

[23] Both S, Wang KKH, Plastaras JP, Deville C, Bar Ad V, Tochner Z, et al. Real-time study of prostate intrafraction motion during external beam radiotherapy with daily endorectal balloon. Int J Radiat Oncol Biol Phys 2011;81:1302–9. doi:10.1016/j.ijrobp.2010.08.052.

[24] Wong AT, Schreiber D, Agarwal M, Polubarov A, Schwartz D. Impact of the use of an endorectal balloon on rectal dosimetry during stereotactic body radiation therapy for localized prostate cancer. Pract Radiat Oncol 2016;6:262–7. doi:10.1016/j.prro.2015.10.019.

[25] Xiang HF, Lu HM, Efstathiou JA, Zietman AL, Armas R De, Harris K, et al. Dosimetric impacts of endorectal balloon in CyberKnife stereotactic body radiation therapy (SBRT) for early-stage prostate cancer. J Appl Clin Med Phys 2017;18:37–43. doi:10.1002/acm2.12063.

[26] Jones BL, Gan G, Kavanagh B, Miften M. Effect of endorectal balloon positioning errors on target deformation and dosimetric quality during prostate SBRT. Phys Med Biol 2013;58:7995–8006. doi:10.1088/0031-9155/58/22/7995.

[27] Lee CH, Akin-Olugbade O, Kirschenbaum A. Overview of Prostate Anatomy, Histology, and Pathology. Endocrinol Metab Clin North Am 2011;40:565–75. doi:10.1016/j.ecl.2011.05.012.

[28] Moore KL, Dalley AF, Agur AMR. Chapter 3: Pelvis and Perineum. Clin. Oriented Anat., 2013, p. 377–9.

[29] Dunn MW, Kazer MW. Prostate Cancer Overview. Semin Oncol Nurs 2011;27:241–50. doi:10.1016/j.soncn.2011.07.002.

[30] Rubin R, Strayer DS. Chapter 17: The lower urinary tract and male reproductive system. Rubin's Pathol. Clin. Found. Med., 2013, p. 856–62.

[31] Chen ME, Johnston DA, Tang K, Babaian RJ, Troncoso P. Detailed Mapping of Prostate Carcinoma Foci. Cancer 2000;89:1800–9.

[32] Buyyounouski MK, Choyke PL, McKenney JK, Sartor O, Sandler HM, Amin MB, et al. Prostate cancer - major changes in the American Joint Committee on Cancer eighth edition cancer staging manual. CA Cancer J Clin 2017;67:245–53. doi:10.3322/caac.21391.

[33] D'Amico A V., Moul J, Carroll PR, Sun L, Lubeck D, Chen MH. Cancer-specific mortality after surgery or radiation for patients with clinically localized prostate cancer managed during the prostate-specific antigen era. J Clin Oncol 2003;21:2163–72. doi:10.1200/JCO.2003.01.075.

[34] Evans E, Staffurth J. Principles of cancer treatment by radiotherapy. Surg 2018;36:111–6. doi:10.1016/j.mpsur.2017.12.002.

[35] Elith C, Dempsey SE, Findlay N, Warren-Forward HM. An introduction to the intensity-modulated radiation therapy (IMRT) techniques, tomotherapy, and VMAT. J Med Imaging Radiat Sci 2011;42:37–43. doi:10.1016/j.jmir.2010.11.005.

[36] Rehman J, Zahra, Ahmad N, Khalid M, Asghar N, Gilani ZA, et al. Intensity modulated radiation therapy: A review of current practice and future directions. J Radiat Res Appl Sci 2018:361–7. doi:10.1177/153303460600500501.

[37] Trotti A, Colevas AD, Setser A, Rusch V, Jaques D, Budach V, et al. CTCAE v3.0: Development of a comprehensive grading system for the adverse effects of cancer treatment. Semin Radiat Oncol 2003;13:176–81. doi:10.1016/S1053-4296(03)00031-6.

[38] Skwarchuk MW, Jackson A, Zelefsky MJ, Venkatraman ES, Cowen DM, Levegrün S, et al. Late rectal toxicity after conformal radiotherapy of prostate cancer (I): Multivariate analysis and dose-response. Int J Radiat Oncol Biol Phys 2000;47:103–13. doi:10.1016/S0360-3016(99)00560-X.

[39] Vargas C, Martinez A, Kestin LL, Yan D, Grills I, Brabbins DS, et al. Dose-volume analysis of predictors for chronic rectal toxicity after treatment of prostate cancer with adaptive image-guided radiotherapy. Int J Radiat Oncol Biol Phys 2005;62:1297–308. doi:10.1016/j.ijrobp.2004.12.052.

[40] van der Laan HP, van den Bergh A, Schilstra C, Vlasman R, Meertens H, Langendijk JA. Grading-System-Dependent Volume Effects for Late Radiation-Induced Rectal Toxicity After Curative Radiotherapy for Prostate Cancer. Int J Radiat Oncol Biol Phys 2008;70:1138–45. doi:10.1016/j.ijrobp.2007.07.2363.

[41] Kim DWN, Cho LC, Straka C, Christie A, Lotan Y, Pistenmaa D, et al. Predictors of rectal tolerance observed in a dose-escalated phase 1-2 trial of stereotactic body radiation therapy for prostate cancer. Int J Radiat Oncol Biol Phys 2014;89:509–17. doi:10.1016/j.ijrobp.2014.03.012.

[42] Nahum AE. The Radiobiology of Hypofractionation. Clin Oncol 2015;27:260–9. doi:10.1016/j.clon.2015.02.001.

[43] Fowler J, Chappell R, Ritter M. Is α/β for prostate tumors really low? Int J Radiat Oncol Biol Phys 2001;50:1021–31. doi:10.1016/S0360-3016(01)01607-8.

[44] Miralbell R, Roberts SA, Zubizarreta E, Hendry JH. Dose-fractionation sensitivity of prostate cancer deduced from radiotherapy outcomes of 5,969 patients in seven international institutional datasets: α/β = 1.4 (0.9-2.2) Gy. Int J Radiat Oncol Biol Phys 2012;82:17–24.

doi:10.1016/j.ijrobp.2010.10.075.

[45] Proust-Lima C, Taylor JMG, Sécher S, Sandler H, Kestin L, Pickles T, et al. Confirmation of a low α/β ratio for prostate cancer treated by external beam radiation therapy alone using a post-treatment repeated-measures model for PSA dynamics. Int J Radiat Oncol Biol Phys 2011;79:195–201. doi:10.1016/j.ijrobp.2009.10.008.

[46] Tucker SL, Thames HD, Michalski JM, Bosch WR, Mohan R, Winter K, et al. Estimation of α/β for late rectal toxicity based on RTOG 94-06. Int J Radiat Oncol Biol Phys 2011;81:600–5. doi:10.1016/j.ijrobp.2010.11.080.

[47] Hegemann N-S, Guckenberger M, Belka C, Ganswindt U, Manapov F, Li M. Hypofractionated radiotherapy for prostate cancer. Radiat Oncol 2014;9. doi:10.1016/S1470-2045(16)30592-7.

[48] Van Herk M, Remeijer P, Rasch C, Lebesque J V. The probability of correct target dosage: Dose-population histograms for deriving treatment margins in radiotherapy. Int J Radiat Oncol Biol Phys 2000;47:1121–35. doi:10.1016/S0360-3016(00)00518-6.

[49] Van Herk M. Errors and Margins in Radiotherapy. Semin Radiat Oncol 2004;14:52–64. doi:10.1053/j.semradonc.2003.10.003.

[50] Litzenberg DW, Balter JM, Hadley SW, Sandler HM, Willoughby TR, Kupelian PA, et al. Influence of intrafraction motion on margins for prostate radiotherapy. Int J Radiat Oncol Biol Phys 2006;65:548–53. doi:10.1016/j.ijrobp.2005.12.033.

[51] Wong JR, Gao Z, Uematsu M, Merrick S, Machernis NP, Chen T, et al. Interfractional Prostate Shifts: Review of 1870 Computed Tomography (CT) Scans Obtained During Image-Guided Radiotherapy Using CT-on-Rails for the Treatment of Prostate Cancer. Int J Radiat Oncol Biol Phys 2008;72:1396–401. doi:10.1016/j.ijrobp.2008.03.045.

[52] Snir JA, Battista JJ, Bauman G, Yartsev S. Evaluation of Inter-fraction Prostate Motion using Kilovoltage Cone Beam Computed Tomography during Radiotherapy. Clin Oncol 2011;23:625–31. doi:10.1016/j.clon.2011.03.007.

[53] Mayyas E, Chetty IJ, Chetvertkov M, Wen N, Neicu T, Nurushev T, et al. Evaluation of multiple image-based modalities for image-guided radiation therapy (IGRT) of prostate carcinoma: A prospective study. Med Phys 2013;40. doi:10.1118/1.4794502.

[54] Mesías MC, Boda-Heggemann J, Thoelking J, Lohr F, Wenz F, Wertz H. Quantification and assessment of interfraction setup errors based on cone beam CT and determination of safety margins for radiotherapy. PLoS One 2016;11:6–13. doi:10.1371/journal.pone.0150326.

[55] Pommer T, Oh JH, Munck af Rosenschöld P, Deasy JO. Simulating intrafraction prostate motion with a random walk model. Adv Radiat Oncol 2017;2:429–36. doi:10.1016/j.adro.2017.03.005.

[56] Ballhausen H, Li M, Hegemann NS, Ganswindt U, Belka C. Intra-fraction motion of the prostate is a random walk. Phys Med Biol 2015;60:549–63. doi:10.1088/0031-9155/60/2/549.

[57] Xie Y, Djajaputra D, King CR, Hossain S, Ma L, Xing L. Intrafractional Motion of the Prostate During Hypofractionated Radiotherapy. Int J Radiat Oncol Biol Phys 2008;72:236–46. doi:10.1038/jid.2014.371.

[58] Langen KM, Willoughby TR, Meeks SL, Santhanam A, Cunningham A, Levine L, et al. Observations on Real-Time Prostate Gland Motion Using Electromagnetic Tracking. Int J

Radiat Oncol Biol Phys 2008;71:1084–90. doi:10.1016/j.ijrobp.2007.11.054.

[59] Tong X, Chen X, Li J, Xu Q, Lin M han, Chen L, et al. Intrafractional prostate motion during external beam radiotherapy monitored by a real-time target localization system. J Appl Clin Med Phys 2015;16:51–61. doi:10.1120/jacmp.v16i2.5013.

[60] Ng JA, Booth JT, Poulsen PR, Fledelius W, Worm ES, Eade T, et al. Kilovoltage intrafraction monitoring for prostate intensity modulated arc therapy: First clinical results. Int J Radiat Oncol Biol Phys 2012;84:e655–61. doi:10.1016/j.ijrobp.2012.07.2367.

[61] Sihono DSK, Ehmann M, Heitmann S, von Swietochowski S, Grimm M, Boda-Heggemann J, et al. Determination of Intrafraction Prostate Motion During External Beam Radiation Therapy With a Transperineal 4-Dimensional Ultrasound Real-Time Tracking System. Int J Radiat Oncol Biol Phys 2018;101:136–43. doi:10.1016/j.ijrobp.2018.01.040.

[62] Shah AP, Kupelian PA, Willoughby TR, Langen KM, Meeks SL. An evaluation of intrafraction motion of the prostate in the prone and supine positions using electromagnetic tracking. Radiother Oncol 2011;99:37–43. doi:10.1016/j.radonc.2011.02.012.

[63] Van De Water S, Valli L, Aluwini S, Lanconelli N, Heijmen B, Hoogeman M. Intrafraction prostate translations and rotations during hypofractionated robotic radiation surgery: Dosimetric impact of correction strategies and margins. Int J Radiat Oncol Biol Phys 2014;88:1154–60. doi:10.1016/j.ijrobp.2013.12.045.

[64] Tang S, Deville C, McDonough J, Tochner Z, Wang KKH, Vapiwala N, et al. Effect of intrafraction prostate motion on proton pencil beam scanning delivery: A quantitative assessment. Int J Radiat Oncol Biol Phys 2013;87:375–82. doi:10.1016/j.ijrobp.2013.05.048.

[65] Hung AY, Garzotto M, Kaurin D. Minimal benefit of an endorectal balloon for prostate immobilization as verified by daily localization. Med Dosim 2011;36:195–9. doi:10.1016/j.meddos.2010.03.003.

[66] Peng C, Ahunbay E, Chen G, Anderson S, Lawton C, Li XA. Characterizing interfraction variations and their dosimetric effects in prostate cancer radiotherapy. Int J Radiat Oncol Biol Phys 2011;79:909–14. doi:10.1016/j.ijrobp.2010.05.008.

[67] Kerkhof EM. Variation in target and rectum dose due to prostate deformation: an assessment by repeated MR imaging and treatment planning. Phys Med Biol 2008;53:5623–34. doi:10.1088/0031-9155/53/20/004.

[68] Zhang X, Dong L, Lee AK, Cox JD, Kuban DA, Zhu RX, et al. Effect of anatomic motion on proton therapy dose distributions in prostate cancer treatment. Int J Radiat Oncol Biol Phys 2007;67:620–9. doi:10.1016/j.ijrobp.2006.10.008.

[69] Wang Y, Efstathiou JA, Sharp GC, Lu HM, Frank Ciernik I, Trofimov A V. Evaluation of the dosimetric impact of interfractional anatomical variations on prostate proton therapy using daily in-room CT images. Med Phys 2011;38:4623–33. doi:10.1118/1.3604152.

[70] Soukup M, Söhn M, Yan D, Liang J, Alber M. Study of Robustness of IMPT and IMRT for Prostate Cancer Against Organ Movement. Int J Radiat Oncol Biol Phys 2009;75:941–9. doi:10.1016/j.ijrobp.2009.04.032.

[71] Faasse-de Hoog M, Hoogeman MS, Nuyttens JJM., Aluwini S. Organ at risk dose parameters increased by daily anatomic changes in prostate cancer SBRT. Radiother Oncol 2016.

[72] Wang Y, Efstathiou JA, Lu HM, Sharp GC, Trofimov A. Hypofractionated proton therapy for prostate cancer: Dose delivery uncertainty due to interfractional motion. Med Phys 2013;40. doi:10.1118/1.4811101.

[73] Moteabbed M, Trofimov A, Khan FH, Wang Y, Sharp GC, Zietman AL, et al. Impact of interfractional motion on hypofractionated pencil beam scanning proton therapy and VMAT delivery for prostate cancer. Med Phys 2018;45:4011–9. doi:10.1002/mp.13091.

[74] Bayman NA, Wylie JP. When Should the Seminal Vesicles be Included in the Target Volume in Prostate Radiotherapy? Clin Oncol 2007;19:302–7. doi:10.1016/j.clon.2007.03.005.

[75] Kestin LL, Goldstein NS, Vicini FA, Yan D, Korman HJ, Martinez AA. Treatment of prostate cancer with radiotherapy: Should the entire seminal vesicles be included in the clinical target volume? Int J Radiat Oncol Biol Phys 2002;54:686–97. doi:10.1016/S0360-3016(02)03011-0.

[76] Weistrand O, Svensson S. The ANACONDA algorithm for deformable image registration in radiotherapy. Med Phys 2015;42:40–53. doi:10.1118/1.4894702.

[77] Aluwini S, Rooij P van, Hoogeman M, Bangma C, Kirkels WJ, Incrocci L, et al. CyberKnife Stereotactic Radiotherapy as Monotherapy for Low- to Intermediate-Stage Prostate Cancer: Early Experience, Feasibility, and Tolerance. J Endourol 2010;24:865–9.

[78] Zhang P, Mah D, Happersett L, Cox B, Hunt M, Mageras G. Determination of action thresholds for electromagnetic tracking system-guided hypofractionated prostate radiotherapy using volumetric modulated arc therapy. Med Phys 2011;38:4001–8. doi:10.1118/1.3596776.

[79] Koike Y, Sumida I, Mizuno H, Shiomi H, Kurosu K, Ota S, et al. Dosimetric impact of intra-fraction prostate motion under a tumour-tracking system in hypofractionated robotic radiosurgery. PLoS One 2018;13:1–10. doi:10.1371/journal.pone.0195296.

[80] Tang S, Deville C, Tochner Z, Wang KKH, McDonough J, Vapiwala N, et al. Impact of intrafraction and residual interfraction effect on prostate proton pencil beam scanning. Int J Radiat Oncol Biol Phys 2014;90:1186–94. doi:10.1016/j.ijrobp.2014.08.015.

[81] Gill S, Dang K, Fox C, Bressel M, Kron T, Bergen N, et al. Seminal vesicle intrafraction motion analysed with cinematic magnetic resonance imaging. 2014. doi:10.1186/1748-717X-9-174.

[82] Sheng Y, Li T, Lee WR, Yin FF, Wu QJ. Exploring the Margin Recipe for Online Adaptive Radiation Therapy for Intermediate-Risk Prostate Cancer: An Intrafractional Seminal Vesicles Motion Analysis. Int J Radiat Oncol Biol Phys 2017;98:473–80. doi:10.1016/j.ijrobp.2017.02.089.

[83] Gill S, Thomas J, Fox C, Kron T, Rolfo A, Leahy M, et al. Acute toxicity in prostate cancer patients treated with and without image-guided radiotherapy. Radiat Oncol 2011;6:1–7. doi:10.1186/1748-717X-6-145.

[84] Zelefsky MJ, Kollmeier M, Cox B, Fidaleo A, Sperling D, Pei X, et al. Improved clinical outcomes with high-dose image guided radiotherapy compared with non-IGRT for the treatment of clinically localized prostate cancer. Int J Radiat Oncol Biol Phys 2012;84:125–9. doi:10.1016/j.ijrobp.2011.11.047.

[85] Singh J, Greer PB, White MA, Parker J, Patterson J, Tang CI, et al. Treatment-related morbidity in prostate cancer: A comparison of 3-dimensional conformal radiation therapy with and without image guidance using implanted fiducial markers. Int J Radiat Oncol Biol Phys 2013;85:1018–23. doi:10.1016/j.ijrobp.2012.07.2376.

[86] Canadian Cancer Society. The Prostate 2019. https://www.cancer.ca/en/cancer-information/cancer-type/prostate/prostate-cancer/the-prostate/?region=on (accessed May 1, 2019).

[87] Ghose DA. Determining the stage of prostate cancer 2019. http://amitghose.com/determining_stage.html (accessed May 1, 2019).

[88] Moreno AC, Frank SJ, Garden AS, Rosenthal DI, Fuller CD, Gunn GB, et al. Intensity modulated proton therapy (IMPT) – The future of IMRT for head and neck cancer. Oral Oncol 2019;88:66–74. doi:10.1016/j.oraloncology.2018.11.015.

Appendices

A. Dose-volume constraints for extremely hypofractionated proton plans

OAR	Volume	Dose (cGy)	Volume constraint	Dose constraint
Anal Canal (bowel inf to CTV_ProstateandVS+5mm)	Maximum point dose (0.01mL)	70% of the prescribed dose		D0.01mL < 2625cGy
	Less than 5mL	40% of the prescribed dose	V1500cGy < 5mL	D5mL < 1500cGy
Bladder	Maximum point dose (0.01mL)	No more than 106% of prescription dose		D0.01mL < 3975cGy
	Less than 10mL	70% of the prescribed dose	V2625cGy < 10mL	D10mL < 2625cGy
Bulb	Maximum point dose (0.01mL)	No more than 100% of prescription dose		D0.01mL < 3750cGy
	Less than 3mL	55% prescribed dose	V2063cGy < 3mL	D3mL < 2063cGy
FemoralHead_L	Maximum point dose (0.01mL)	60% of the prescribed dose		D0.01mL < 2250cGy
FemoralHead_R	Maximum point dose (0.01mL)	60% of the prescribed dose		D0.01mL < 2250cGy
Heupen (FemoralHeads)	Less than 10mL cumulative (both sides)	55% prescribed dose	V2063cGy < 10mL	D10mL < 2063cGy
Rectum (Volume)	Less than 2mL	No more than 105% of the prescription dose	V3938cGy < 2mL	D2mL < 3938cGy
Rectum (Volume)	Less than 5mL	Less than 95% of the prescription dose	V3563cGy < 5mL	D5mL < 3563cGy
Rectum (superior to CTV_ProstateandVS+5mm)	Maximum point dose (0.01mL)	80% of the prescribed dose		D0.01mL < 3000cGy
	Less than 10mL	60% of the prescribed dose	V2250cGy < 10mL	D10mL < 2250cGy
Rectum_wall_ant	Maximum point dose (0.01mL)	No more than 105% of the prescription dose		D0.01mL < 3938cGy
Rectum_wall_post	Maximum point dose (0.01mL)	No more than 50% of the prescription dose		D0.01mL < 1875cGy
Skin5mm	Maximum point dose (0.01mL)	40% of the prescribed dose		D0.01mL < 1500cGy

B. Objective list of the pencil beam scanning proton plans for all patients

Patient 1

Function	Constraint	Dose	ROI	Description	Robust	Weight	Value
Physical Composite Objective							
Min Dose		Beam Set	CTV_Prostate	Min Dose 3800 cGy, All beams	★	500.00	
Dose Fall-Off		Plan	BODY	Dose Fall-Off [H]4750 cGy [L]0 cGy, Low dose distance 2.40 cm		1.00	0.0077
Max Dose		Plan	Wallprostate+1cm	Max Dose 3800 cGy		100.00	
Dose Fall-Off		Plan	BODY	Dose Fall-Off [H]4750 cGy [L]1850 cGy, Low dose distance 1.50 cm		1.00	1.1174E-4
Max Dose		Beam Set	CTV_Prostate	Max Dose 4000 cGy, All beams	★	100.00	
Dose Fall-Off		Plan	CTV_VS	Dose Fall-Off [H]4500 cGy [L]3000 cGy, Low dose distance 0.85 cm		1.00	1.7424E-5
Min Dose		Beam Set	CTV_VS-CTV_Prostate+1.0cm	Min Dose 3050 cGy, All beams	★	500.00	
Max Dose		Beam Set	CTV_VS-CTV_Prostate+1.0cm	Max Dose 3210 cGy, All beams	★	100.00	
Max Dose		Plan	CTV_VS+1cm-CTV_Prostaat+1cm	Max Dose 3050 cGy		100.00	0.0170
Min Dose		Beam Set	CTV_Prostate	Min Dose 3800 cGy, All beams		200.00	
Max Dose		Beam Set	CTV_Prostate	Max Dose 4000 cGy, All beams		250.00	
Min Dose		Beam Set	CTV_VS-CTV_Prostate+1.0cm	Min Dose 3050 cGy, All beams		200.00	
Max Dose		Beam Set	CTV_VS-CTV_Prostate+1.0cm	Max Dose 3210 cGy, All beams		100.00	
Max Dose		Plan	Bladder	Max Dose 3900 cGy		2500.00	5.0539E-4
Max Dose		Plan	Rectum_wall_post	Max Dose 1800 cGy		1000.00	0.0024
Max Dose		Plan	Rectum_wall_ant	Max Dose 3900 cGy		1000.00	2.1492E-4
Dose Fall-Off		Plan	Bulb	Dose Fall-Off [H]4500 cGy [L]1850 cGy, Low dose distance 0.85 cm		1.00	0.0140
Dose Fall-Off		Plan	Bladder	Dose Fall-Off [H]4500 cGy [L]1850 cGy, Low dose distance 0.85 cm		1.00	0.0072
Dose Fall-Off		Plan	Rectum	Dose Fall-Off [H]4500 cGy [L]1850 cGy, Low dose distance 0.85 cm		1.00	0.0068
Dose Fall-Off		Plan	Anal Canal (bowel inf to CTV_ProstateandVS+5mm)	Dose Fall-Off [H]4500 cGy [L]1850 cGy, Low dose distance 0.85 cm		1.00	2.9303E-8
Max Dose		Plan	Anal Canal (bowel inf to CTV_ProstateandVS+5mm)	Max Dose 2600 cGy		1000.00	0.0000

Patient 2

Function	Constraint	Dose	ROI	Description	Robust	Weight	Value
Physical Composite Objective							
Uniform Dose		Beam Set	CTV_Prostate	Uniform Dose 3850 cGy, All beams	★	500.00	
Dose Fall-Off		Plan	BODY	Dose Fall-Off [H]4750 cGy [L]0 cGy, Low dose distance 2.40 cm		1.00	0.0044
Dose Fall-Off		Plan	CTV_VS	Dose Fall-Off [H]4500 cGy [L]3000 cGy, Low dose distance 0.85 cm		50.00	0.0013
Max Dose		Plan	BODY	Max Dose 3940 cGy		1000.00	8.8718E-6
Max Dose		Plan	CTV_VS+1cm-CTV_Prostaat+1cm	Max Dose 3150 cGy		100.00	
Dose Fall-Off		Plan	BODY	Dose Fall-Off [H]4750 cGy [L]1850 cGy, Low dose distance 1.50 cm		50.00	0.0024
Max Dose		Plan	Bulb	Max Dose 3750 cGy		2000.00	6.7316E-6
Max Dose		Plan	Rectum_wall_post	Max Dose 1875 cGy		4000.00	0.0043
Max Dose		Plan	Skin5mm	Max Dose 1500 cGy		5000.00	0.0000
Max Dose		Plan	Rectum_wall_ant	Max Dose 3938 cGy		4000.00	2.1814E-5
Dose Fall-Off		Plan	Rectum	Dose Fall-Off [H]4125 cGy [L]0 cGy, Low dose distance 2.00 cm		5.00	0.0117
Dose Fall-Off		Plan	Anal Canal (bowel inf to CTV_ProstateandVS+5mm)	Dose Fall-Off [H]4125 cGy [L]0 cGy, Low dose distance 2.00 cm		5.00	5.5597E-4
Min Dose		Beam Set	CTV_VS+0.8 post-CTV_Prostate+1.5	Min Dose 3000 cGy, All beams	★	1000.00	

Patient 3

Function	Constraint	Dose	ROI	Description	Robust	Weight	Value
Physical Composite Objective							
Min Dose		Beam Set	CTV_Prostate	Min Dose 3800 cGy, All beams	★	500.00	
Dose Fall-Off		Plan	BODY	Dose Fall-Off [H]4750 cGy [L]0 cGy, Low dose distance 2.40 cm		1.00	0.0041
Max Dose		Plan	Wallprostate+1cm	Max Dose 3800 cGy		100.00	
Dose Fall-Off		Plan	BODY	Dose Fall-Off [H]4750 cGy [L]1850 cGy, Low dose distance 1.50 cm		1.00	5.2304E-5
Max Dose		Beam Set	CTV_Prostate	Max Dose 4000 cGy, All beams	★	100.00	
Dose Fall-Off		Plan	CTV_VS	Dose Fall-Off [H]4500 cGy [L]3000 cGy, Low dose distance 0.85 cm		1.00	4.2392E-5
Min Dose		Beam Set	CTV_VS-CTV_Prostate+1.0cm	Min Dose 3050 cGy, All beams	★	500.00	
Max Dose		Beam Set	CTV_VS-CTV_Prostate+1.0cm	Max Dose 3210 cGy, All beams	★	50.00	
Max Dose		Plan	CTV_VS+1cm-CTV_Prostaat+1cm	Max Dose 3050 cGy		100.00	
Min Dose		Beam Set	CTV_Prostate	Min Dose 3800 cGy, All beams		200.00	
Max Dose		Beam Set	CTV_Prostate	Max Dose 4000 cGy, All beams		500.00	
Min Dose		Beam Set	CTV_VS-CTV_Prostate+1.0cm	Min Dose 3050 cGy, All beams		200.00	
Max Dose		Beam Set	CTV_VS-CTV_Prostate+1.0cm	Max Dose 3210 cGy, All beams		100.00	
Max Dose		Plan	Bladder	Max Dose 3900 cGy		2500.00	1.6838E-4
Max Dose		Plan	Rectum_wall_post	Max Dose 1800 cGy		1000.00	1.2776E-4
Max Dose		Plan	Rectum_wall_ant	Max Dose 3900 cGy		1000.00	1.0414E-5
Dose Fall-Off		Plan	Bulb	Dose Fall-Off [H]4500 cGy [L]1850 cGy, Low dose distance 0.85 cm		1.00	0.0151
Dose Fall-Off		Plan	Bladder	Dose Fall-Off [H]4500 cGy [L]1850 cGy, Low dose distance 0.85 cm		1.00	0.0091
Dose Fall-Off		Plan	Rectum	Dose Fall-Off [H]4500 cGy [L]1850 cGy, Low dose distance 0.85 cm		1.00	0.0048
Dose Fall-Off		Plan	Anal Canal (bowel inf to CTV_ProstateandVS+5mm)	Dose Fall-Off [H]4500 cGy [L]1850 cGy, Low dose distance 0.85 cm		1.00	6.2506E-6
Max Dose		Plan	Anal Canal (bowel inf to CTV_ProstateandVS+5mm)	Max Dose 2600 cGy		1000.00	0.0000

Patient 4

Function	Constraint	Dose	ROI	Description	Robust	Weight	Value
Physical Composite Objective							
Min Dose		Beam Set	CTV_Prostate	Min Dose 3820 cGy, All beams	★	500.00	
Dose Fall-Off		Plan	BODY	Dose Fall-Off [H]4750 cGy [L]0 cGy, Low dose distance 2.40 cm		0.10	6.0770E-4
Max Dose		Plan	Wallprostate+1cm	Max Dose 3820 cGy		200.00	0.0217
Dose Fall-Off		Plan	BODY	Dose Fall-Off [H]4750 cGy [L]1850 cGy, Low dose distance 1.50 cm		1.00	8.0977E-5
Max Dose		Beam Set	CTV_Prostate	Max Dose 4020 cGy, All beams	★	100.00	
Dose Fall-Off		Plan	CTV_VS	Dose Fall-Off [H]4500 cGy [L]3000 cGy, Low dose distance 0.85 cm		1.00	0.0026
Max Dose		Plan	CTV_VS+1cm-CTV_Prostaat+1cm	Max Dose 3070 cGy		1.00	0.0034
Min Dose		Beam Set	CTV_Prostate	Min Dose 3820 cGy, All beams		300.00	
Max Dose		Beam Set	CTV_Prostate	Max Dose 4020 cGy, All beams		200.00	
Max Dose		Plan	Bladder	Max Dose 3900 cGy		3500.00	6.7781E-5
Max Dose		Plan	Rectum_wall_post	Max Dose 1800 cGy		1000.00	0.0000
Max Dose		Plan	Rectum_wall_ant	Max Dose 3900 cGy		1000.00	1.4155E-5
Dose Fall-Off		Plan	Bulb	Dose Fall-Off [H]4500 cGy [L]1850 cGy, Low dose distance 0.85 cm		2.00	0.0363
Dose Fall-Off		Plan	Bladder	Dose Fall-Off [H]4500 cGy [L]1850 cGy, Low dose distance 0.85 cm		1.00	0.0133
Dose Fall-Off		Plan	Rectum	Dose Fall-Off [H]4500 cGy [L]1850 cGy, Low dose distance 0.85 cm		1.00	0.0042
Min Dose		Beam Set	CTV_VS-CTV_Prostate+1.0cm	Min Dose 3070 cGy, All beams		300.00	
Max Dose		Beam Set	CTV_VS-CTV_Prostate+1.0cm	Max Dose 3230 cGy, All beams		0.10	
Max Dose		Plan	Bulb	Max Dose 3750 cGy		100.00	0.0039
Dose Fall-Off		Plan	Anal Canal (bowel inf to CTV_ProstateandVS+5mm)	Dose Fall-Off [H]4500 cGy [L]1850 cGy, Low dose distance 0.85 cm		1.00	7.5076E-5
Max Dose		Plan	Anal Canal (bowel inf to CTV_ProstateandVS+5mm)	Max Dose 2600 cGy		1000.00	0.0012
Max Dose		Beam Set	CTV_VS-CTV_Prostate+1.0cm	Max Dose 3230 cGy, All beams	★	0.10	
Min Dose		Beam Set	CTV_VS-CTV_Prostate+1.0cm	Min Dose 3070 cGy, All beams	★	500.00	

Patient 5

Function	Constraint	Dose	ROI	Description	Robust	Weight	Value
Physical Composite Objective							
Min Dose		Beam Set	CTV_Prostate	Min Dose 3800 cGy, All beams	★	750.00	
Dose Fall-Off		Plan	BODY	Dose Fall-Off [H]4750 cGy [L]0 cGy, Low dose distance 2.40 cm		1.00	0.0059
Max Dose		Plan	Wallprostate+1cm	Max Dose 3800 cGy		100.00	
Dose Fall-Off		Plan	BODY	Dose Fall-Off [H]4750 cGy [L]1850 cGy, Low dose distance 1.50 cm		1.00	9.6212E-5
Max Dose		Beam Set	CTV_Prostate	Max Dose 4000 cGy, All beams	★	100.00	
Dose Fall-Off		Plan	CTV_VS	Dose Fall-Off [H]4500 cGy [L]3000 cGy, Low dose distance 0.85 cm		1.00	1.7692E-5
Min Dose		Beam Set	CTV_VS-CTV_Prostate+1.0cm	Min Dose 3050 cGy, All beams	★	500.00	
Max Dose		Beam Set	CTV_VS-CTV_Prostate+1.0cm	Max Dose 3210 cGy, All beams	★	100.00	
Max Dose		Plan	CTV_VS+1cm-CTV_Prostaat+1cm	Max Dose 3050 cGy		100.00	
Min Dose		Beam Set	CTV_Prostate	Min Dose 3800 cGy, All beams		200.00	
Max Dose		Beam Set	CTV_Prostate	Max Dose 4000 cGy, All beams		2000.00	
Min Dose		Beam Set	CTV_VS-CTV_Prostate+1.0cm	Min Dose 3050 cGy, All beams		200.00	
Max Dose		Beam Set	CTV_VS-CTV_Prostate+1.0cm	Max Dose 3210 cGy, All beams		100.00	
Max Dose		Plan	Bladder	Max Dose 3900 cGy		2500.00	0.0020
Max Dose		Plan	Rectum_wall_post	Max Dose 1800 cGy		1000.00	0.0053
Max Dose		Plan	Rectum_wall_ant	Max Dose 3900 cGy		2000.00	0.0015
Dose Fall-Off		Plan	Bulb	Dose Fall-Off [H]4500 cGy [L]1850 cGy, Low dose distance 0.85 cm		1.00	0.0000
Dose Fall-Off		Plan	Bladder	Dose Fall-Off [H]4500 cGy [L]1850 cGy, Low dose distance 0.85 cm		1.00	0.0257
Dose Fall-Off		Plan	Rectum	Dose Fall-Off [H]4500 cGy [L]1850 cGy, Low dose distance 0.85 cm		1.00	0.0028
Dose Fall-Off		Plan	Anal Canal (bowel inf to CTV_ProstateandVS+5mm)	Dose Fall-Off [H]4500 cGy [L]1850 cGy, Low dose distance 0.85 cm		1.00	6.5387E-5
Max Dose		Plan	Anal Canal (bowel inf to CTV_ProstateandVS+5mm)	Max Dose 2600 cGy		50.00	0.0166

C. Additional Results Chapter 2

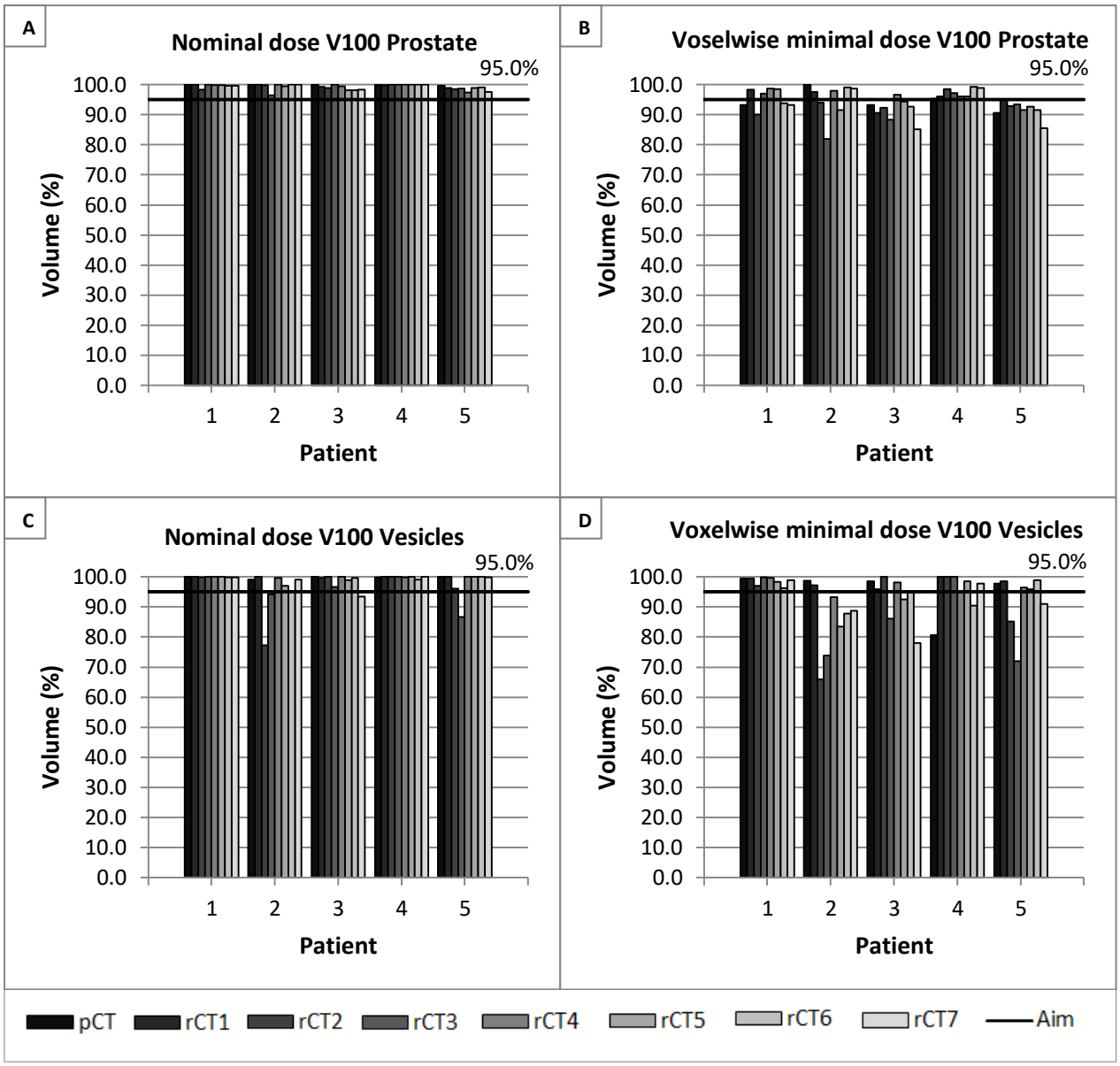

Figure 1: V100 of the nominal (A and C) and voxelwise minimal dose (B and D) of the prostate (A and B) and the proximal part of the seminal vesicles (C and D) for the pCT and rCTs of all patients. The black lines indicate the aim of the prostate and proximal part of the seminal vesicles (95.0%).

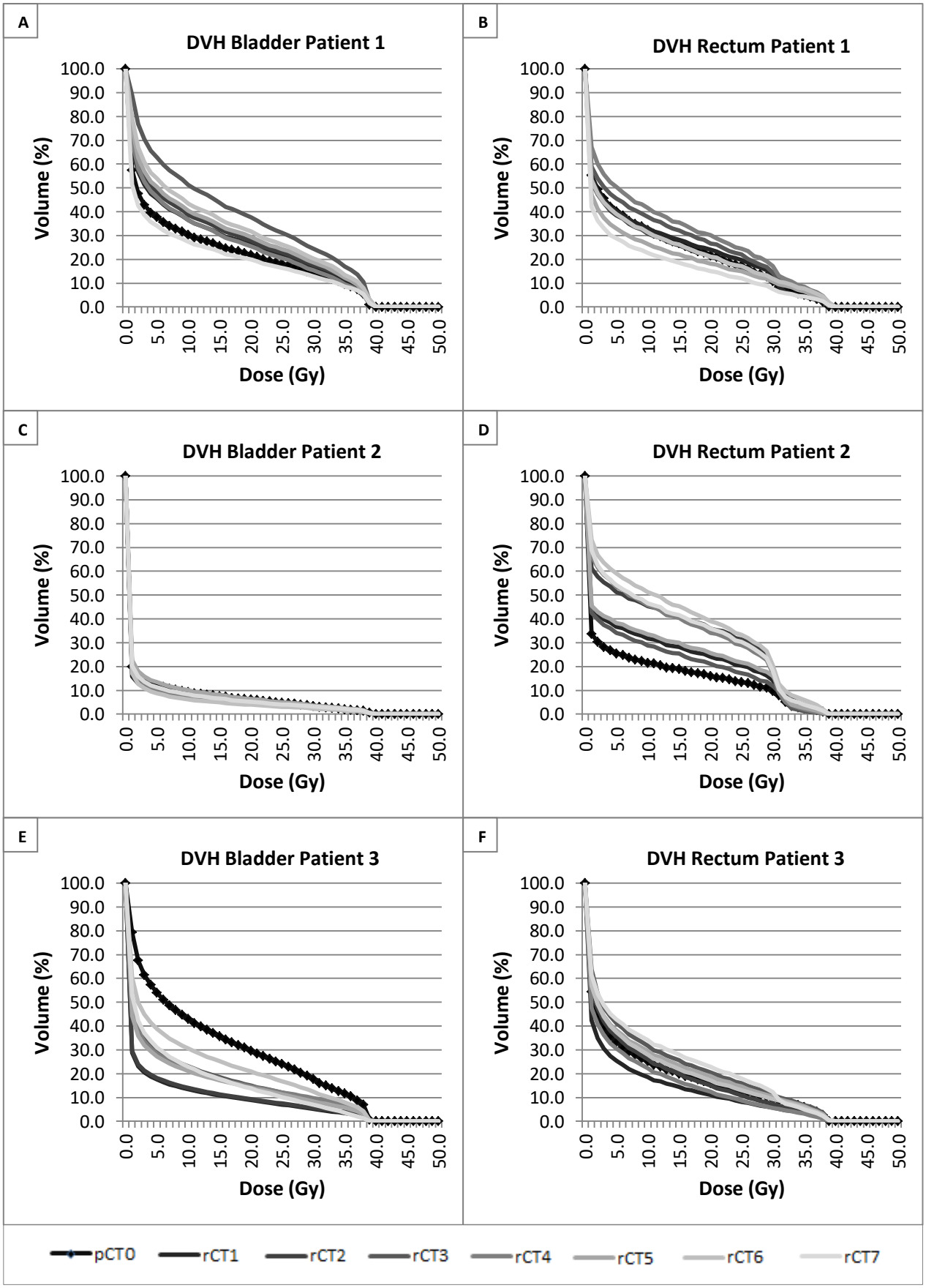

Figure 2: Dose-volume histograms of bladder and rectum for pCT and rCTs of patients 1-3.

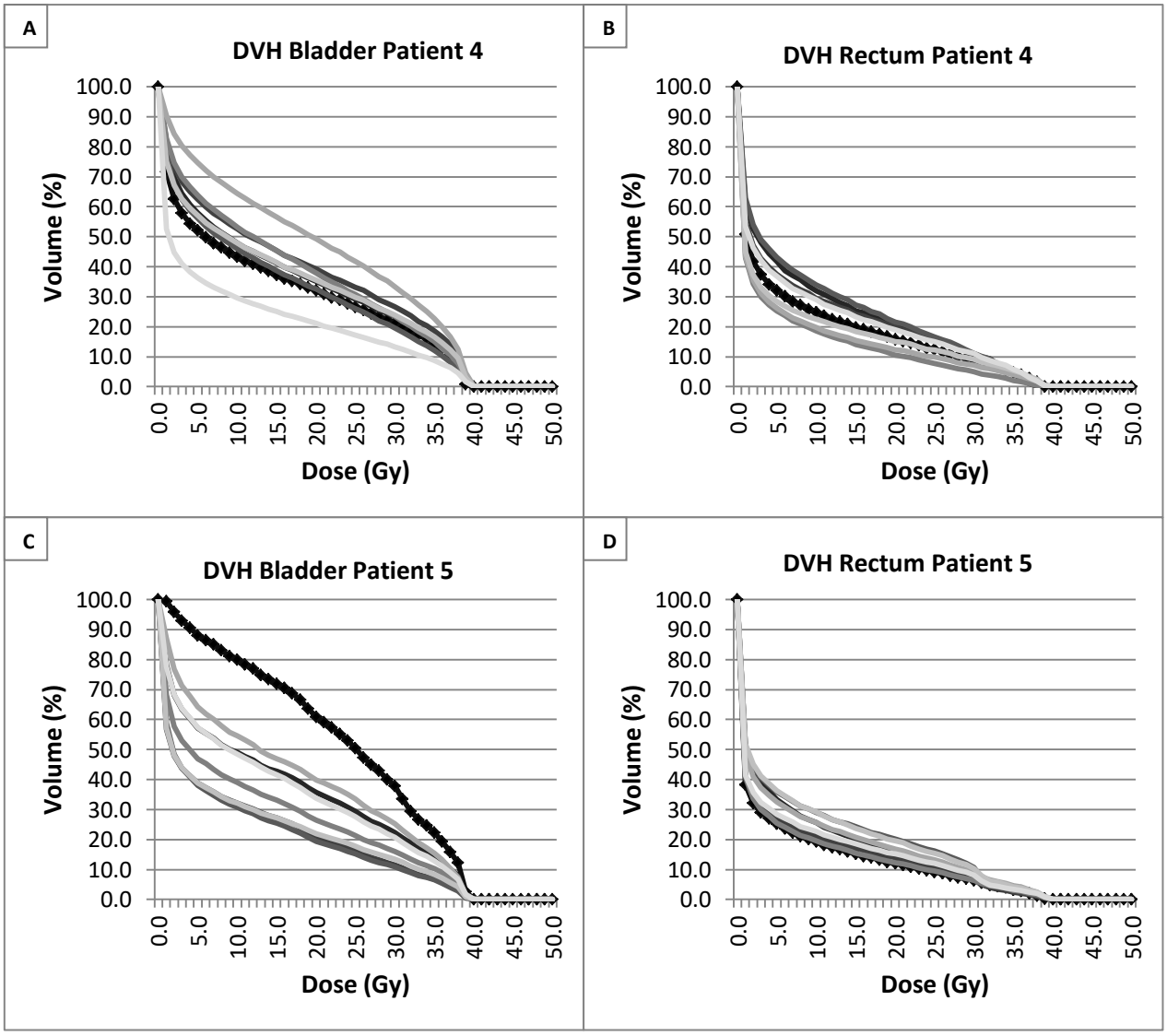

Figure 3: Dose-volume histograms of bladder and rectum for pCT and rCTs of patients 4 and 5.

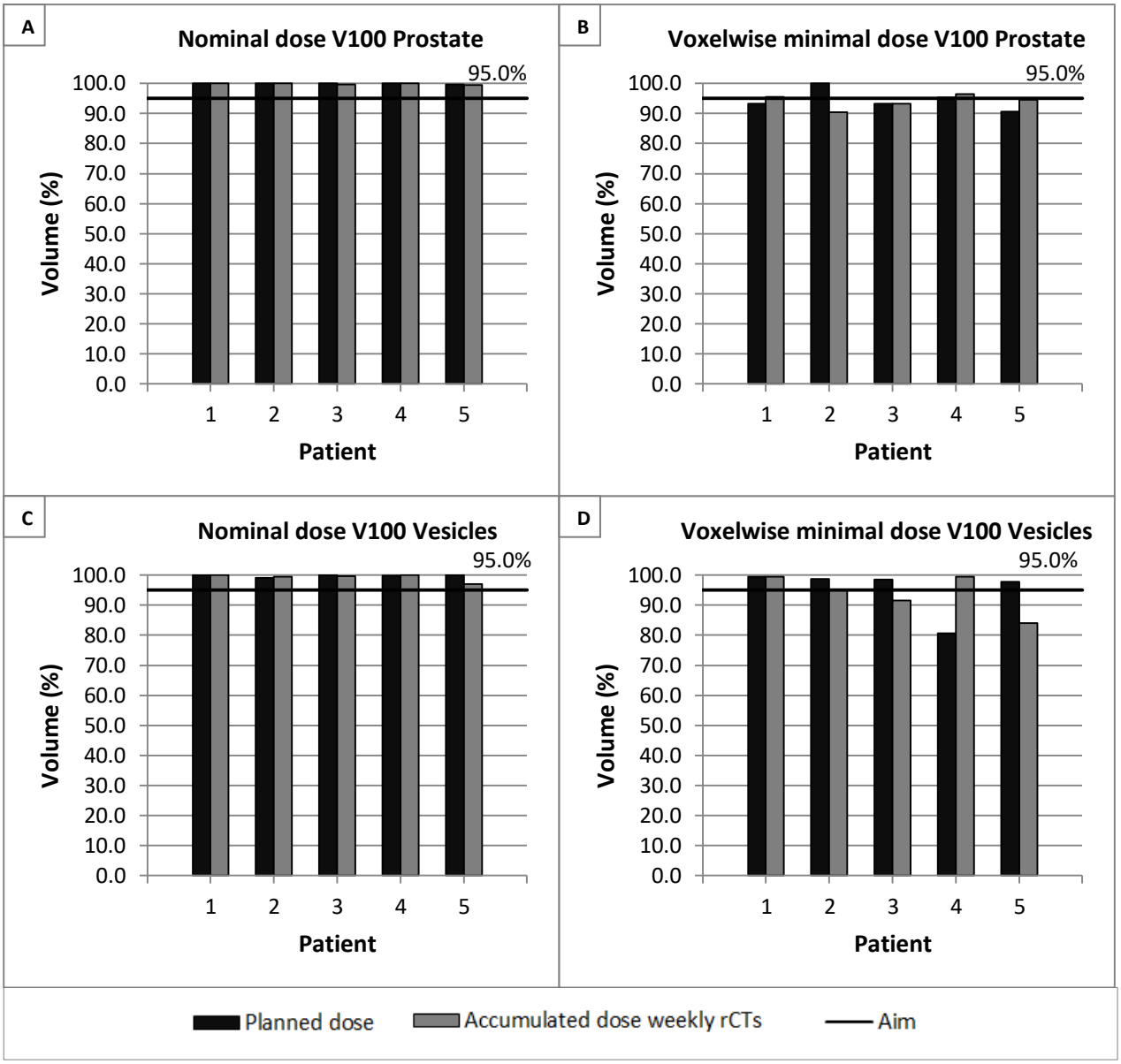

Figure 4: V100 of the nominal (A and C) and voxelwise minimal doses (B and D) of the prostate (A and B) and the proximal part of the seminal vesicles (C and D) for the planned dose and the accumulated dose on the first five weekly rCTs. The black lines indicate the aim of 95.0%.

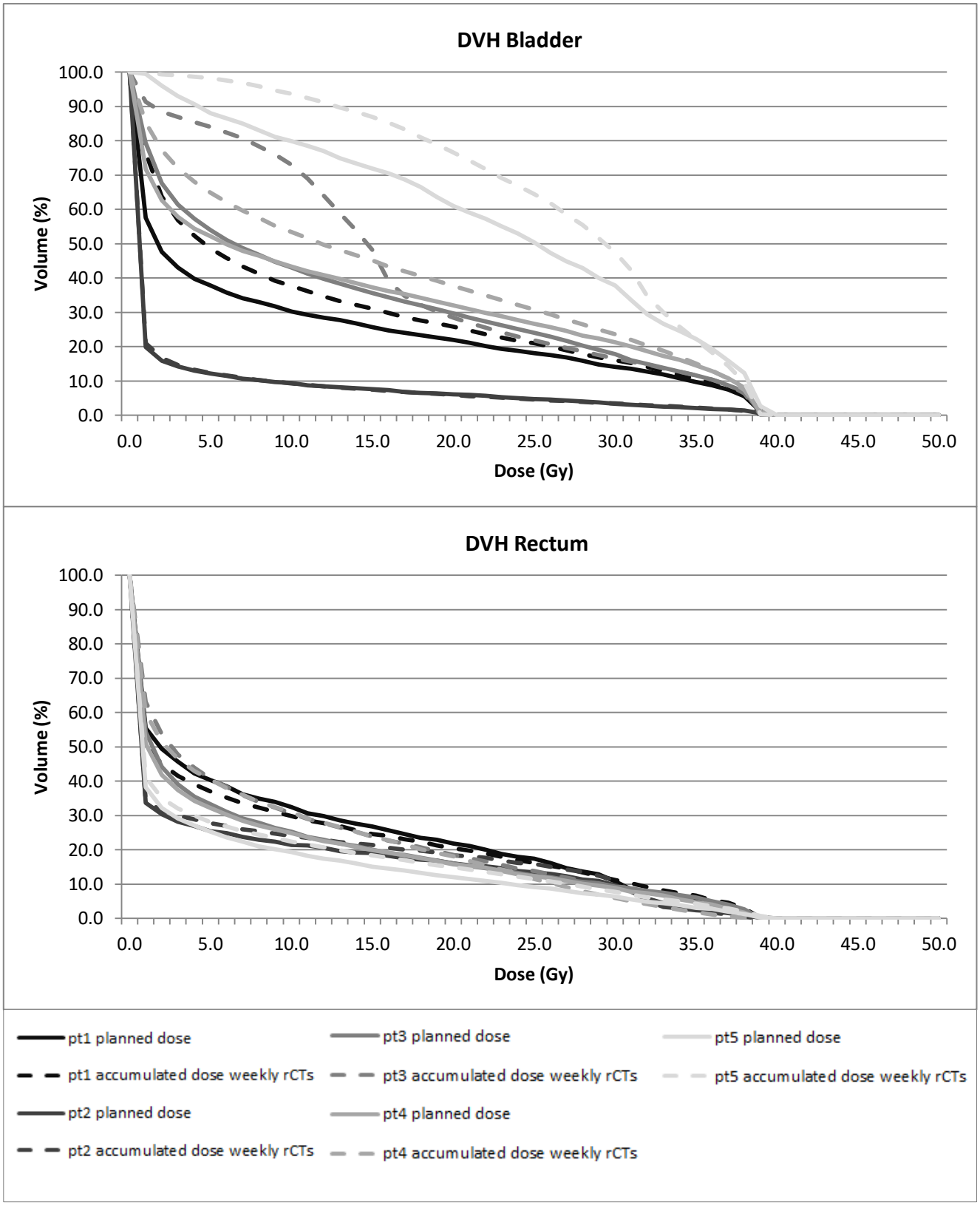

Figure 5: Dose-volume histograms of bladder and rectum for the planned dose and the accumulated dose on the first five weekly rCTs.

D. User manual for creating virtual CTs in RayStation 7.99 Research

- Copy the CT in which you want to displace e.g. the CTV.
    - RayStation Research:
        - Open the patient.
        - DICOM export → select the right export target and select the CT image that you want to export.
    - Bendicomedit:
        - Select file → select the right directory → select all slices (ctrl + a).
        - DICOM Pixel Data: preview of the selected CT image.
        - Batch list: all DICOM tags.
        - DICOM Tags: Select StudyInstanceUID and SeriesInstanceUID, press >> and replace the value of these DICOM Tags, add for instance .1
        - Save files to: original file path (files are saved under subdirectory ''mod'').
        - Save all.
    - RayStation Research:
        - Open the patient.
        - DICOM import → import to current patient/case → Source = File, choose the right directory: mod.
        - Preview
        - Import
        - Change the name and image system of the copied CT:
            - Patient Data Management, select the CT image → Properties → change the image set name in e.g. CT_copy and the imaging system in the same as of the original CT.
        - Copy the structures of the original CT to the copied CT:
            - Patient modeling → structure definition → new ROI geometry → copy ROI geometries. Source structure set = CT. Geometry: all structures. Target structure set = CT_copy. OK.
- Translate the CTV using the calculated motion (RayStation Research)
    - Create a centroid of the CTV in the original and copied CT.
        - Patient modeling → structure definition → POI tools → New POI geometry → ROI center: CTV → New POI: name = Centroid_CTV.
    - Translate the CTV manually in the CT_copy using the calculated motion (x-, y-, and z-direction).
        - Patient modeling → structure definition → Current ROI = CTV → 3D mode → translate in the different directions.
        - Translate the CTV in the different directions using the following slices:
            - X-direction (left/right motion): transversal slice.
            - Y-direction (superior/inferior direction): sagittal slice.
            - Z-direction (anterior/posterior direction): transversal slice.
    - Check the position of the x-, y-, and z-coordinates of the centroid of the copied CT.

        - Patient modeling → structure definition → POI tools → select the POI Centroid_CTV → Edit POI geometry → Point specification: ROI center: CTV, OK.
    - If the difference between the POI coordinates of the original and copied CT equals the calculated motion, continue with the next step. Otherwise repeat the described translation and checking process.
- Creation of a virtual, deformed CT
    - Create a deformation vector field of the translation of the CTV.
        - Patient modeling → deformable registration → create + evaluate → New registration → Hybrid intensity and structure based → Reference image set = CT_copy; Target image set = CT. Controlling ROI(s): CTV and the surrounding bony structures. Deformation strategy = default, deformation grid, resolution = 0.25. OK.
    - View the deformation vector field.
        - Select → registration → reference = CT_copy, target = CT.
    - View the deformed CT using the following options:
        - Side by side evaluation.
        - Image comparison → target view (deformed).
    - Create the virtual, deformed CT
        - Run script ConsoleAndStateTree
            - State viewer: You can search which case and registration you have to call and you can check everything.
            - Example of Command: case.Registrations[0].StructureRegstrations['HybridDefReg'].CreateDeformedExamination(ExaminationName="pCT",SizeSimilarToTargetImage="false")
- Map the structures
    - Map the structures deformable from the CT → CT_copy.
        - Patient modeling → Deformable Registration → Create and Evaluate → Map structures → map ROIs. Select the right Deformable registration (reference = CT_copy, target = CT).
        - Map structures: reverse direction, create new geometry, ***select all except CTV***!
    - Map the structures rigidly from the CT_copy → virtual, deformed CT.
        - Patient modeling → structure definition → select layout (prim+sec). CT_copy = primary, vCT = secondary.
        - Patient modeling → structure definition → new ROI geometries → Copy ROI geometries → Select all.

E. MATLAB script for selection of worst-case intrafraction prostate motion

```
clear all
close all
clc
for p = 1 % Patient
    clearvars -except p
    % load data of one patient
    [FileName, PathName] = uigetfile('*.*','MultiSelect', 'on');
    completename = fullfile(PathName, FileName);
    delimiterIn = ' '; % column separator character
    headerlinesIn = 1; % number of text header lines
    for n = 1:length(completename) % n = number of fractions
        A(n) = importdata(completename{n}, delimiterIn, headerlinesIn);
        xvalue{:,n} = A(n).data(:,1) - A(n).data(1,1); % measured x values minus
begin x value in mm
        yvalue{:,n} = A(n).data(:,2) - A(n).data(1,2); % measured y values minus
begin y value in mm
        zvalue{:,n} = A(n).data(:,3) - A(n).data(1,3); % measured z values minus
begin z value in mm
        threed{:,n} = A(n).data(:,4); % 3D motion in mm
        time{:,n} = A(n).data(:,5); % tracking time in seconds
        % plot area under the curve
        figure(n);
        auc_plot(n) = area(time{:,n},threed{:,n});
        hold on
        if p<22
           title(sprintf('AUC 3D motion Fraction %d Patient %d (Balloon)',n,p));
        else
           title(sprintf('AUC 3D motion Fraction %d Patient %d (Non-
Balloon)',n,p));
        end
        xlabel('Tracking time in seconds');
        ylabel('3D motion in mm');
        axis([0 240 0 25]);
        if p<22
            saveas(figure(n),sprintf('AUC 3D motion Fraction %d Patient %d
(Balloon).png',n,p));
        else
            saveas(figure(n),sprintf('AUC 3D motion Fraction %d Patient %d
(NB).png',n,p));
        end
        close all
            % time1 = 0-4 minutes
            time1{:,n}=time{:,n}(time{:,n}<=240); % time1 = 0-4 minutes
            itime1{:,n}=find(time{:,n}<=240); % find indices of time1
            xvalue1{:,n}=xvalue{:,n}(itime1{:,n}); % xvalues 0-4 minutes
            yvalue1{:,n}=yvalue{:,n}(itime1{:,n}); % yvalues 0-4 minutes
            zvalue1{:,n}=zvalue{:,n}(itime1{:,n}); % zvalues 0-4 minutes
            threed1{:,n}=threed{:,n}(itime1{:,n}); % 3D motion 0-4 minutes
            % determine the index of the first and last value of the
            % different time intervals (TIME INTERVAL 1)
            for j = 1:length(time1{:,n}); % 1 = first index.
                valtime_first1{:,n}(j) = time1{:,n}(j); % first value of time
interval
                interval = 15; % time interval = 15 seconds
                valtime_second1{:,n}(j) = (valtime_first1{:,n}(j)+interval); %
second value time interval
                if valtime_second1{:,n}(j)>time1{:,n}(length(time1{:,n}));
                j=j-1;
                else
                itime_first1{:,n}(j) = j;
                [~,itime_second1{:,n}(j)] = min(abs(time1{:,n}-
valtime_second1{:,n}(j))); % real number cannot be selected, so value closest to
time+15 seconds
                end
                if j==0;
```

```
                    auc_cal1{:,n}=[];
                    itime_first1{:,n}=[];
                    itime_second1{:,n}=[];
                    break
                end
                if valtime_second1{:,n}(j)>time1{:,n}(length(time1{:,n}));
                    break
                end
                if time1{:,n}(itime_second1{:,n}(j))-
time1{:,n}(itime_first1{:,n}(j))<14 % if time interval is not 15 seconds, break.
                    break
                end

                % calculate area under the curve for the different time intervals
                auc_cal1{:,n}(j) =
trapz(time1{:,n}(itime_first1{:,n}(j):itime_second1{:,n}(j)),threed1{:,n}(itime_fir
st1{:,n}(j):itime_second1{:,n}(j)));
            end

            % calculate the maximal area under the curve of the time interval of 15
seconds in the fraction.
             if isempty(auc_cal1{:,n})
                maxarea1{:,n} = NaN;
                imax1{:,n} = NaN;
                itimeinterval_first1{:,n} = [];
                itimeinterval_second1{:,n} = [];
             else
                maxarea1{:,n} = max(auc_cal1{:,n}); % max area under the curve
                imax1{:,n} = find(auc_cal1{:,n}==max(auc_cal1{:,n})); % i for which
area is maximal.
                itimeinterval_first1{:,n} = itime_first1{:,n}(imax1{:,n}); % first
index of time interval
                itimeinterval_second1{:,n} = itime_second1{:,n}(imax1{:,n}); %
second index of time interval
             end
            % determine the values for the time interval, x-, y-, and z-coordinates
            if isempty(time1{:,n});
                timeinterval1{:,n}=NaN;
                valthreed1{:,n}=NaN;
                valx1{:,n}=NaN;
                valy1{:,n}=NaN;
                valz1{:,n}=NaN;
            end
            if isempty(itimeinterval_first1{:,n})
                timeinterval1{:,n}=NaN;
                valthreed1{:,n}=NaN;
                valx1{:,n}=NaN;
                valy1{:,n}=NaN;
                valz1{:,n}=NaN;
            end
            for o = itimeinterval_first1{:,n}:itimeinterval_second1{:,n}
                timeinterval1{:,n}(o-(itimeinterval_first1{:,n}-1)) =
time1{:,n}(o);
                valthreed1{:,n}(o-(itimeinterval_first1{:,n}-1)) = threed1{:,n}(o);
                valx1{:,n}(o-(itimeinterval_first1{:,n}-1)) = xvalue1{:,n}(o);
                valy1{:,n}(o-(itimeinterval_first1{:,n}-1)) = yvalue1{:,n}(o);
                valz1{:,n}(o-(itimeinterval_first1{:,n}-1)) = zvalue1{:,n}(o);
            end
            % save data to Excel files
            if p<22
                filename1 = sprintf('Max aucs 3D Time Interval 0-4min Patient %d
(Balloon).xlsx',p);
            else
                filename1 = sprintf('Max aucs 3D Time Interval 0-4min Patient %d
(Non-Balloon).xlsx',p);
            end
            xlswrite(filename1, {'AUCs', 'TIME INTERVAL', 'X VALUE', 'Y VALUE', 'Z
VALUE', '3D MOTION'}, sprintf('Fraction%d',n), 'A1');
```

```
            xlswrite(filename1, maxarea1{:,n}', sprintf('Fraction%d',n), 'A2');
            xlswrite(filename1, timeinterval1{:,n}', sprintf('Fraction%d',n),
'B2');
            xlswrite(filename1, valx1{:,n}', sprintf('Fraction%d',n), 'C2');
            xlswrite(filename1, valy1{:,n}', sprintf('Fraction%d',n), 'D2');
            xlswrite(filename1, valz1{:,n}', sprintf('Fraction%d',n), 'E2');
            xlswrite(filename1, valthreed1{:,n}', sprintf('Fraction%d',n), 'F2');
   end
end
```

F. Selected worst-case intrafraction motion of Calypso patient with endorectal balloon

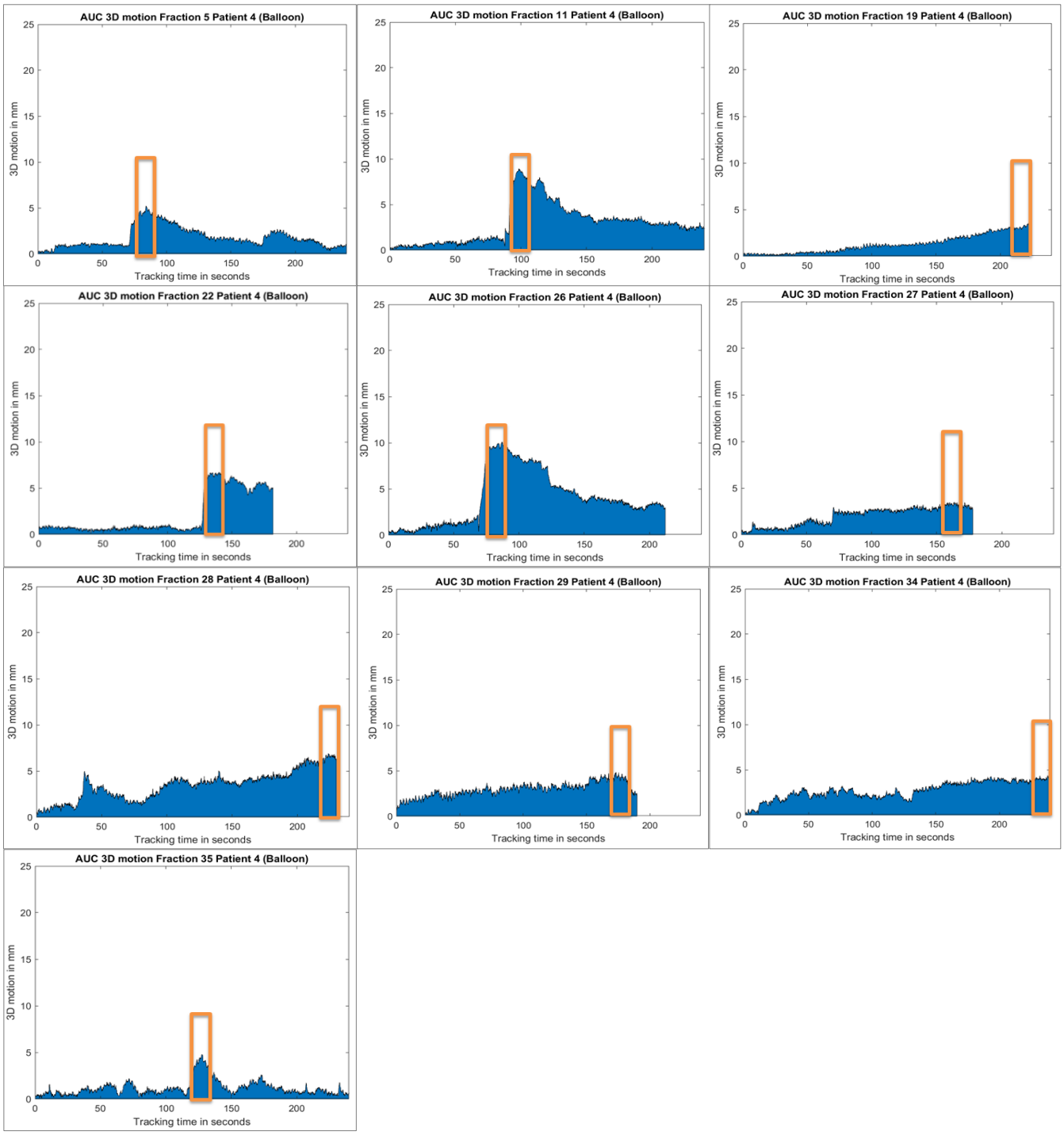

G. Selected worst-case intrafraction motion of Calypso patient without endorectal balloon

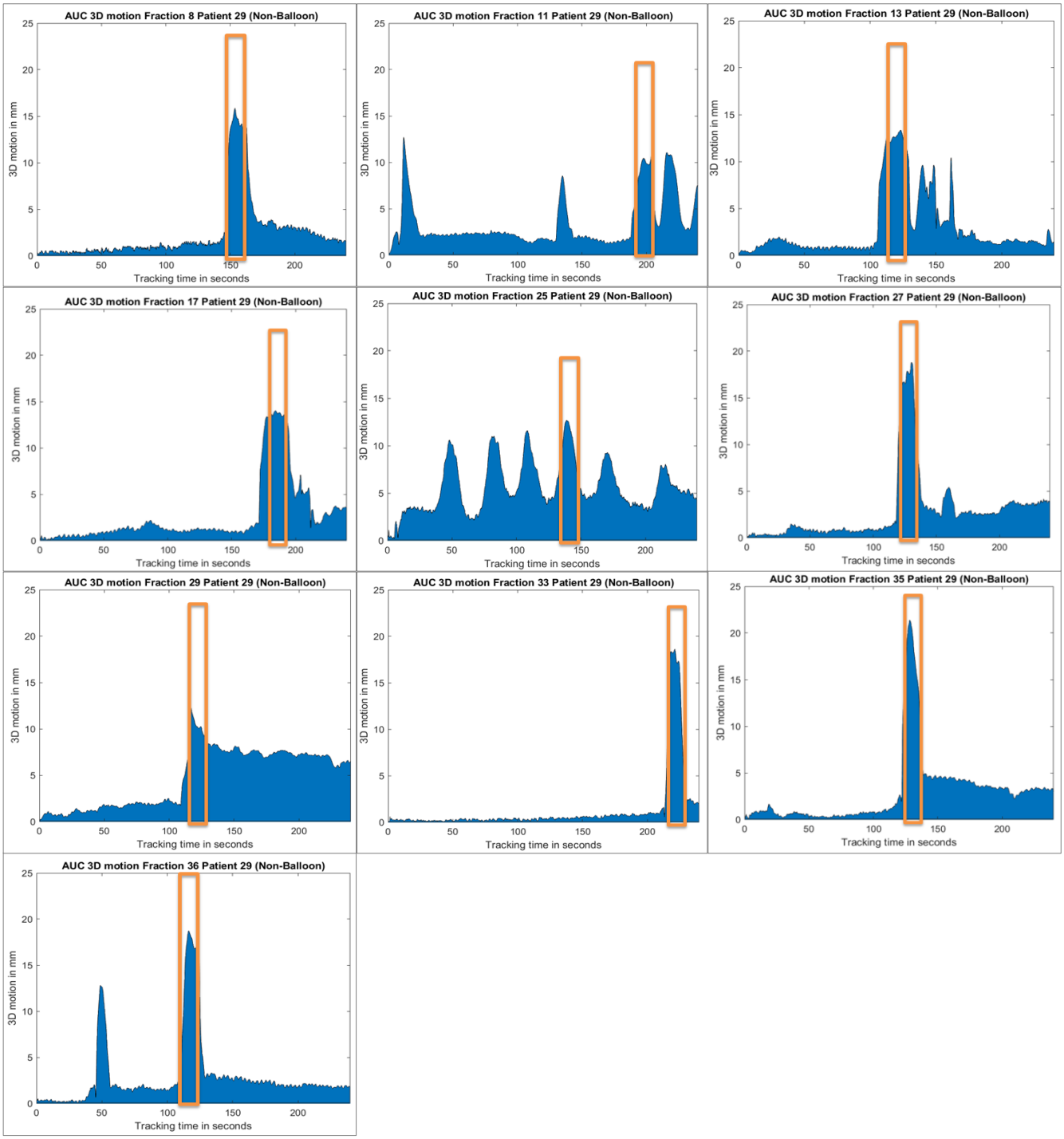

H. Additional results Chapter 3

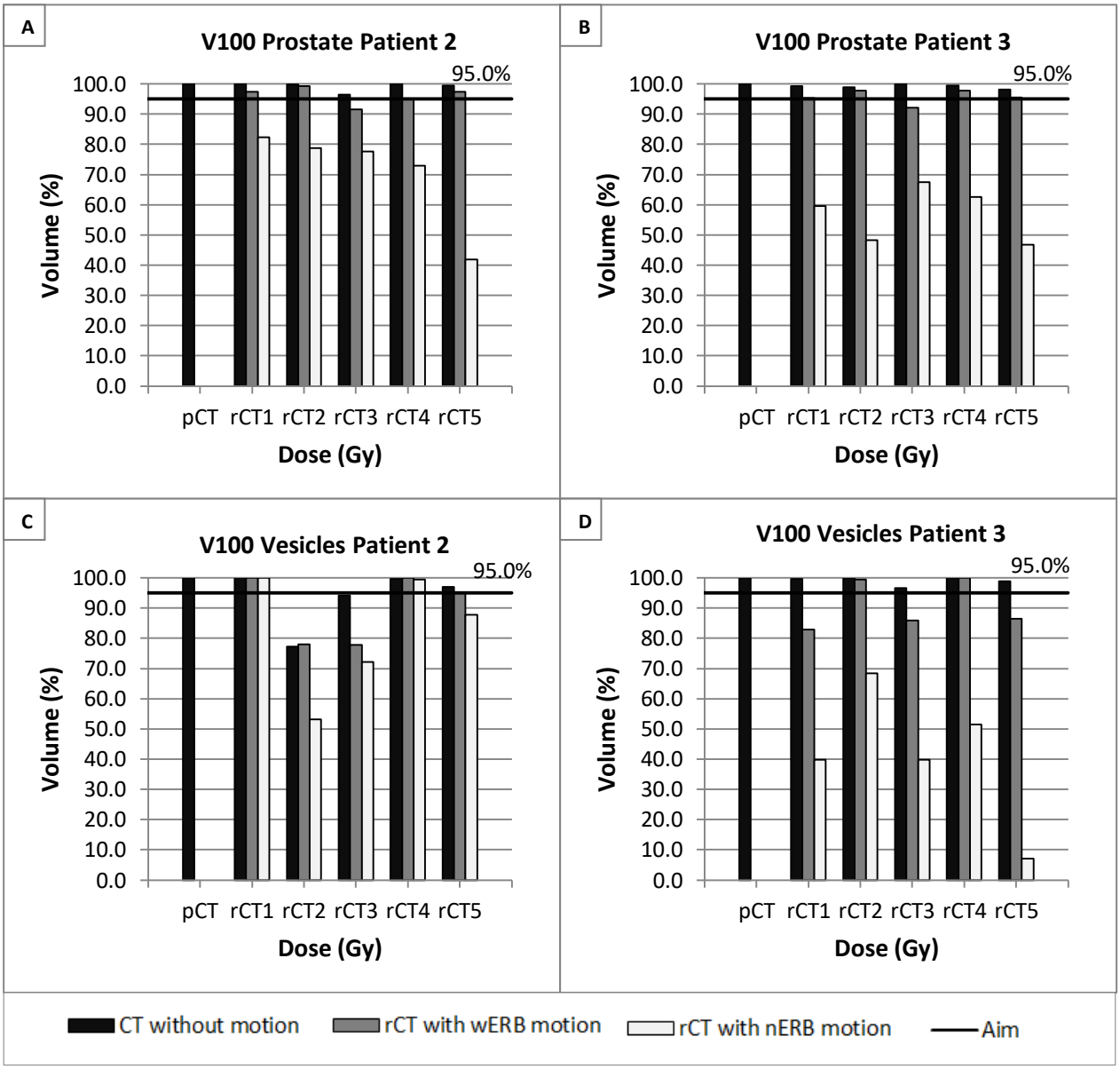

Figure 1: V100 of the 4D fractional dose for the prostate (A and B) and proximal part of the seminal vesicles (C and D) for patient 2 (A and C) and patient 3 (B and D). The aim of V100 was 95.0% for both the prostate and the proximal part of the seminal vesicles. Abbreviations: with endorectal balloon (wERB) and without endorectal balloon (nERB).

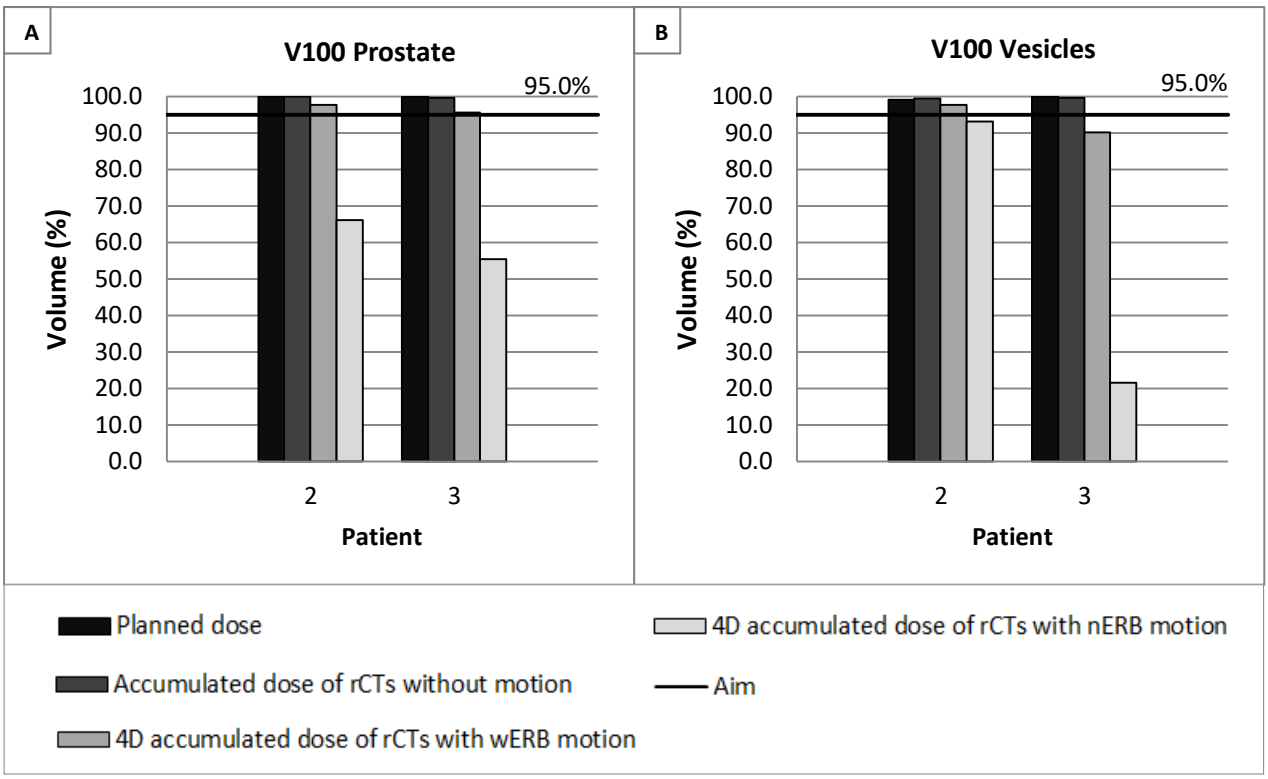

Figure 2: V100 of the prostate (A) and proximal part of the seminal vesicles (B) for the planned dose, accumulated dose of rCTs without motion and the 4D accumulated doses of rCTs with wERB and nERB motion. Abbreviations: repeated CT (rCT), with endorectal balloon (wERB), without endorectal balloon (nERB).

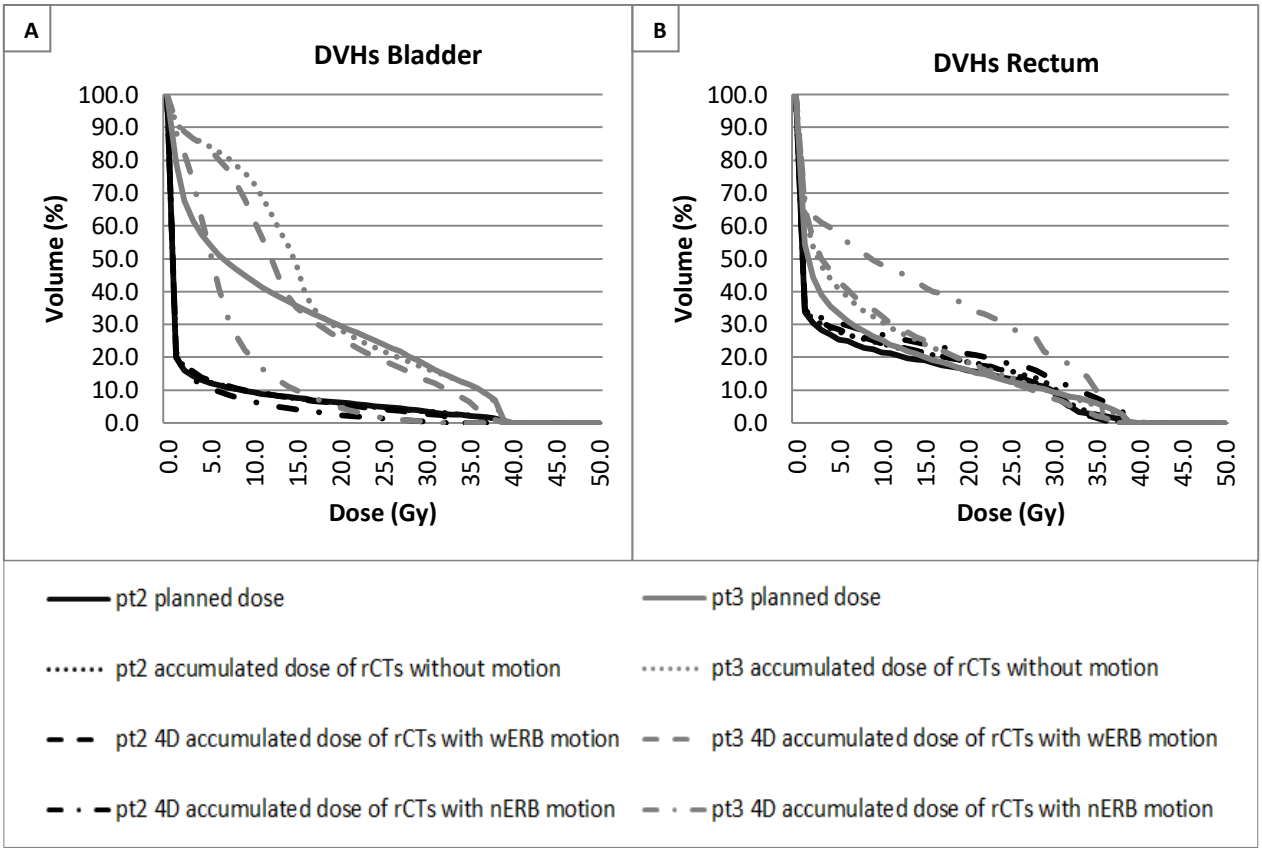

Figure 3: Dose-volume histograms of the bladder (A) and rectum (B) for patient 2 and 3. The straight lines indicate the planned dose, the dotted line indicates the accumulated dose of the rCTs without motion, the dashed lines indicate the 4D accumulated dose of the rCTs with wERB motion and the dashed-dotted lines indicate the 4D accumulated dose of the rCTs with nERB motion. Abbreviations: repeated CT (rCT), with endorectal balloon (wERB), without endorectal balloon (nERB).